



RESEARCH MEMORANDUM

DATA FROM LARGE-SCALE LOW-SPEED TESTS OF AIRPLANE
CONFIGURATIONS WITH A THIN 45° SWEPT WING
INCORPORATING SEVERAL LEADING-EDGE
CONTOUR MODIFICATIONS

By William T. Evans

Ames Aeronautical Laboratory
Moffett Field, Calif.

LIBRARY
JUN 11 1956
LANGLEY RESEARCH CENTER
LIBRARY, NASA
LANGLEY STATION
HAMPTON, VIRGINIA

NATIONAL ADVISORY COMMITTEE
FOR AERONAUTICS

WASHINGTON

May 7, 1956

Declassified March 20, 1958

NATIONAL ADVISORY COMMITTEE FOR AERONAUTICS

RESEARCH MEMORANDUM

DATA FROM LARGE-SCALE LOW-SPEED TESTS OF AIRPLANE

CONFIGURATIONS WITH A THIN 45° SWEEP WING

INCORPORATING SEVERAL LEADING-EDGE

CONTOUR MODIFICATIONS

By William T. Evans

SUMMARY

Force tests have been made of airplane configurations with a thin swept wing incorporating several wing-contour modifications forward of maximum thickness. Both longitudinal and lateral characteristics are presented. The basic wing had an aspect ratio of 3, a taper ratio of 0.4, a leading-edge sweep of 45° , and an NACA 64A006 airfoil section normal to the quarter-chord line. The four principal modifications consisted of increases in leading-edge radius, and in two cases, slight forward camber. In two cases, the modified airfoil sections were constant over the span, while in the other two, they varied spanwise from thin-nosed sections at the root to maximum modifications at the tip. A fifth modification, tested briefly, consisted of an abrupt change of section at 40-percent semispan. The detailed derivation of all modifications is indicated.

The complete airplane configuration consisted of the wing, a body, either of two vertical tails, and an all-movable horizontal tail, which could be installed at various heights relative to the wing chord plane. Tests were made with and without the empennage components, and, in addition, the basic wing was tested alone, without the body. Fences, chord extensions, split flaps, and simulated ailerons were tested on the model. Tests were made at Reynolds numbers from 4.4 to 21×10^6 , the corresponding Mach number range being from 0.05 to 0.29.

No analysis is made of the data presented.

INTRODUCTION

The fundamental results of an investigation of the effects of a wing-contour modification designed to improve the low-speed characteristics of a thin swept wing have been reported and analyzed in reference 1. The modification consisted of a greatly increased leading-edge radius and slight forward camber. Data were presented in the report from tests at low subsonic, high subsonic, and supersonic speeds.

Besides the data reported in reference 1, a considerable amount of additional low-speed data was obtained in the course of the investigation, which was not directly relevant to the basic analysis of reference 1. Specifically, data were obtained on three less extreme wing-contour modifications. Also, for each wing, data were obtained on the effects of horizontal and vertical tails, and on the effects of fences. Some limited data were obtained on the effects of chord extensions, split flaps, and simulated (split-flap-type) ailerons. All testing was done in the Ames 40- by 80-foot wind tunnel.

It is the purpose of this report to present these data. While no analysis is made herein, it is hoped that the report will provide a useful fund of information on a representative interceptor-type configuration. (For the sake of completeness, the low-speed data of ref. 1 are repeated in this report.) It is also hoped that it will provide an indication, when considered in conjunction with the analysis of reference 1, of the possibilities and limitations of leading-edge contour design for a thin swept wing.

In addition to the high-speed data available in reference 1, additional data obtained at high speeds and/or low Reynolds numbers from tests of wings having the same plan form with various airfoil sections can be found in references 2 through 7. Reference 5 includes data on a wing modification essentially the same as modification 3 of this report. Data on the use of spoilers as lateral controls on the subject model can be found in reference 8.

NOTATION

The sign convention used for presentation of the data is shown in figure 1.

C_D drag coefficient, $\frac{\text{drag}}{qS}$

C_{D_0}	drag coefficient at zero lift
C_L	lift coefficient, $\frac{\text{lift}}{qS}$
C_l	rolling-moment coefficient, $\frac{\text{rolling moment}}{qSb}$
C_m	pitching-moment coefficient, $\frac{\text{pitching moment}}{qS\bar{c}}$
C_n	yawing-moment coefficient, $\frac{\text{yawing moment}}{qSb}$
C_Y	side-force coefficient, $\frac{\text{side force}}{qS}$
M	Mach number
R	Reynolds number, based on \bar{c} of basic wing
S	area of basic wing, sq ft
S_t	area of horizontal tail, sq ft
V	free-stream velocity, ft/sec
a	arbitrary coefficient
b	wing span, ft
b_t	horizontal-tail span, ft
c	local streamwise chord of basic wing, ft
c'	local chord of NACA 64A006 section of basic wing, lying normal to 39.45° sweep line, ft
\bar{c}	mean aerodynamic chord of basic wing, $\frac{\int_0^{b/2} c^2 dy}{\int_0^{b/2} c dy}$
c_l	section-lift coefficient
d_η	leading-edge droop of modified wing section, percent of local basic-wing chord
i_t	incidence of horizontal tail relative to body axis, deg

l_t	longitudinal distance from moment center to pivot line of horizontal tail, ft
q	dynamic pressure, $\frac{1}{2} \rho V^2$
r_η	leading-edge radius, percent of local basic-wing chord
x	longitudinal coordinate parallel to model center line, ft
y	lateral coordinate perpendicular to plane of symmetry, ft
z	vertical coordinate perpendicular to basic-wing chord plane, ft
α	angle of attack, referred to body axis, deg
β	angle of sideslip, deg
δ_f	flap deflection (angle between split flap and lower surface of wing), measured in plane perpendicular to hinge line, deg
ϵ_{av}	average effective downwash, deg
η	$\frac{y}{b/2}$
λ	taper ratio
ρ	air density, slugs/cu ft

Subscript

max maximum

The following code designation of model configurations is used on all data figures:

W	basic wing
WM _n	wing with modification n
B	body
V _Δ	triangular vertical tail
V _Λ	swept vertical tail
hH_i	horizontal tail at height $h = z/(b/2)$, and at incidence i , deg

η^F	fences at spanwise location η
E	chord extensions
$\eta^{SF\delta}$	split flaps of spanwise extent η , at deflection δ , deg
A	simulated ailerons
\pm	with and without
\sim	variable

DESCRIPTION OF MODEL

A two-view drawing with pertinent dimensions is given in figure 2. Geometric data are tabulated in table I. A photograph of a typical installation of the model in the tunnel is given in figure 3.

Basic Configuration

The basic wing had an aspect ratio of 3, taper ratio of 0.4, sweep-back of the leading edge of 45° , and an NACA 64A006 airfoil section normal to its own quarter-chord line, which was swept 39.45° .

The body was a Sears-Haack body of fineness ratio 12.5. The general formula for such bodies is

$$r = r_{\max} \left[1 - \left(1 - \frac{x}{l/2} \right)^2 \right]^{3/4}$$

where r is the radius, x the axial distance from the nose, and l the body length.

Either of two vertical tails was used. The triangular vertical tail had an aspect ratio of 1 and a modified NACA 0005 section in the streamwise direction. The modification consisted of a straight fairing from 67-percent chord aft.

The swept vertical tail had a plan form the same as the basic wing semispan. The streamwise section had a constant 6-percent thickness from 11- to 74-percent chord, a semiellipse forward of 11-percent chord, and a straight fairing from 75-percent chord aft. There was an arbitrary fairing from 74- to 75-percent chord.

The horizontal tail had an unswept midchord line and a modified diamond section. The original diamond section of 5.6-percent thickness was modified by rounding the maximum-thickness ridge to a radius of curvature of 4.48-percent chord; the resulting section had a maximum thickness of 4.2-percent chord. The tail was all-movable and pivoted about a line connecting the leading edges of the tips. When the tail was mounted on the body, in the chord plane of the wing, the aspect ratio was 4.4 and the taper ratio 0.46; above the chord plane, on either vertical tail, the aspect ratio was 4.0 and the taper ratio 0.50. The tail was tested at heights $z/(b/2)$ of 0, 0.12, 0.21, and 0.41.

Wing-Contour Modifications

Wing-section coordinates defining all modifications are tabulated in table II, and the sections are illustrated in figure 4. All the sections are taken normal to the 39.45° sweep line, which was the quarter-chord line of the NACA 64A006 section of the basic wing.

Modifications 1 and 1(b).— Modification 1 consisted of the same modified section over the entire span. The leading-edge radius and droop were 1.19- and 1.38-percent chord, respectively.¹ The section was designed to attain a given low-speed value of $c_{l_{max}}$, about equal to that to be expected from the use of a leading-edge flap on the NACA 64A006 section. Further information is given in reference 1, including the detailed derivation of the section, its experimental two-dimensional lift curve, and an analysis of the fundamental longitudinal characteristics of the wing with this modification.

Modification 1(b) was the same as modification 1 from $0.4 b/2$ to the wing tip, but consisted of the basic wing inboard of $0.4 b/2$. It was tested with and without a fairing of the spanwise discontinuity. It was designed as a less extreme modification which might be expected to retain the stability benefit of the full-span modification. For a detailed discussion and analysis of test results, see reference 1.

Modifications 2 and 3.— These were both based on the basic-wing section at the wing root and the thickness distribution of modification 1 at the wing tip. Modification 2 retained the camber of modification 1 at the tip, while modification 3 was uncambered. Intermediate sections were the result of linear elements between root and tip. The resulting spanwise variations of leading-edge radius and droop are given by the formulas

¹When referring to a modified section, the term "percent chord" shall be understood to mean "percent of the local basic-wing chord."

$$r_{\eta} = \left[\frac{(1 - \eta)\sqrt{r_{\text{root}}} + \eta\lambda\sqrt{r_{\text{tip}}}}{1 - (1 - \lambda)\eta} \right]^2$$

and

$$d_{\eta} = \frac{(1 - \eta)d_{\text{root}} + \eta\lambda d_{\text{tip}}}{1 - (1 - \lambda)\eta}$$

where r_{η} and d_{η} are, respectively, the radius and droop at span station η , both in percent of the local chord. These variations are plotted in figure 5.

These modifications were designed to effect compromises between the low-speed characteristics of modification 1 and the high-speed characteristics of the basic wing-body configuration. (As reported in ref. 1, the high-speed increment of C_{D_0} due to modification 1 was as much as 0.0075 at $M = 1.9$ and $R = 2.9 \times 10^6$.)

There were minor design differences between the two modifications. Modification 2 was intended to approximate a similar model tested in the Ames 6- by 6-foot supersonic wind tunnel.² The wing for that model had been designed in terms of streamwise sections, having the streamwise section of the basic wing along the wing center line, and what was essentially the streamwise section of modification 1 at the wing tip. On the other hand, modification 3 was designed in terms of sections lying normal to the 39.45° sweep line, as were all the wings except modification 2. The "root" section of modification 3, that is, the imaginary section with its leading edge on the wing center line and lying in the extended wing panel, was the NACA 64A006. The section with its leading edge at the wing tip was essentially the uncambered thickness distribution of the section of modification 1. (Actually, since modification 1 protruded forward of the leading edge of the basic wing by 1.5-percent chord, and had a constant maximum-thickness region over approximately 19-percent chord, the "tip" section of modification 3 was shortened in the maximum-thickness region by 1.5-percent chord.)³

Modification 4.- This was uncambered, and consisted of the same section over the entire span. The forward 20-percent chord of the section

²The data obtained in that test program have not been published. These data indicated trends very similar to those obtained for a model incorporating what was essentially modification 3. The latter data have been reported in reference 5.

³For further data on a similar model, including high-speed data, see reference 5.

was described by an equation of the type used to derive NACA OOOX sections:

$y = a_0 \sqrt{x} + a_1 x + a_2 x^2 + a_3 x^3$. The coefficients of the equation were determined by setting the leading-edge radius equal to 0.9-percent chord, the ordinate at 20-percent chord equal to 3-percent chord, and the slope and curvature at 20-percent chord equal to zero. From 20-percent chord, a constant-thickness region extended back to the location of maximum thickness of the NACA 64A006 section (39-percent chord).

This modification was designed to have the best low-speed stalling characteristics attainable without the introduction of camber. Because of high-speed drag considerations, a leading-edge radius was chosen only slightly larger than the minimum considered necessary for attainment of maximum low-speed benefit. The conclusion that there exists a magnitude of leading-edge radius above which no increasing benefit can be expected is based on the empirical relation between $c_{l_{max}}$ and leading-edge radius for symmetrical 6-percent-thick sections shown in figure 6, taken from reference 1. The relation indicates that increases of leading-edge radius beyond 0.8-percent chord do not result in increases of $c_{l_{max}}$. For the subject modification, a leading-edge radius of 0.9-percent chord was chosen to provide a slight margin of safety.

Because swept wings are often designed in terms of streamwise sections, it is perhaps well to note that the streamwise sections of all the subject wings differed significantly from the corresponding sections normal to the 39.45° sweep line, which have been described above. The former were approximately 5 percent thick and had leading-edge radii, in percent chord, equal to 68 percent of the leading-edge radii of the latter.

Fences and Chord Extensions

Fences were tested on the basic wing and all modifications, except 1(b). They were of 5-percent-chord height and extended from 25-percent chord on the lower surface around the leading edge to 100-percent chord on the upper surface.

Chord extensions were tested on the basic wing only. They were of 15-percent chord in the streamwise direction. The section normal to the 39.45° sweep line had NACA 64A006 ordinates back to the point of maximum thickness, and a flat slab from that point back to the point of maximum thickness of the original wing.

Considerable data on fences and chord extensions were obtained on the basic wing. The configurations selected for presentation of test results are representative of the most stabilizing configurations tested.

Flaps and Ailerons

Split flaps were tested with modifications 1, 2, and 4. Their streamwise chord was 25 percent of the local streamwise chord of the basic wing. The outboard end of each flap was cut perpendicular to the hinge line. The inboard end was cut to make a rough fit to the contour of the body and was adjusted for each deflection. The gap was unsealed. Two spanwise extents of flap were tested: the outboard end of the trailing edge, when the flap was undeflected, was located at either 55 or 75 percent of the wing semispan.

Ailerons, simulated by split flaps, were tested with modification 4 only. Their hinge line coincided with that of the flaps, and their ends were cut off perpendicular to the hinge line. Their trailing edges, when undeflected, extended from 50 to 75 percent of the wing semispan. They were tested at a differential deflection of $\pm 17^\circ$ only.

TESTS AND CORRECTIONS

The model was tested in the Ames 40- by 80-foot wind tunnel and was supported on a conventional three-strut support system. Six-component force data were obtained at angles of attack from -4° to $+26^\circ$, and at angles of sideslip from -2° to $+12^\circ$. The Reynolds number for most of the data was from 9.5 to 10×10^6 , the corresponding Mach number being approximately 0.13, and the corresponding dynamic pressure being approximately 25 pounds per square foot. Some data were obtained at Reynolds numbers from 4.4 to 21×10^6 , the corresponding Mach number range being 0.05 to 0.29, and the corresponding range of dynamic pressures being 5 to 120 pounds per square foot. The variation of Mach number with Reynolds number is shown in figure 7. All data have been corrected for air-stream inclination, wind-tunnel-wall effects, and support-strut interference. The wall-effect corrections added were as follows:

$$\alpha_T = 0.70 C_L$$

$$C_{D_T} = 0.0122 C_L^2$$

$$C_{m_T} = 0.0152 C_L \text{ for the horizontal tail} \\ \text{in the wing chord plane}$$

$$C_{m_T} = 0.0144 C_L \text{ for the horizontal tail} \\ \text{above the wing chord plane}$$

All angles of attack are referred to the chord plane of the basic wing (i.e., to the body axis). All force and moment coefficients are based on the area and mean aerodynamic chord of the basic wing. All

moments for horizontal-tail-off configurations are computed about the appropriate axis through the quarter-chord point of the mean aerodynamic chord of the basic wing.

All moments for horizontal-tail-on configurations are computed about centers such that a value of $(dC_m/dC_L)_{C_L=0} \approx -0.06$ would be obtained when controls and flaps were undeflected. The maximum deviation from this value is in the case of modification 1.

Pressure-distribution data were obtained on the basic wing and on modifications 1 and 4, and are available for inspection at the Ames Laboratory of the NACA. No pressure-distribution data are presented herein. (The data were obtained from rows of pressure orifices located on the right wing panel at 0.15, 0.30, 0.45, 0.60, 0.75, 0.90, and 0.95 $b/2$; on the basic wing alone, additional rows were located at 0 and 0.05 $b/2$.)

PRESENTATION OF RESULTS

An index to all figures presenting force data is given in table III. The figures are grouped by wing contour, with the final two figures presenting certain intercomparisons among the wings.

Any slight discrepancies that may be apparent among figures presenting the same data are due to the fact that test runs for certain configurations were repeated, often after the wing had been refinished. The run data chosen for presentation in a given figure are considered the most valid for the particular comparison to be brought out by that figure.

Ames Aeronautical Laboratory
National Advisory Committee for Aeronautics
Moffett Field, Calif., Feb. 17, 1956

REFERENCES

1. Graham, David, and Evans, William T.: Investigation of the Effects of an Airfoil Section Modification on the Aerodynamic Characteristics at Subsonic and Supersonic Speeds of a Thin Swept Wing of Aspect Ratio 3 in Combination With a Body. NACA RM A55D11, 1955.
2. Hall, Charles F.: Lift, Drag, and Pitching Moment of Low-Aspect-Ratio Wings at Subsonic and Supersonic Speeds. NACA RM A53A30, 1953.

3. Holdaway, George H.: A Flight Investigation at Transonic Speeds and Small Angles of Attack of the Aerodynamic Characteristics of a Model Having a 45° Sweptback Wing of Aspect Ratio 3 With an NACA 64A006 Airfoil Section. NACA RM A54I17, 1955.
4. Knechtel, Earl D., and Summers, James L.: Effects of Sweep and Taper Ratio on the Longitudinal Characteristics of an Aspect Ratio 3 Wing-Body Combination at Mach numbers From 0.6 to 1.4. NACA RM A55A03, 1955.
5. Boyd, John W., Migotsky, Eugene, and Wetzel, Benton E.: A Study of Conical Camber for Triangular and Sweptback Wings. NACA RM A55G19, 1955.
6. Wetzel, Benton E.: Effect of Leading-Edge Sweepback on Lift, Drag, and Pitching-Moment Characteristics of Thin Wings of Aspect Ratio 3 and Taper Ratio 0.4 at Subsonic and Supersonic Speeds. NACA RM A55H04a, 1955.
7. Bandettini, Angelo: An Investigation at Subsonic Speeds of the Rolling Effectiveness of a Small Perforated Spoiler on a Wing Having 45° of Sweepback. NACA RM A52G02, 1952.
8. Franks, Ralph W.: Tests in the Ames 40- by 80-Foot Wind Tunnel of the Aerodynamic Characteristics of Airplane Models With Plain Spoiler Ailerons. NACA RM A54H26, 1954.

TABLE I.- GEOMETRIC DATA

Wing	Basic Wing and Modifications		
	3 and 4	Modifica- tion 1	Modifica- tion 2
Area, sq ft	312.5	318.8	313.4
Span, ft	30.62	30.62	30.62
Mean aerodynamic chord, ft	10.83	11.05	10.87
Aspect ratio	3	2.94	2.99
Taper ratio	0.4	0.4	0.408
Leading-edge sweep, deg	45	45.33	44.77
Sweep of $c'/4$, deg	39.45	- - -	- - -
Incidence of root chord, deg	0	-0.74	0
Dihedral (referred to $c'/4$), deg	0	-0.32	-0.21
Twist (washout), deg	0	0	-0.74
Body			
Length, ft			56.16
Maximum diameter, ft			4.49
Fineness ratio			12.5
Vertical tail		Triangular	Swept
Exposed area, sq ft		52.5	63.1
Aspect ratio		1	1.5
Taper Ratio		0	0.4
Leading-edge sweep, deg		63.43	45
Horizontal tail		On triangular vertical tail	On swept vertical tail
Aspect ratio	On body 4.4	4	4
Taper ratio	0.46	0.50	0.50
S_t/S	0.246	0.200	0.200
b_t/b	0.602	0.517	0.517
Moment center for $z/(b/2) = 0$	0.348	- - -	- - -
Moment center for $z/(b/2) = 0.12$	- - -	0.358	- - -
Moment center for $z/(b/2) = 0.21$	- - -	0.358	0.358
Moment center for $z/(b/2) = 0.41$	- - -	0.408	0.438
l_t/\bar{c} for $z/(b/2) = 0$	1.748	- - -	- - -
l_t/\bar{c} for $z/(b/2) = 0.12$	- - -	1.738	- - -
l_t/\bar{c} for $z/(b/2) = 0.21$	- - -	1.738	1.623
l_t/\bar{c} for $z/(b/2) = 0.41$	- - -	1.688	1.777

TABLE II.- WING-SECTION COORDINATES DEFINING THE WING MODIFICATIONS

[All sections are taken normal to the quarter-chord line of the NACA 64A006 section of the basic wing. All coordinates are referred to the chord of the NACA 64A006 section and are in terms of percent of that chord. Asterisks indicate coordinates that are identical to those of the NACA 64A006 section.]

Station	NACA 64A006	Modification 1 ¹		Modification 3 ²		Modification 4	Station	Modification 2 ² - Leading edge at tip		Station	Modification 2 ² - Leading edge at 0.5 b/2	
		Ordinates		Ordinates				Ordinates			Ordinates	
		Upper surface	Lower surface	Leading edge at tip	Leading edge at 0.5 b/2			Upper surface	Lower surface		Upper surface	Lower surface
-1.50		-1.38	-1.38				-1.50	-1.38	-1.38	-0.43	-0.40	-0.40
-1.25		-.60	-2.065				-1.13	-.47	-2.18	-.05	.18	-.93
-1.00		-.34	-2.315				-.57	-.01	-2.56	.51	.49	-1.19
-.75		-.145	-2.49				.36	.46	-2.94	1.45		-1.47
-.25		.16	-2.75				2.25		-3.30	3.34		-1.80
0	0	.29	-2.855	0	0	0	4.17		-3.43	5.27		-2.01
.25		.395	-2.955				6.11		-3.50	7.23		-2.18
.50		.49	-3.04	.98	.625	.891	10.07		-3.56	11.20		-2.43
.75			-3.10	1.18	.755	1.075	14.13		-3.50	15.26		-2.60
1.25	.739		-3.22	1.465	.945	1.354	18.31		-3.37	19.46		-2.74
2.5	1.016		-3.405	1.915	1.275	1.818	22.61		-3.21	23.80		-2.83
5.0	1.399		-3.60	2.355	1.67	2.355	27.03		-3.12	28.23		-2.92
7.5	1.684		-3.67	2.59	1.94	2.699	35		-2.98	35		-2.98
10	1.919		-3.68	2.73	2.15	2.836						
15	2.283		-3.61	2.91	2.455	2.981						
20	2.737		-3.45	2.997	2.68	3.000						
25	2.757		-3.235	3.000	2.83	3.000						
30	2.896		-3.095	3.000	2.925	3.000						
35	2.977		-3.02	3.000	2.985	3.000						
40	2.999		-3.000	2.999	2.999	2.999						
45	2.945											
50	2.825											
55	2.653											
60	2.438											
65	2.188											
70	1.907											
75	1.602											
80	1.285											
85	.967											
90	.649											
95	.331											
100	.013											
Max. radius 0.246		1.19		1.19	0.44	0.90		1.19			0.44	
Maximum thickness of modification 1 and modification 2 (tip) in percent of true chord: 5.91												
Maximum camber of modification 1 and modification 2 (tip) in percent of true chord: 0.90												

¹Modification 1(b) consisted of the same section outboard of 0.4 b/2, the basic wing inboard.

²Sections of the wing other than those for which ordinates are given were the result of linear elements between corresponding tabulated chordwise stations. It should be noted that linear elements do not result in a linear variation of percent-chord ordinates. Note also that linear elements of modification 2 do not lie strictly along constant-percent-chord lines.

TABLE III.- INDEX TO DATA FIGURES

[W basic wing; WM_n wing with modification n; B body; V_Δ triangular vertical tail; V_Δ swept vertical tail; hH₁ horizontal tail at height $h = z/(b/2)$, and at incidence i , deg; η F fences at spanwise location η ; E chord extensions; η SF₈ split flaps of spanwise extent η , at deflection δ , deg; A simulated ailerons; \pm with and without; * also published in reference 1.]

Figure	Configuration	R $\times 10^{-6}$	β	Data
(a) Basic Wing				
8	W	4,8,10,14,16	0	C _L vs. α , C _m , C _D
9(a)	W	10	0,12	C _L vs. α , C _m , C _D
9(b)	W	10	0,3,6,12	C _L vs. C _l , C _y , C _n
10	W,W+B	10	0	C _L vs. α , C _m , C _D
11	W+B	4.5,8,10,14,20	0	C _L vs. α , C _m , C _D *
12(a)	W+B+V _Δ	10	0,12	C _L vs. α , C _m , C _D
12(b)	W+B+V _Δ	10	0,3,6,9,12	C _L vs. C _l , C _y , C _n
13	W+B+V _Δ +0.2H ₀ , -2, -8	10,8	0	C _L vs. α , C _m , C _D
14	W+B+V _Δ +0.12H ₀	10	0	C _L vs. α , C _m , C _D
15	W+B+V _Δ +0.21H ₀ , -2, -8	10,8	0	C _L vs. α , C _m , C _D
16	W+B+V _Δ +0.41H ₀ , -2, -8	10,8	0	C _L vs. α , C _m , C _D
17	W+B+V _Δ +0, 0.12, 0.21, 0.41H ₀	10,8	0	C _L vs. C _m
18	W+B+V _Δ +0, 0.21, 0.41H	10,8	0	ϵ_{av} vs. α
19	W+B+V _Δ +0.7F \pm E	10	0	C _L vs. α , C _m , C _D
20	W+B+V _Δ +0.12H ₀ +0.7F \pm E	10,8	0	C _L vs. α , C _m , C _D
21	W+B+V _Δ +0.21H ₀ +0.7F \pm E	10,8	0	C _L vs. α , C _m , C _D
(b) Modifications 1 and 1(b)				
22	WM ₁ +B	4,8,10,14,20	0	C _L vs. α , C _m , C _D *
23	WM ₁ +B+V _Δ ; WM _{1(b)} +B+V _Δ	10	0	C _L vs. α , C _m , C _D *
24(a)	WM ₁ +B+V _Δ	10	0,12	C _L vs. α , C _m , C _D
24(b)	WM ₁ +B+V _Δ	10	0,3,6,9,12	C _L vs. C _l , C _y , C _n
25	WM ₁ +B+V _Δ +0.2H ₀ , -2, -8	10,8	0	C _L vs. α , C _m , C _D
26	WM ₁ +B+V _Δ +0.21H ₀ , -2, -8	10,8	0	C _L vs. α , C _m , C _D
27	WM ₁ +B+V _Δ +0.41H ₀ , -2, -8	10,8	0	C _L vs. α , C _m , C _D
28	WM ₁ +B+V _Δ +0, 0.21, 0.41H ₀	10,8	0	C _L vs. C _m
29	WM ₁ +B+V _Δ +0, 0.21, 0.41H	10,8	0	ϵ_{av} vs. α
30	WM ₁ +B+V _Δ +0.55SF ₄₀	10	0	C _L vs. α , C _m , C _D *
31	WM ₁ +B+V _Δ +0.75F	10	0	C _L vs. α , C _m , C _D

TABLE III.- INDEX TO DATA FIGURES - Concluded

Figure	Configuration	$R \times 10^{-6}$	β	Data
(c) Modification 2				
32	WM_2+B	4,6,8,10,14,20	0	C_L vs. α , C_m , C_D
33(a)	WM_2+B	10	0,12	C_L vs. α , C_m , C_D
33(b)	WM_2+B	10	0,3,6,9,12	C_L vs. C_l , C_Y , C_n
34(a)	$WM_2+B+V_{\Delta} \pm 0.6F$	10	0,12	C_L vs. α , C_m , C_D
34(b)	$WM_2+B+V_{\Delta} \pm 0.6F$	10	0,3,6,9,12	C_L vs. C_l , C_Y , C_n
35(a)	$WM_2+B+V_{\Delta} \pm 0.21H_0$	10,8	0,12	C_L vs. α , C_m , C_D
35(b)	$WM_2+B+V_{\Delta} \pm 0.21H_0$	10,8	0,3,6,9,12	C_L vs. C_l , C_Y , C_n
36	$WM_2+B \pm 0.55SF_{17,37,57}$	10	0	C_L vs. α , C_m , C_D
37	$WM_2+B \pm 0.75SF_{17,37,57}$	10	0	C_L vs. α , C_m , C_D
(d) Modification 3				
38	WM_3+B	10	0	C_L vs. α , C_m , C_D
39(a)	$WM_3+B+V_{\Delta} \pm 0.6F$	10	0,6	C_L vs. α , C_m , C_D
39(b)	$WM_3+B+V_{\Delta} \pm 0.6F$	10	0,3,6,9	C_L vs. C_l , C_Y , C_n
40	$WM_3+B+V_{\Delta} \pm 0.21H_0$; $WM_3+B+V_{\Delta} \pm 0.41H_0 \pm 0.6F$	10,8	0	C_L vs. α , C_m , C_D
(e) Modification 4				
41	WM_4+B	4,6,8,10,14,20	0	C_L vs. α , C_m , C_D
42(a)	WM_4+B+V_{Δ}	10	0,12	C_L vs. α , C_m , C_D
42(b)	WM_4+B+V_{Δ}	10	0,3,6,9,12	C_L vs. C_l , C_Y , C_n
43	$WM_4+B+V_{\Delta} \pm 0.2H_0, -2, -6, -10$	10,8	0	C_L vs. α , C_m , C_D
44	$WM_4+B+V_{\Delta} \pm 0.21, 0.41H_0$	10,8	0	C_L vs. α , C_m , C_D
45	$WM_4+B+V_{\Delta} \pm 0.55SF_{17,37,57}$	10	0	C_L vs. α , C_m , C_D
46	$WM_4+B+V_{\Delta} \pm 0.75SF_{17,37,57}$	10	0	C_L vs. α , C_m , C_D
47(a)	$WM_4+B+V_{\Delta} \pm 0.55SF_{37}$	10	0,12	C_L vs. α , C_m , C_D
47(b)	$WM_4+B+V_{\Delta} \pm 0.55SF_{37}$	10	0,3,6,9,12	C_L vs. C_l , C_Y , C_n
48	$WM_4+B+V_{\Delta} \pm 0.2H_0, -2, -6, -10$	10,8	0	C_L vs. α , C_m , C_D
49	$WM_4+B+V_{\Delta} \pm 0.55SF_{37}$	10,8	0	e_{av} vs. α
50	$WM_4+B+V_{\Delta} \pm A$	10	(1)	$C_L, C_m, C_D, C_l, C_Y, C_n$ vs. β
51	$WM_4+B+V_{\Delta} \pm 0.2H_0 \pm A$	10	(1)	$C_L, C_m, C_D, C_l, C_Y, C_n$ vs. β
52	$WM_4+B+V_{\Delta} \pm 0.6, 0.75F$	10	0	C_L vs. α , C_m , C_D
(f) Intercomparisons among the wings				
53	$(W, WM_{1,2,3,4})+B; WM_{1(b)}+B+V_{\Delta}$	10	0	C_L vs. α , C_m , C_D
54	$(W, WM_1)+B+V_{\Delta} \pm 0.2H_0; WM_4+B+V_{\Delta} \pm 0.2H_0$	10,8	0	C_L vs. α , C_m , C_D

¹ β varied at $\alpha = 0^\circ, 6^\circ$, and 12° .

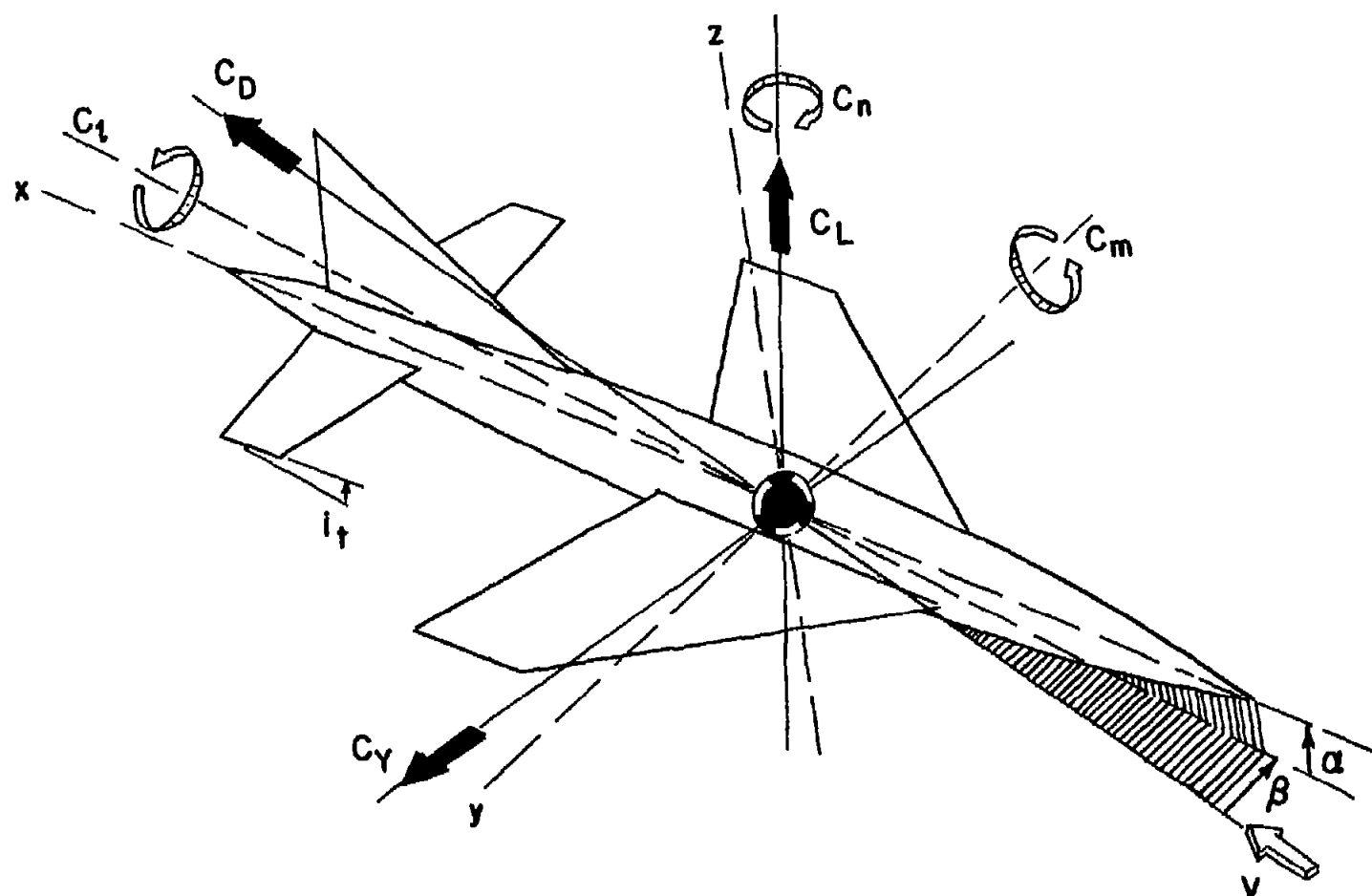


Figure 1.- Sign convention used in presentation of the data. All coefficients and angles are shown as positive.

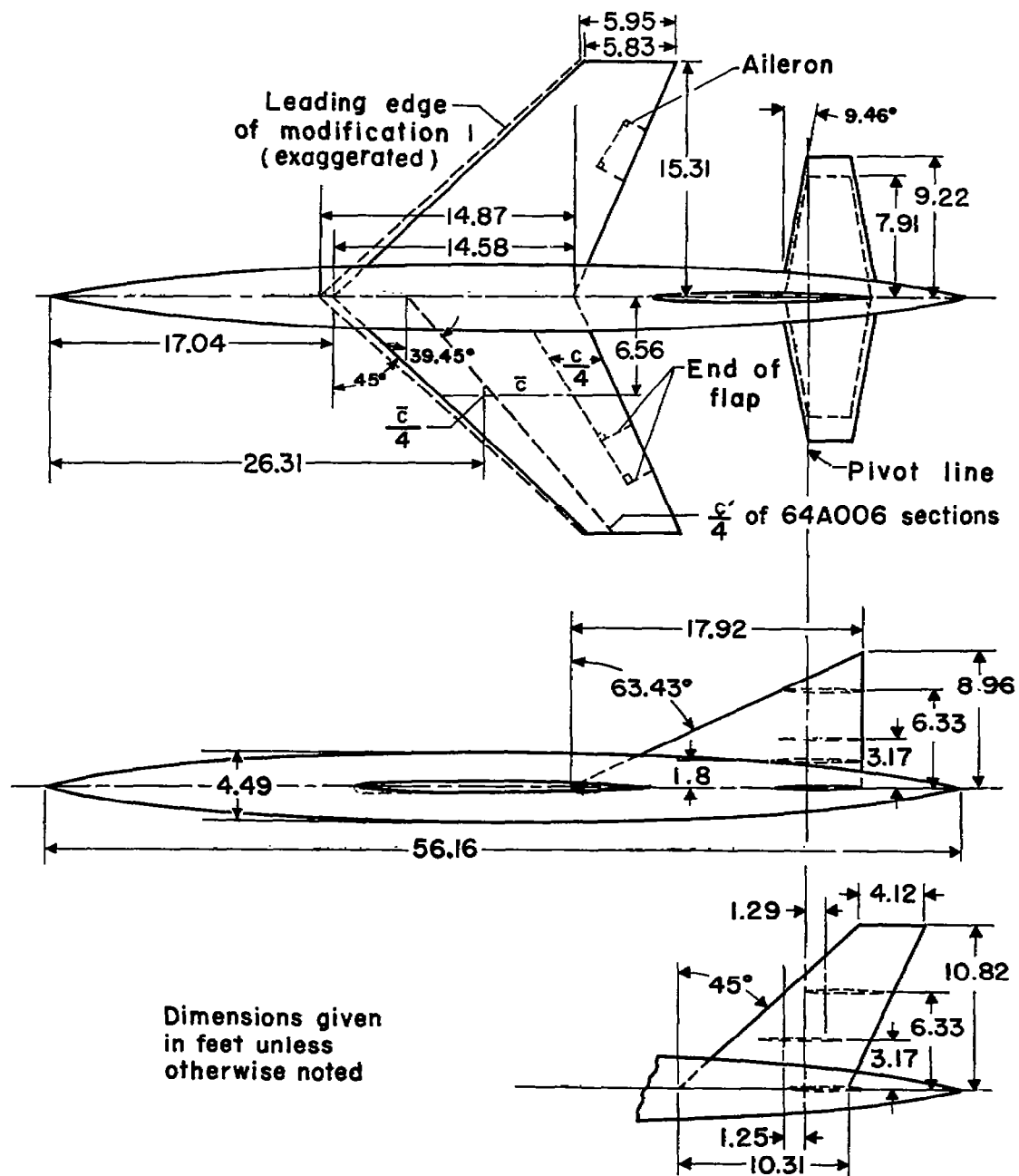
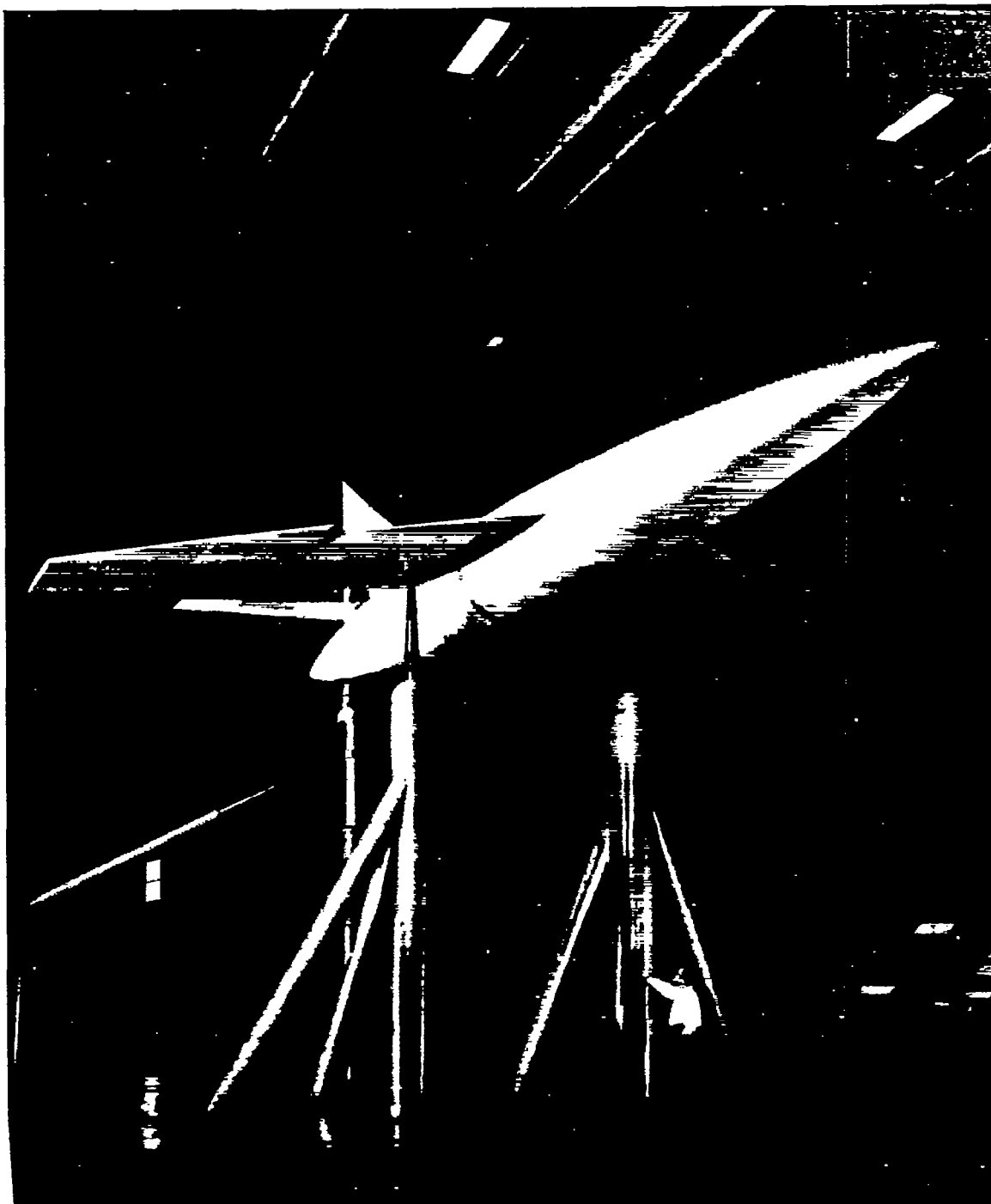


Figure 2.- Drawing of the model.



A-17818

Figure 3.- Typical installation of the model in the wind tunnel.

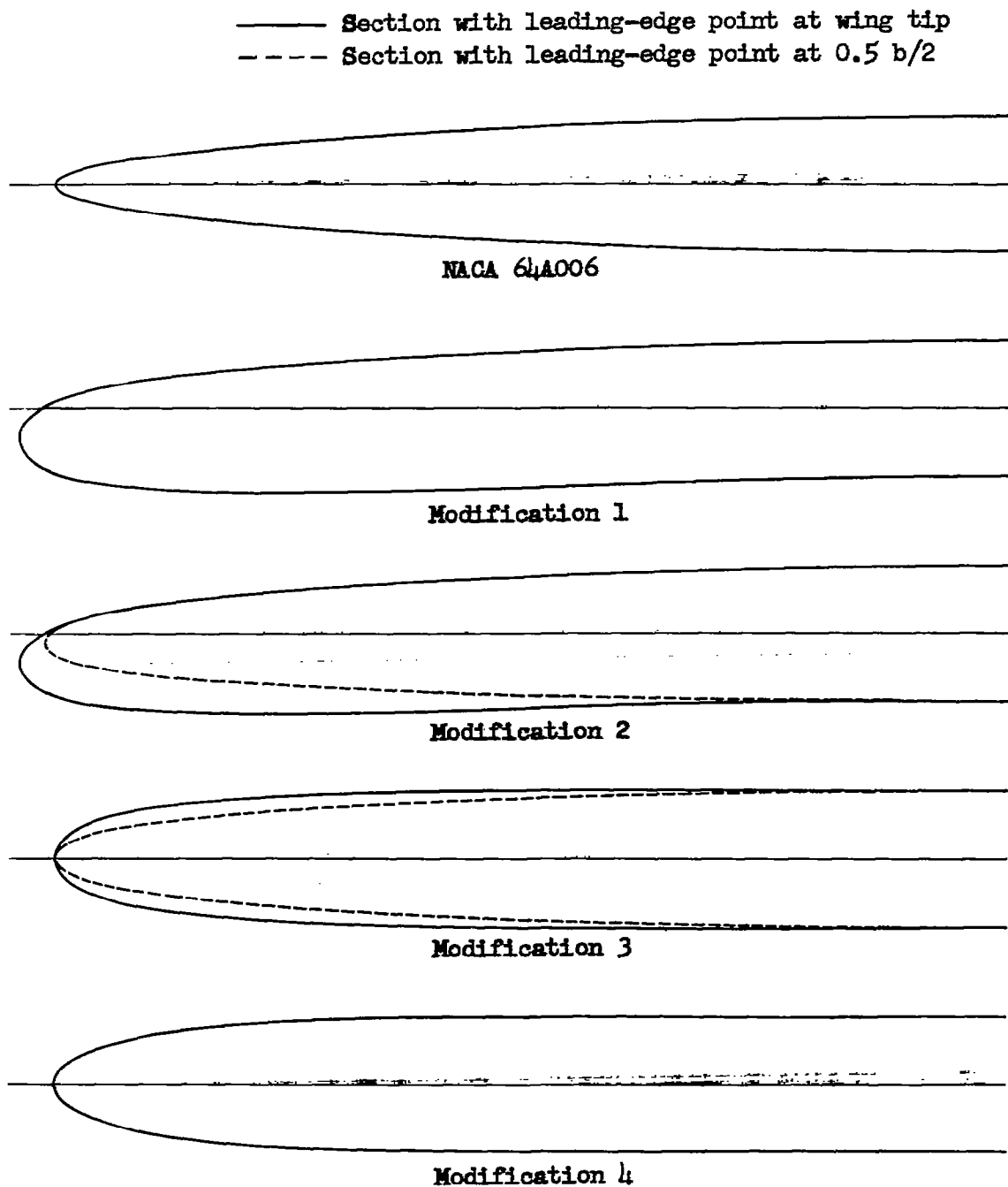


Figure 4.- Basic and modified wing sections normal to the 39.45° sweep line.

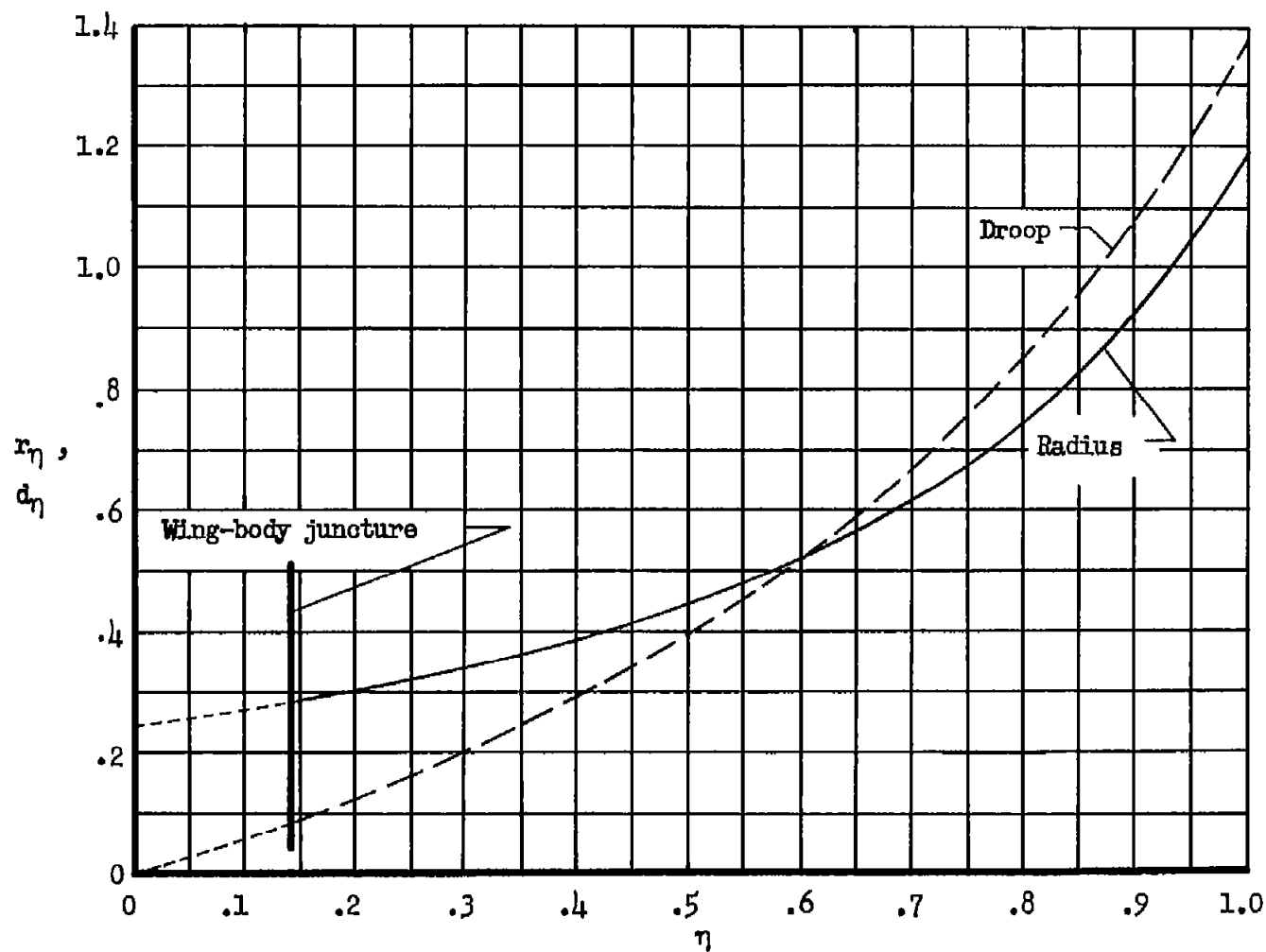


Figure 5.- Spanwise variation of leading-edge radius for modifications 2 and 3, and spanwise variation of leading-edge droop for modification 2.

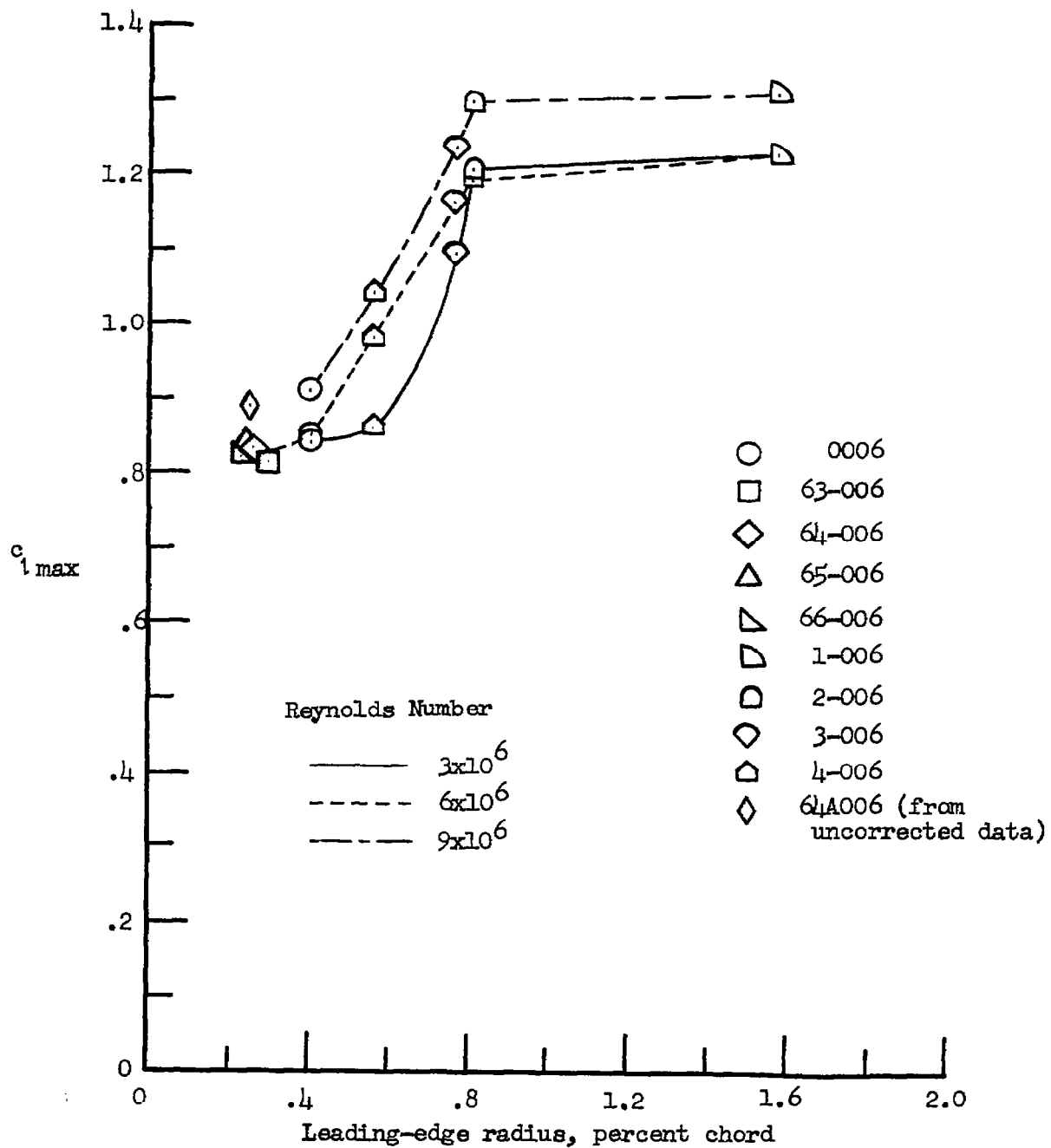


Figure 6.- Effect of leading-edge radius on maximum lift at low speeds of symmetrical 6-percent-thick airfoil sections.

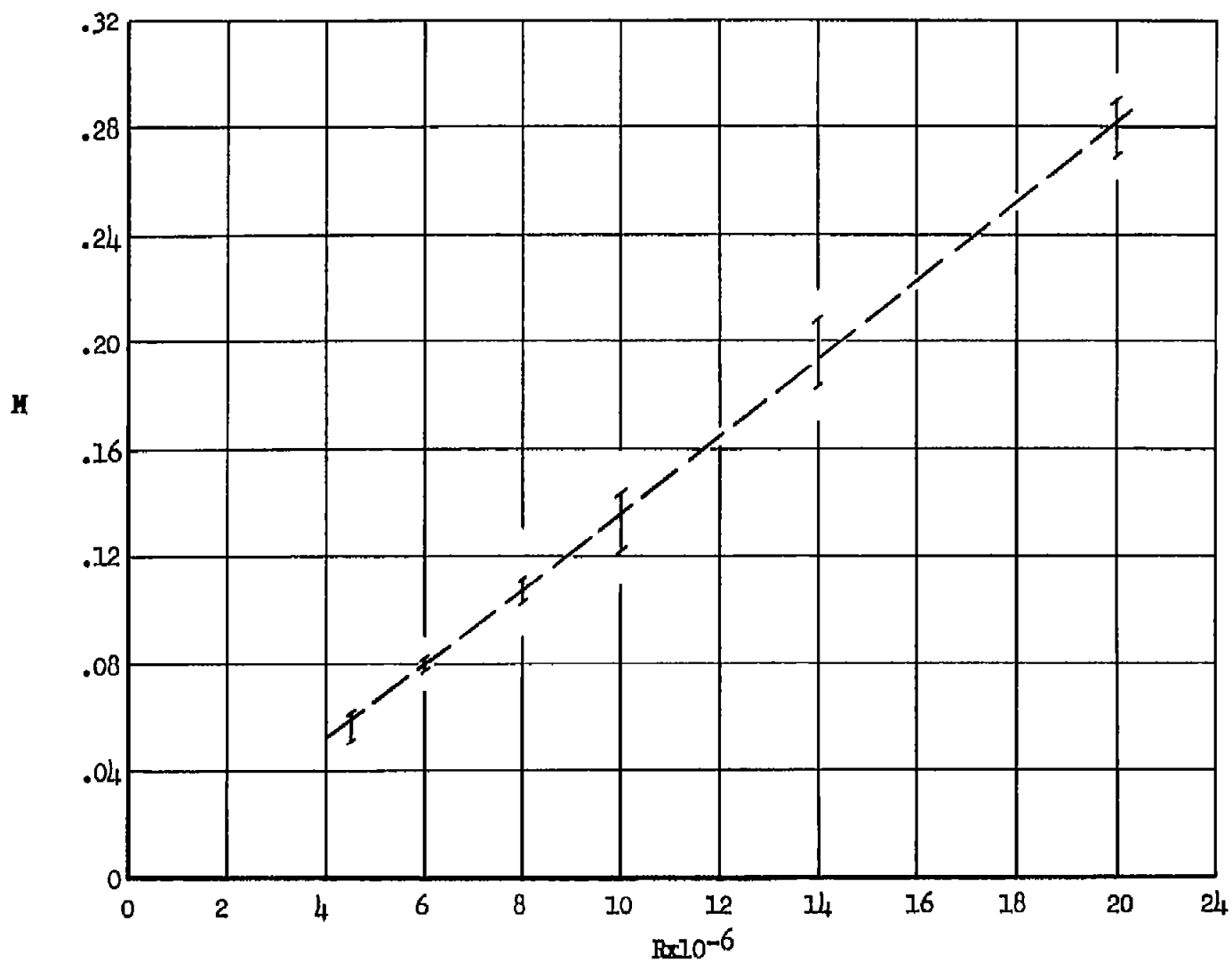
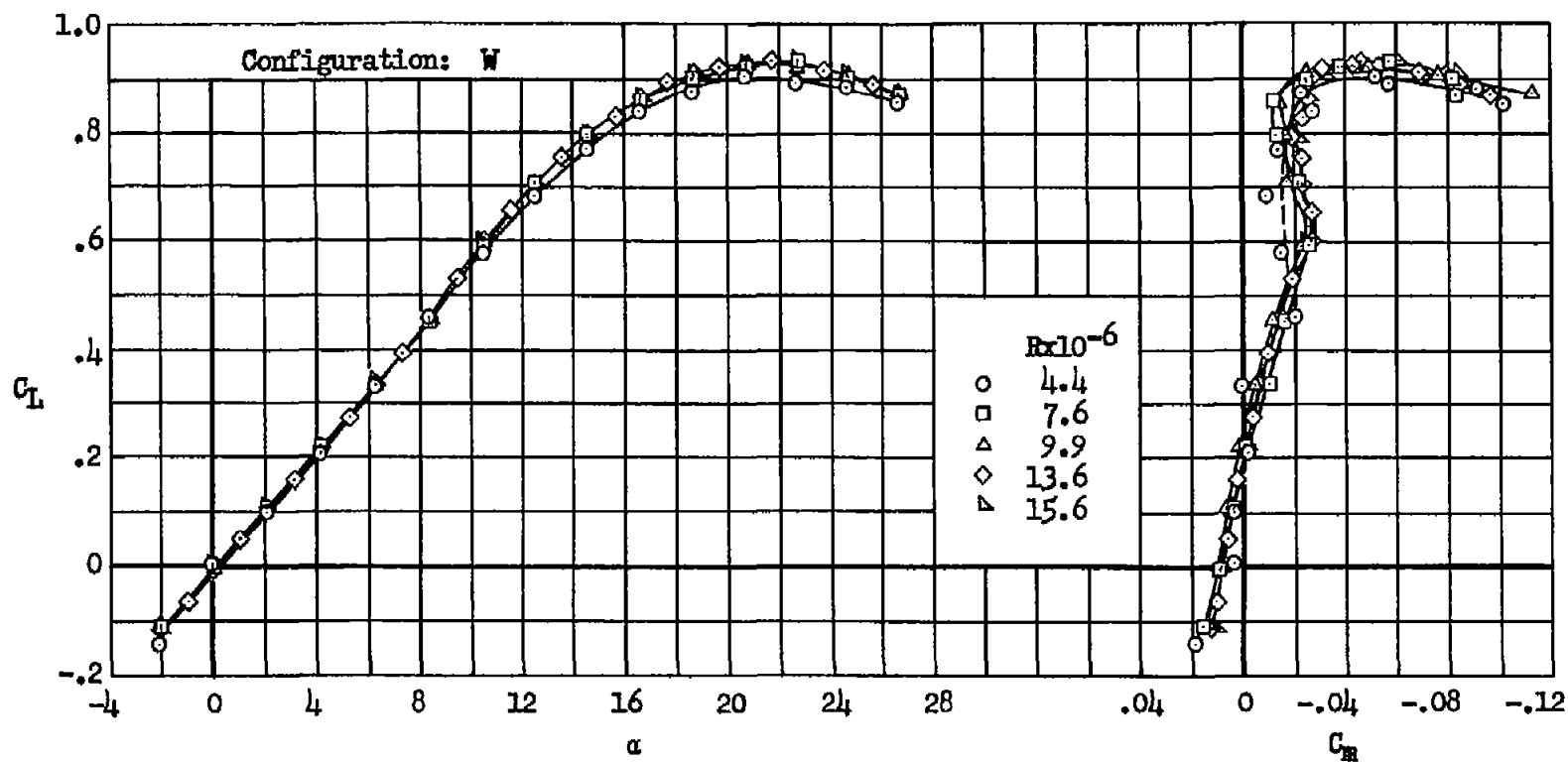
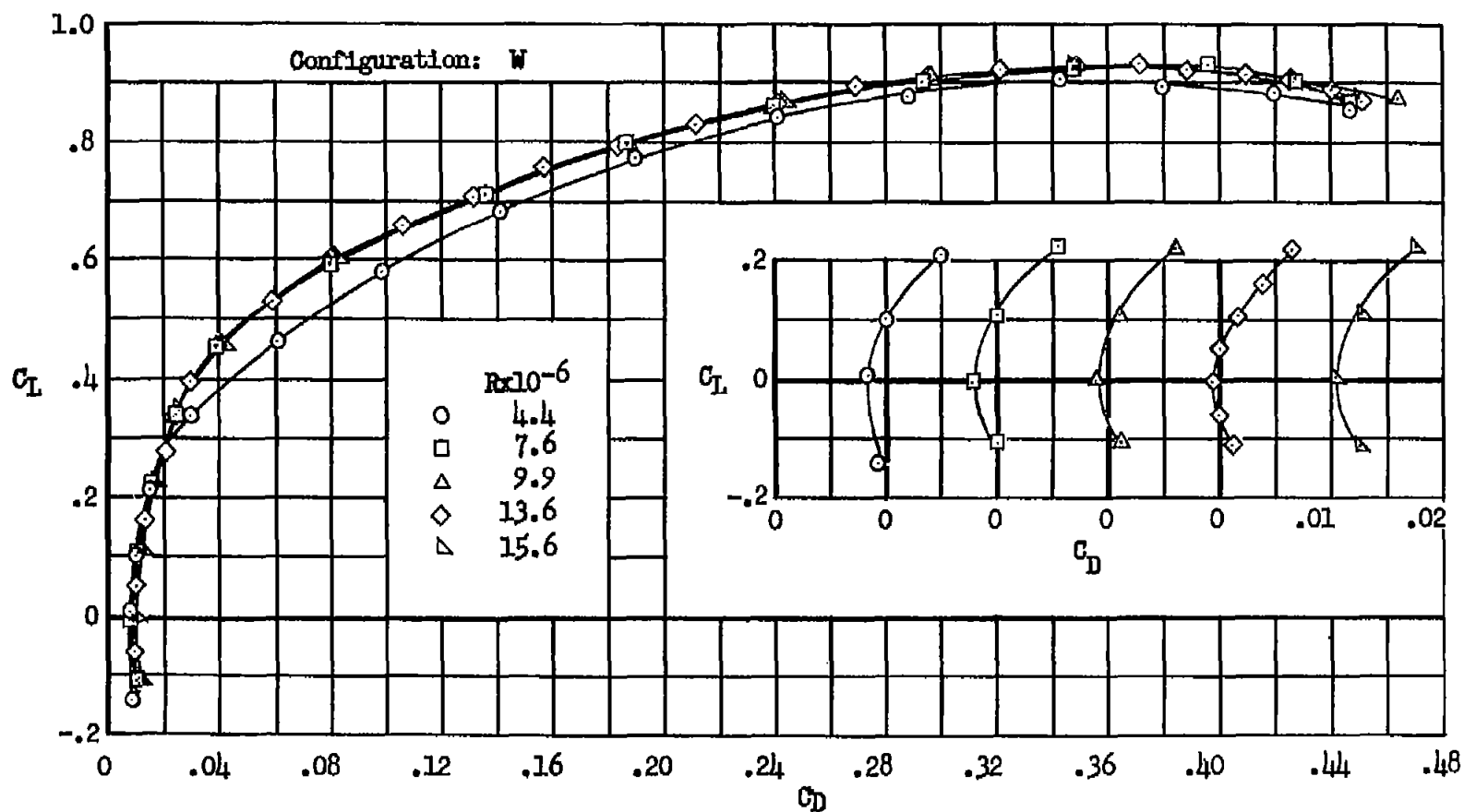


Figure 7.- Variation of Mach number with Reynolds number. Range of Mach number for each test Reynolds number is indicated.



(a) C_L vs. α , C_m

Figure 8.- Basic wing; longitudinal characteristics of the wing alone at several Reynolds numbers.



(Note: Absolute values of minimum drag have not been corrected for the presence of tubing from pressure orifices, which was run down the tail strut and was partly exposed to the air stream.)

(b) C_L vs. C_D

Figure 8.- Concluded.

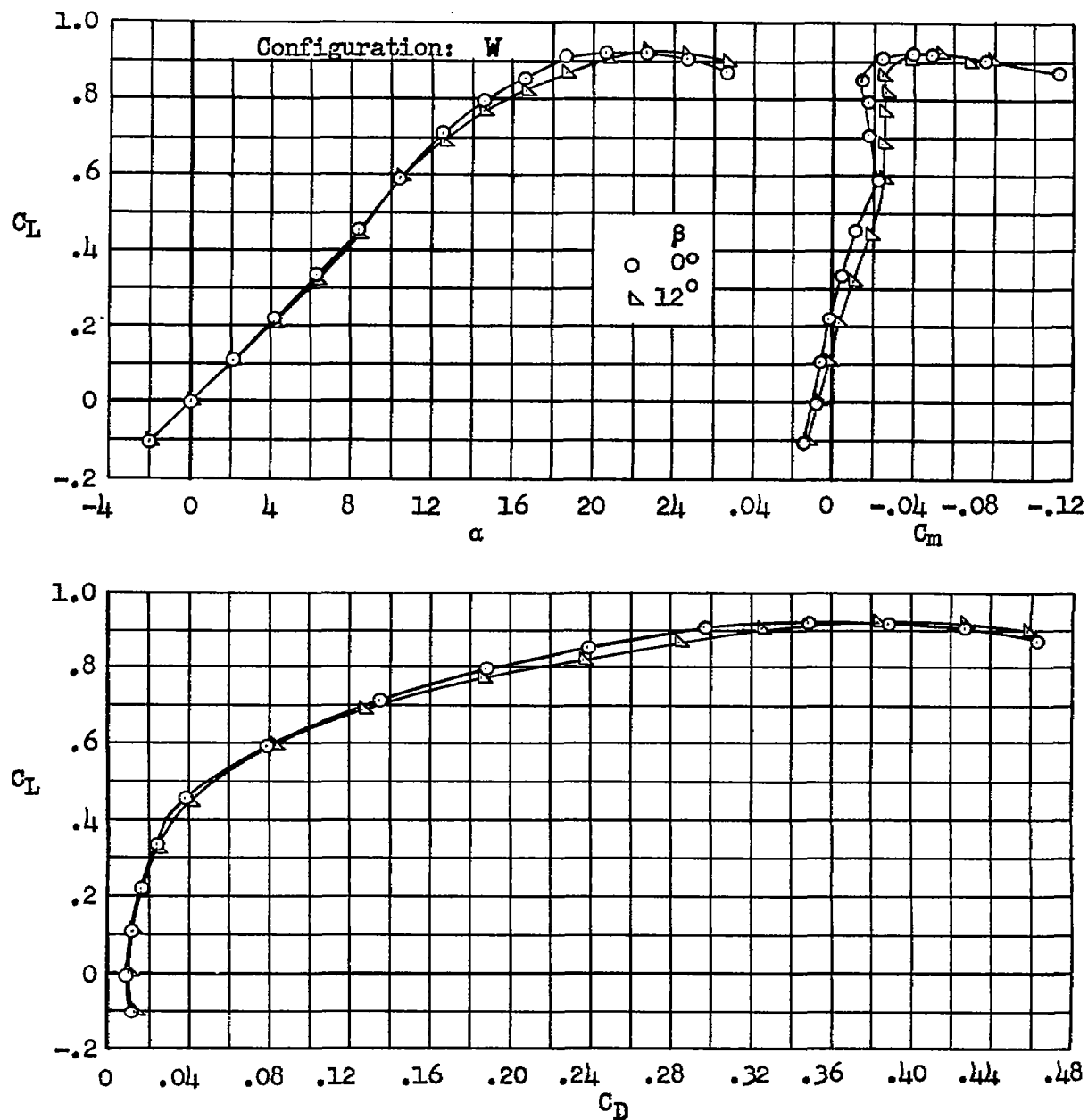
(a) C_L vs. α , C_m , C_D

Figure 9.- Basic wing; characteristics of the wing alone in sideslip, Reynolds number 10×10^6 .

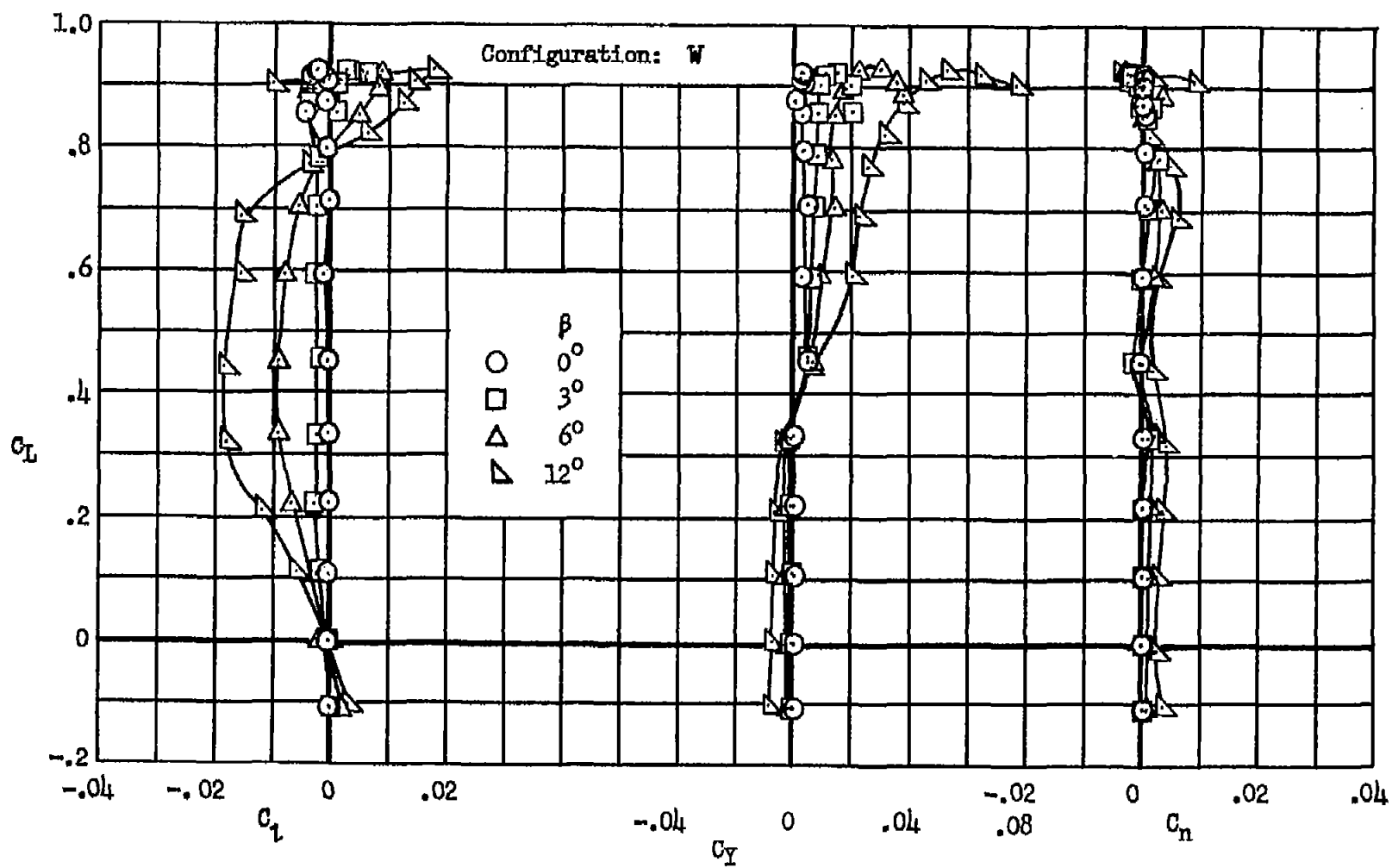
(b) C_L vs. C_D , C_Y , C_N

Figure 9.- Concluded.

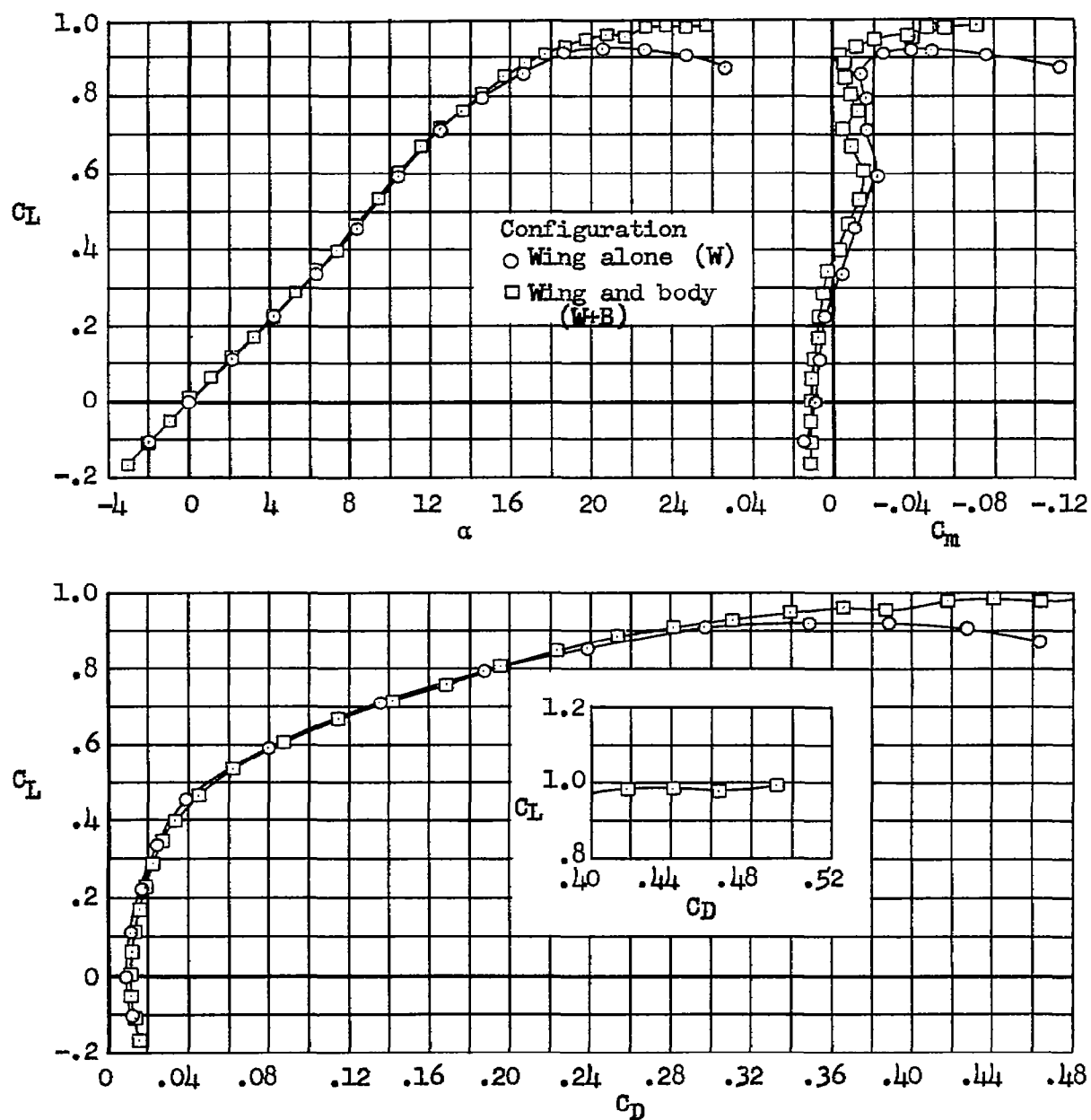


Figure 10.- Basic wing; comparison of the longitudinal characteristics of the wing alone and in combination with the body, Reynolds number 10×10^6 .

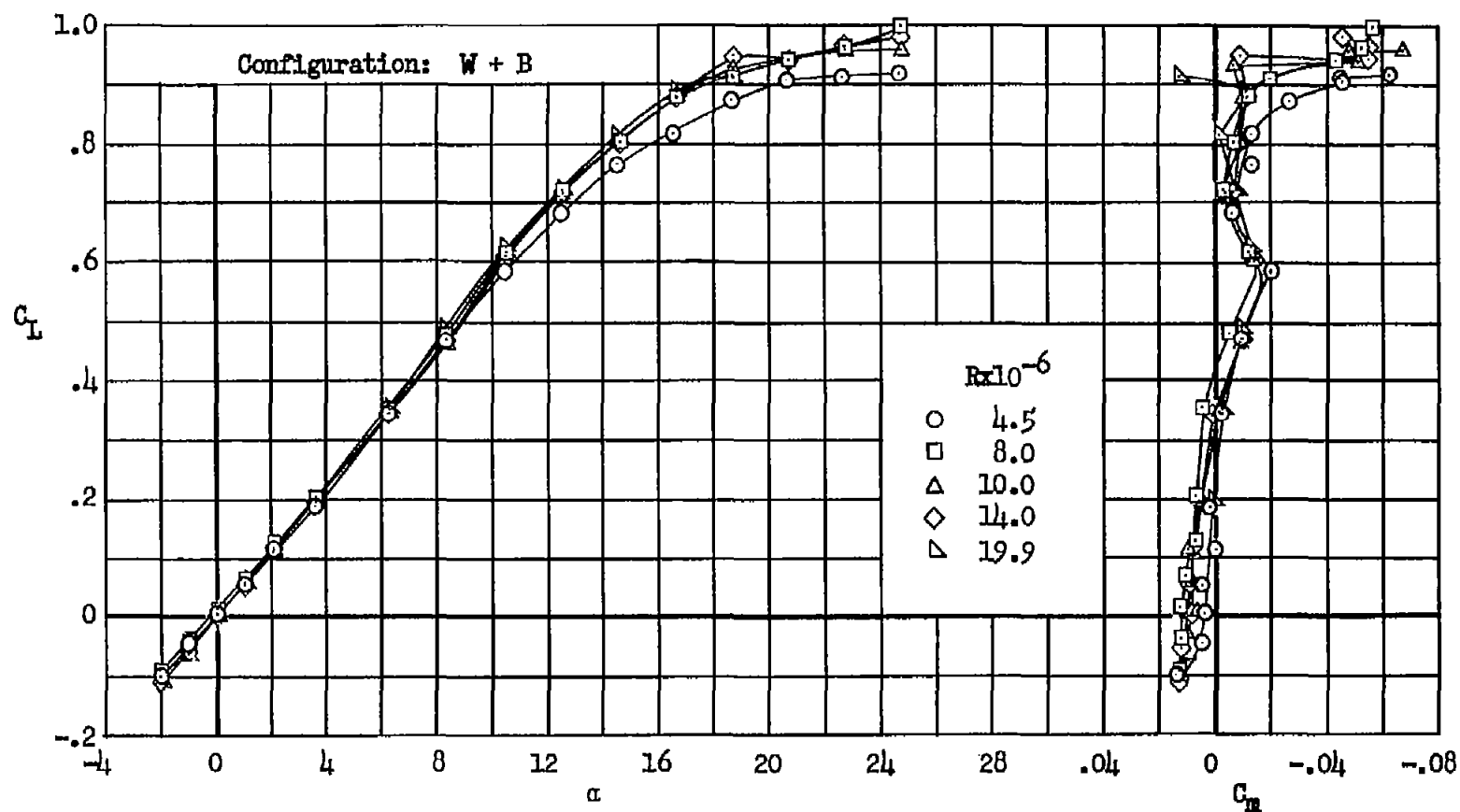
(a) C_L vs. α , C_m

Figure 11.- Basic wing; longitudinal characteristics of the wing and body at several Reynolds numbers.

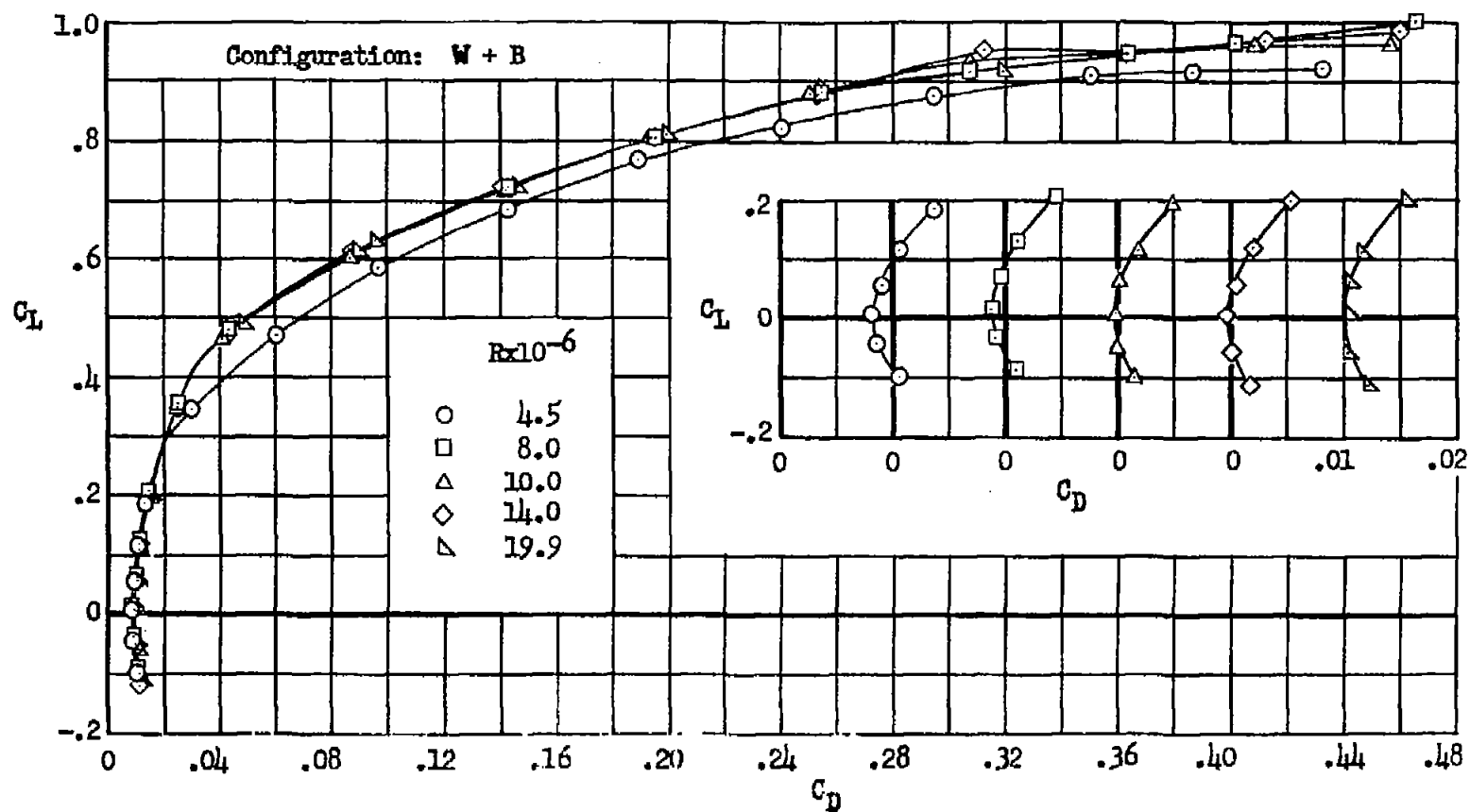
(b) C_L vs. C_D

Figure 11.- Concluded.

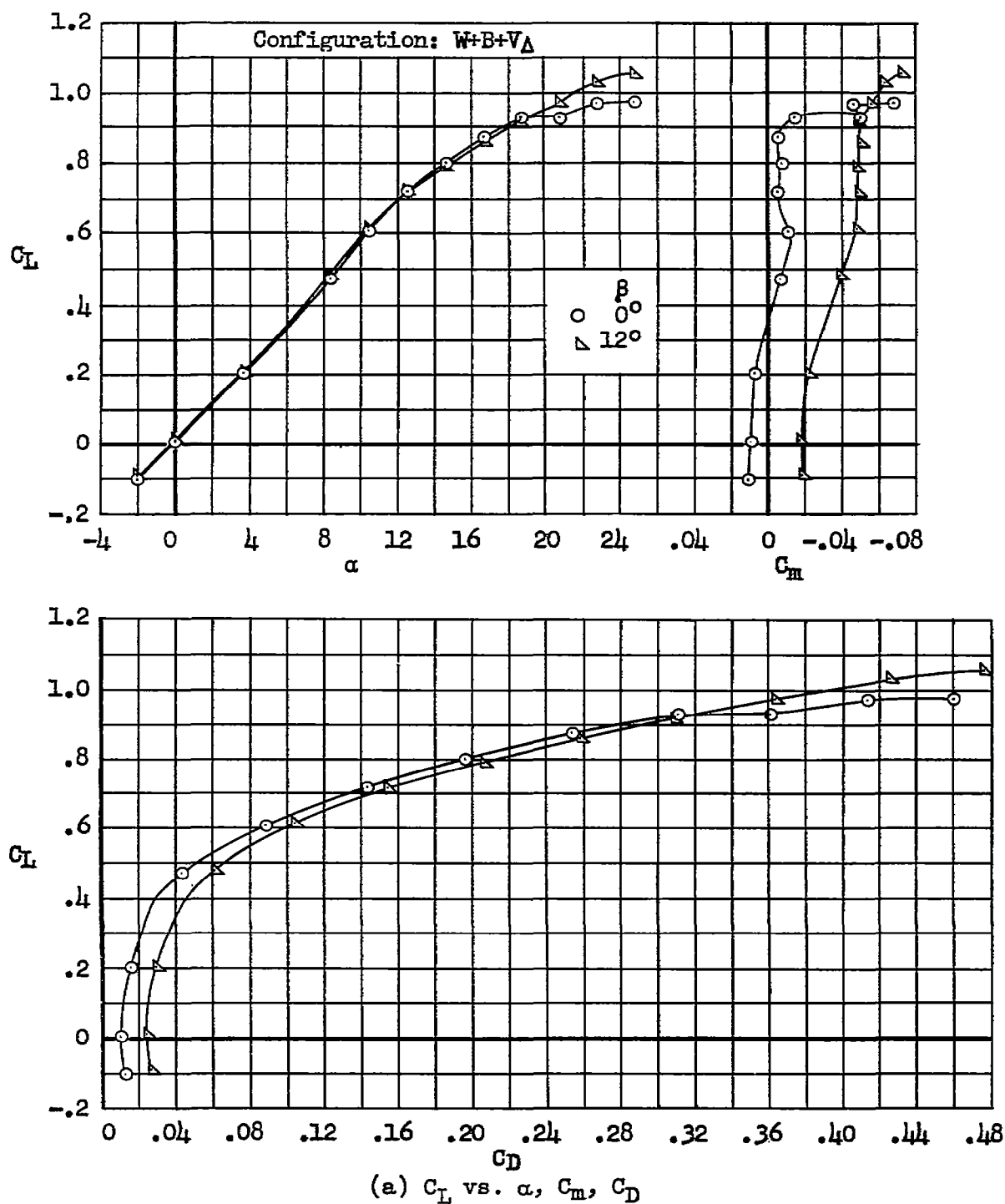
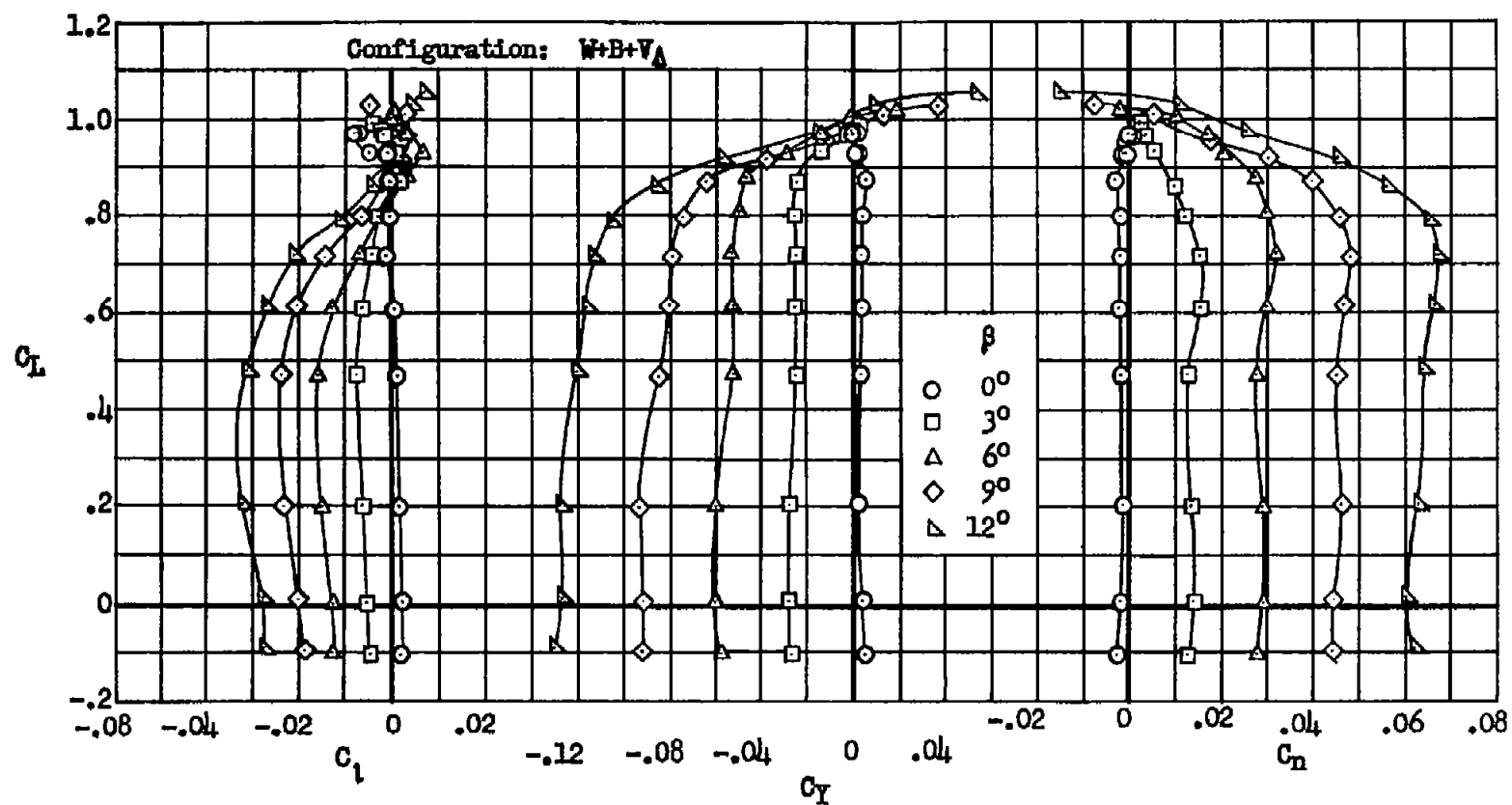
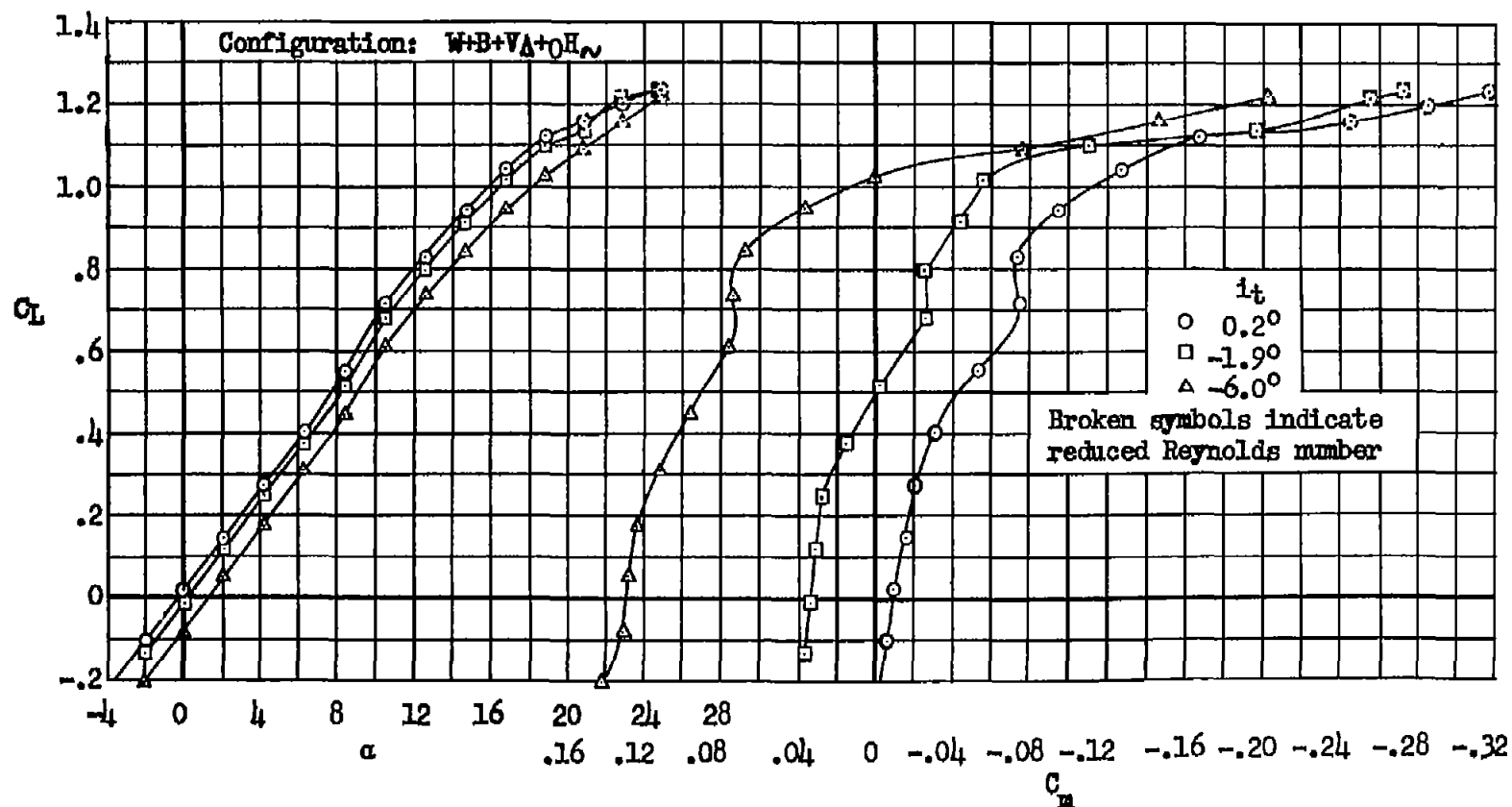


Figure 12.- Basic wing; characteristics in sideslip of the model with the triangular vertical tail, without the horizontal tail; Reynolds number 10×10^6 .



(b) C_L vs. C_D , C_Y , C_N

Figure 12.- Concluded.



(a) C_L vs. α , C_m

Figure 13.- Basic wing; longitudinal characteristics of the model with the horizontal tail in the wing chord plane, moment center at 0.34 \bar{c} , Reynolds numbers 10 and 8×10^6 .

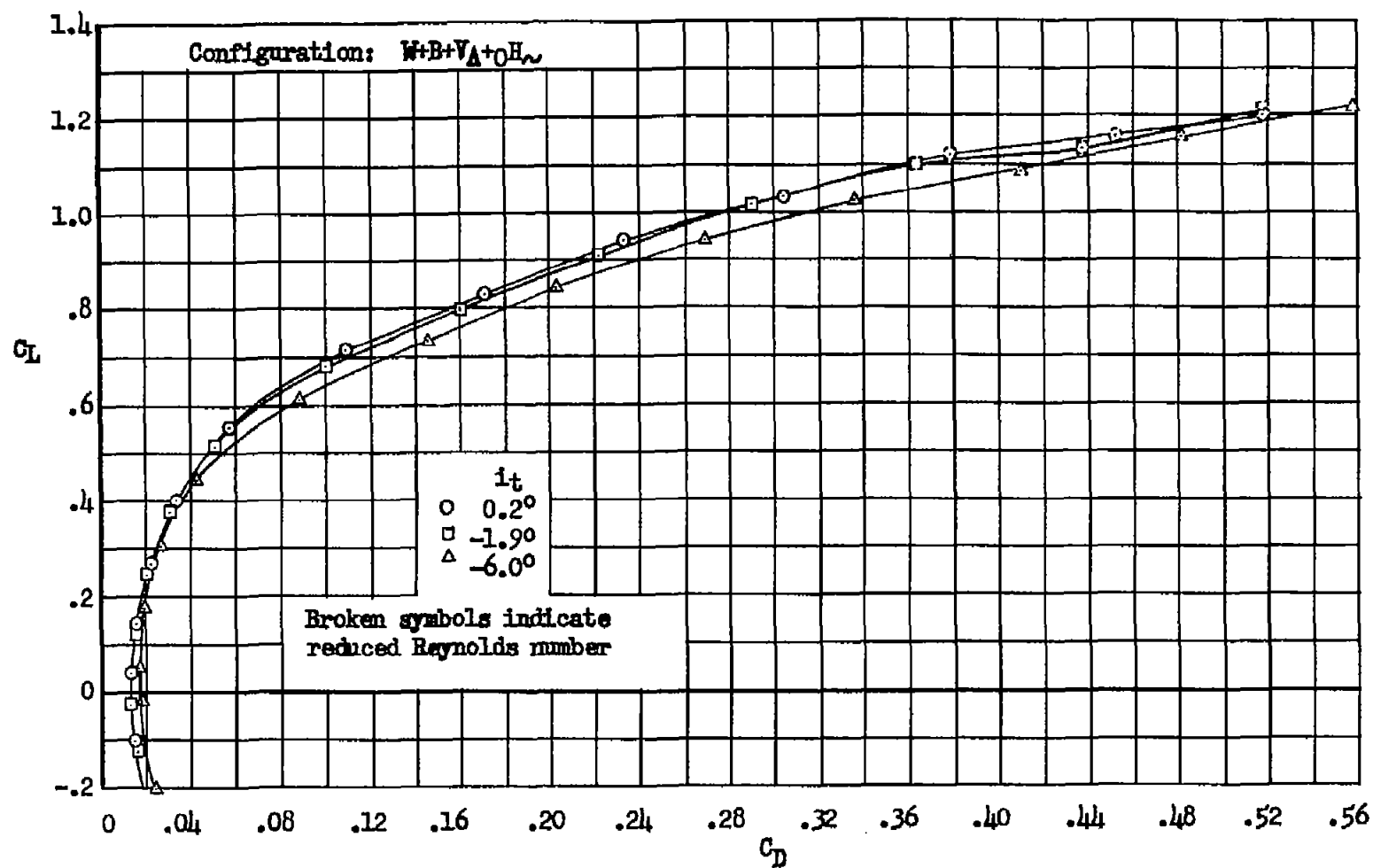
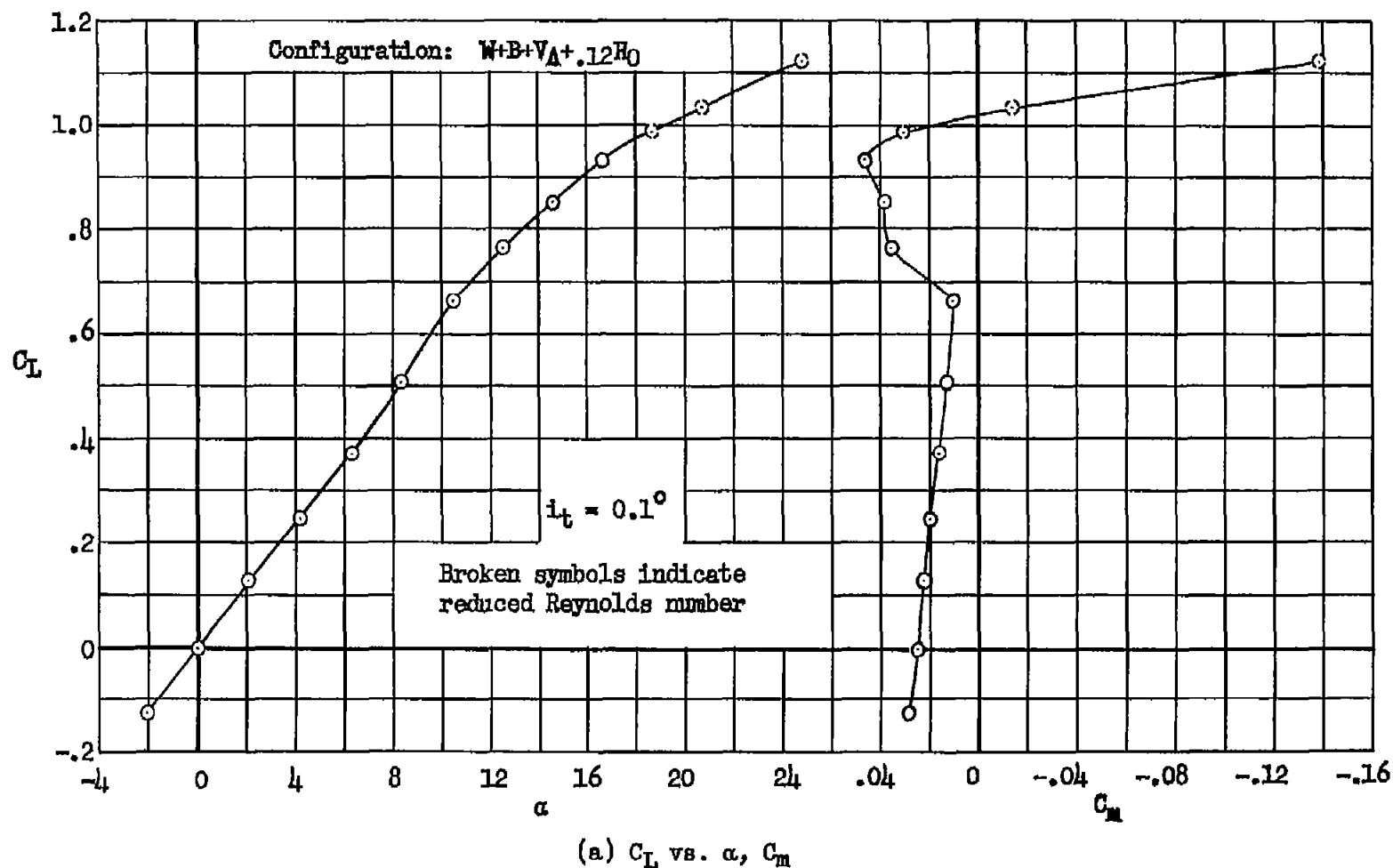
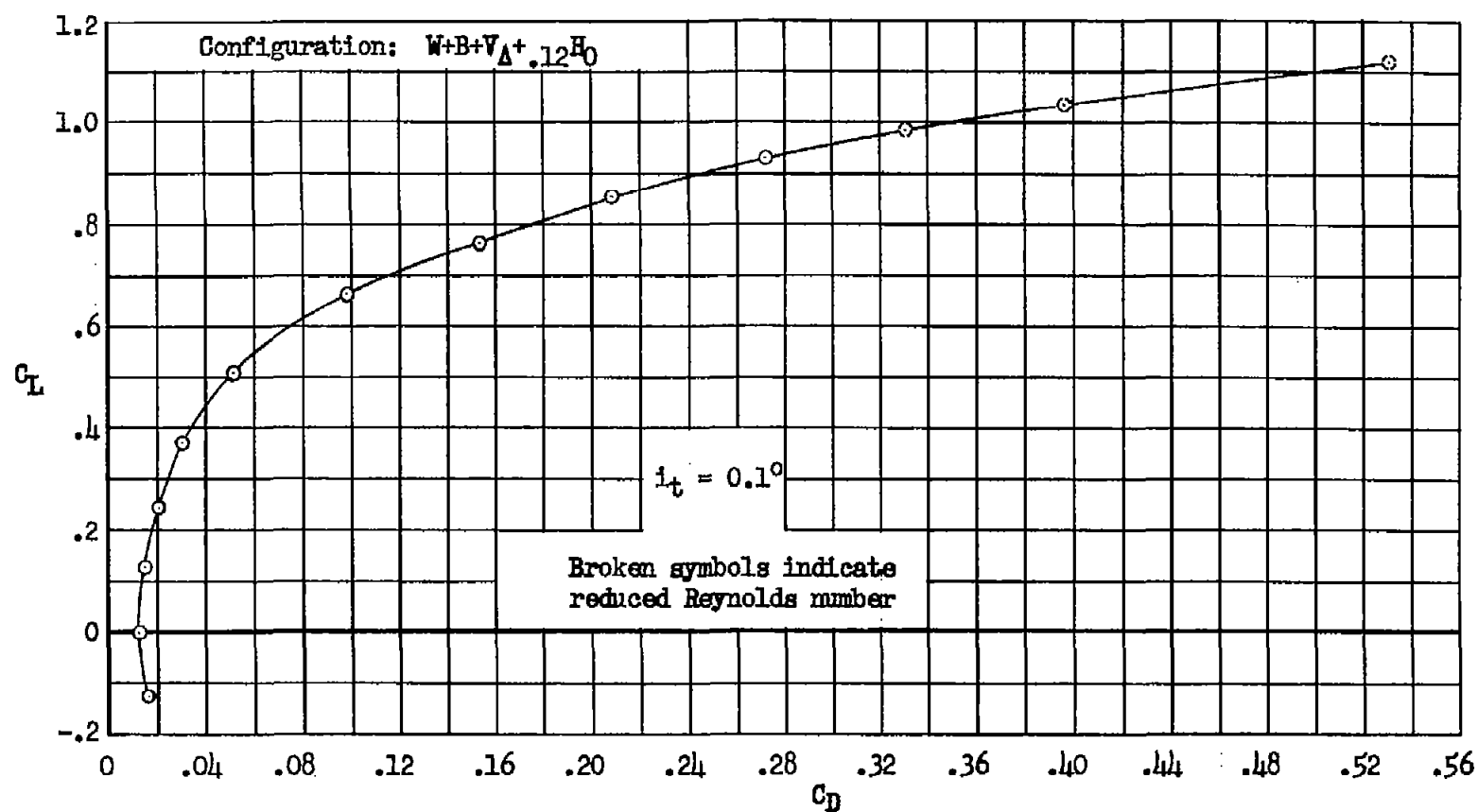
(b) C_L vs. C_D

Figure 13.- Concluded.





(b) C_L vs. C_D

Figure 14.- Concluded.

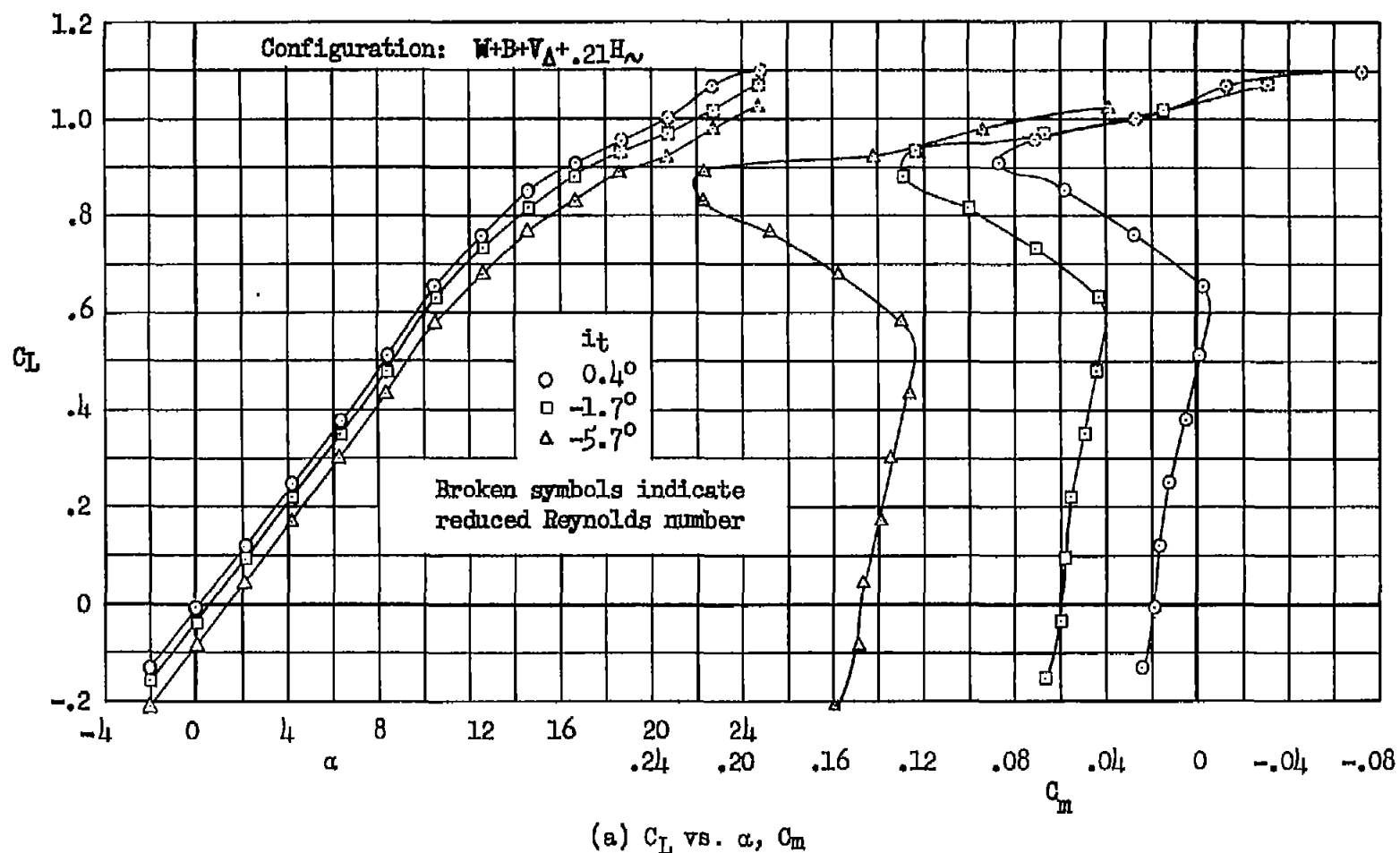


Figure 15.- Basic wing; longitudinal characteristics of the model with the tail mounted on the triangular vertical tail at $z/(b/2) = 0.21$, moment center at $0.35\bar{c}$, Reynolds numbers 10 and 8×10^6 .

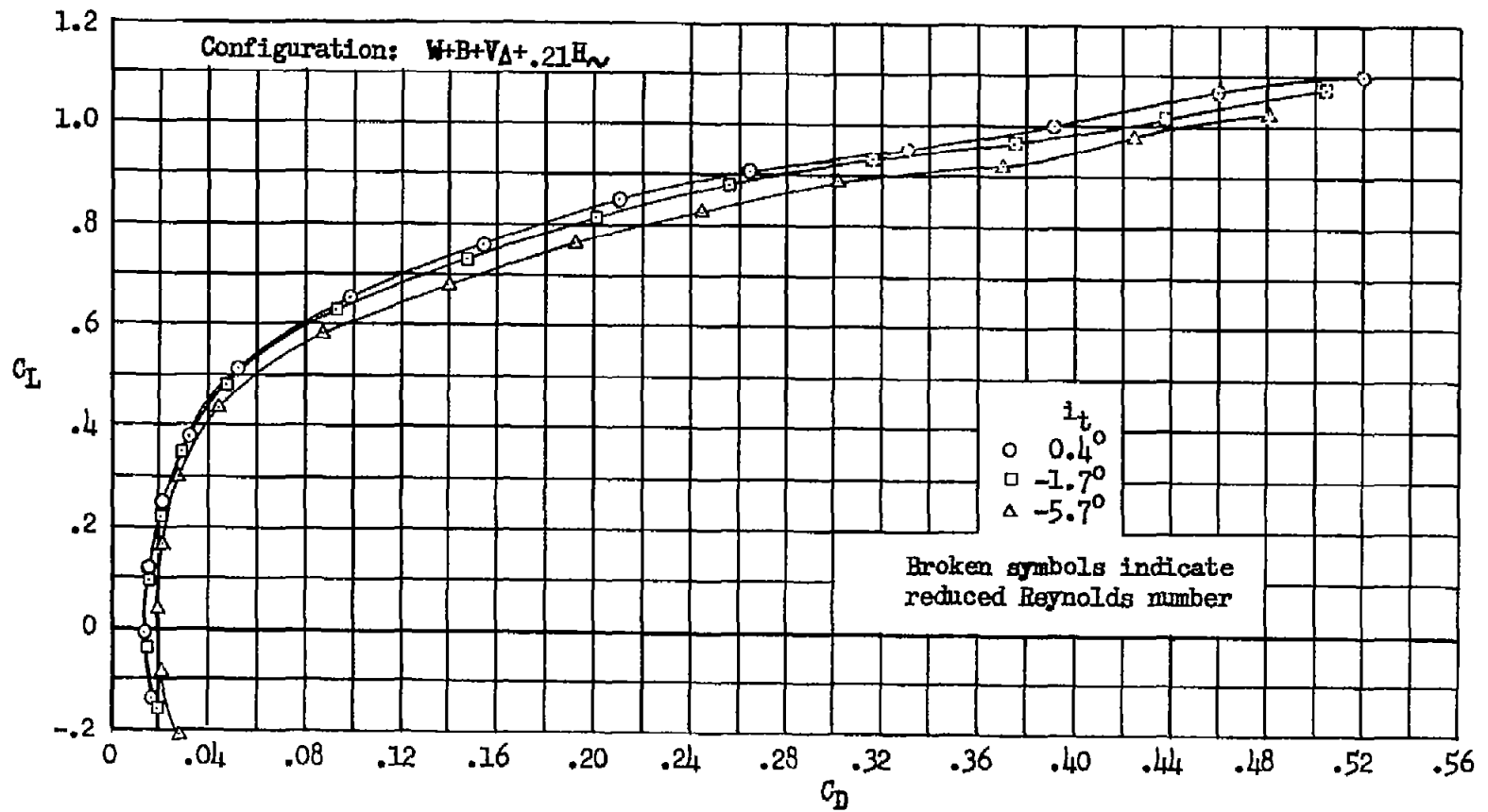
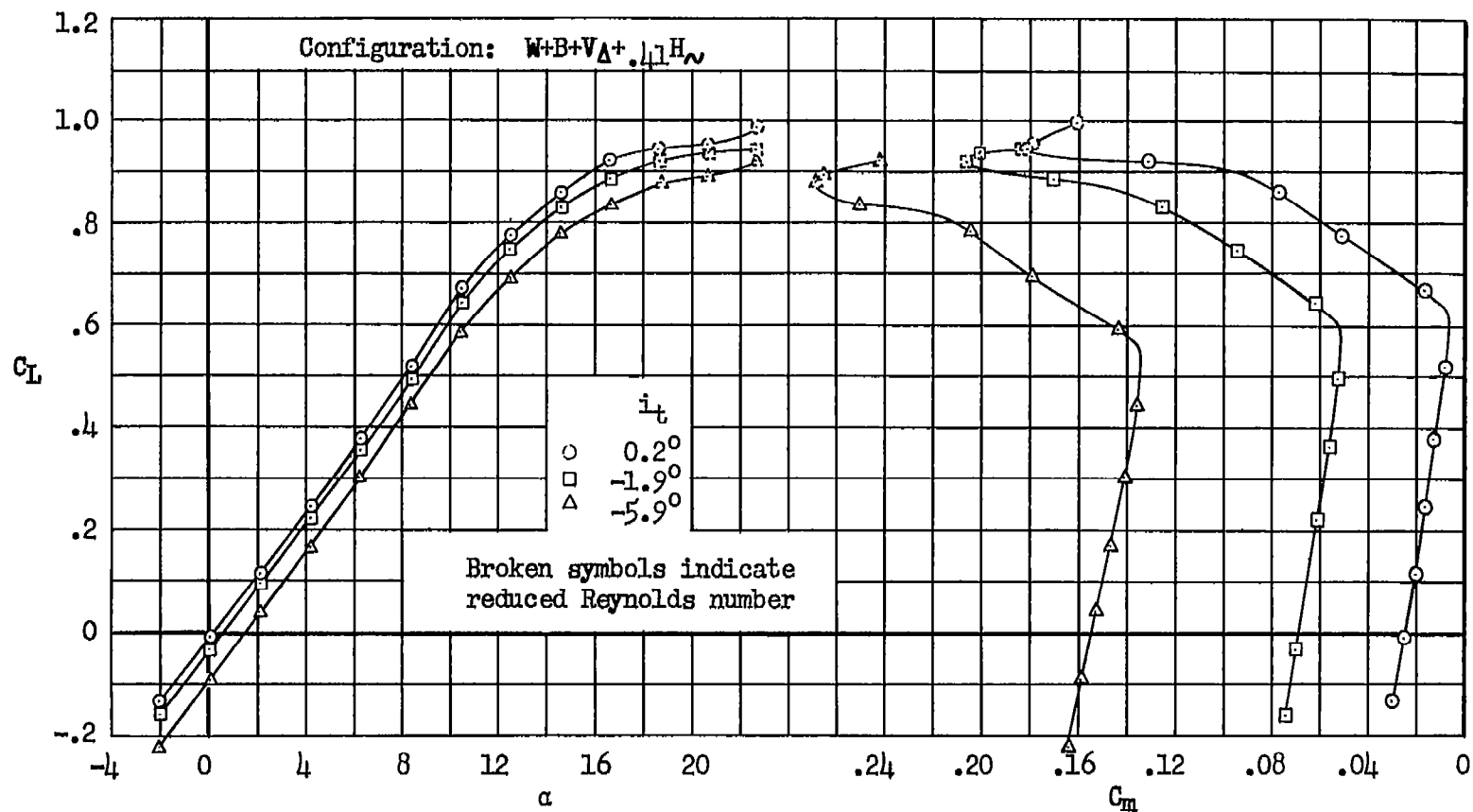
(b) C_L vs. C_D

Figure 15.- Concluded.



(a) C_L vs. α , C_m

Figure 16.- Basic wing; longitudinal characteristics of the model with the tail mounted on the triangular vertical tail at $z/(b/2) = 0.41$, moment center at 0.40 \bar{c} , Reynolds numbers 10 and 8×10^6 .

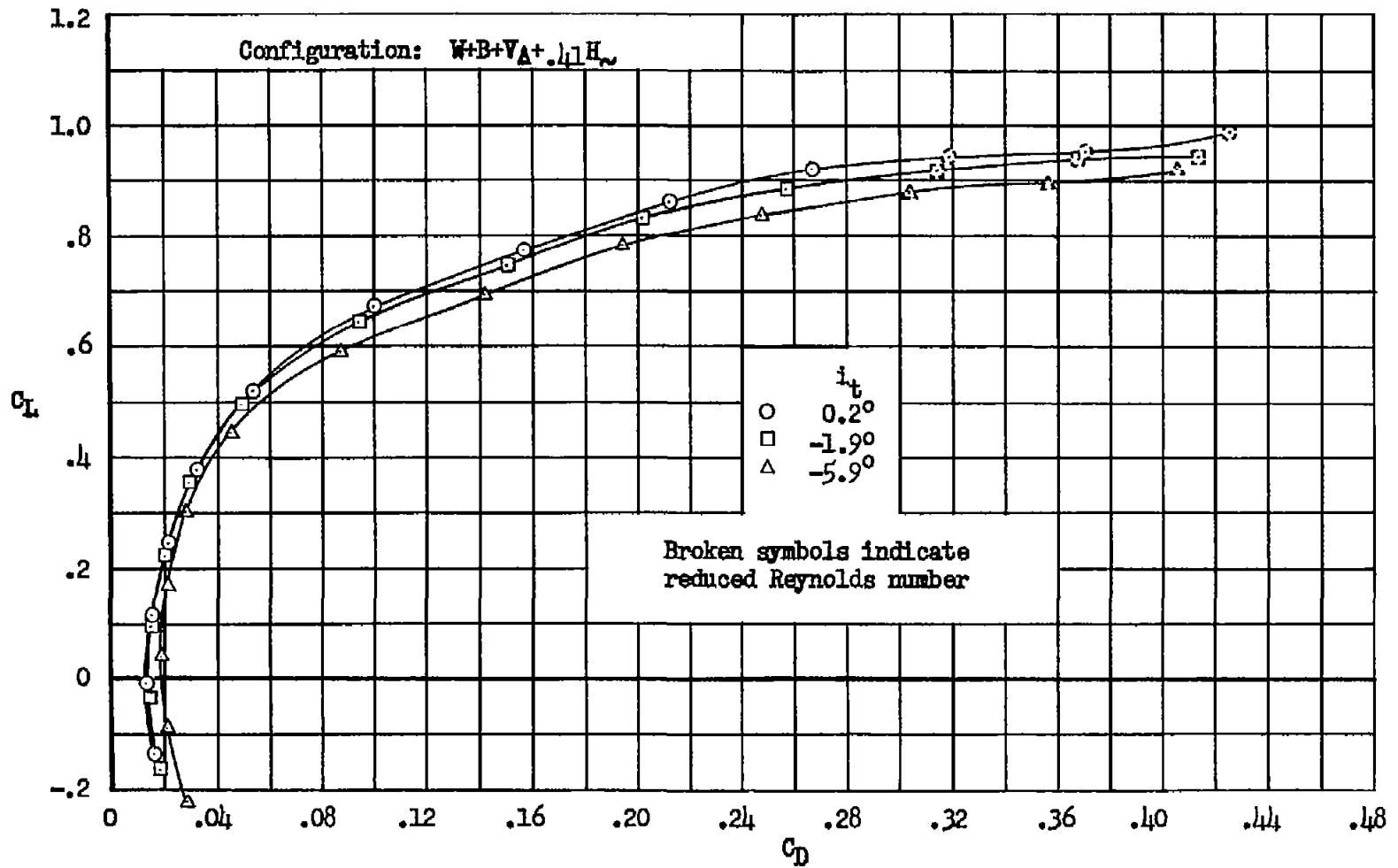
(b) C_L vs. C_D

Figure 16.- Concluded.

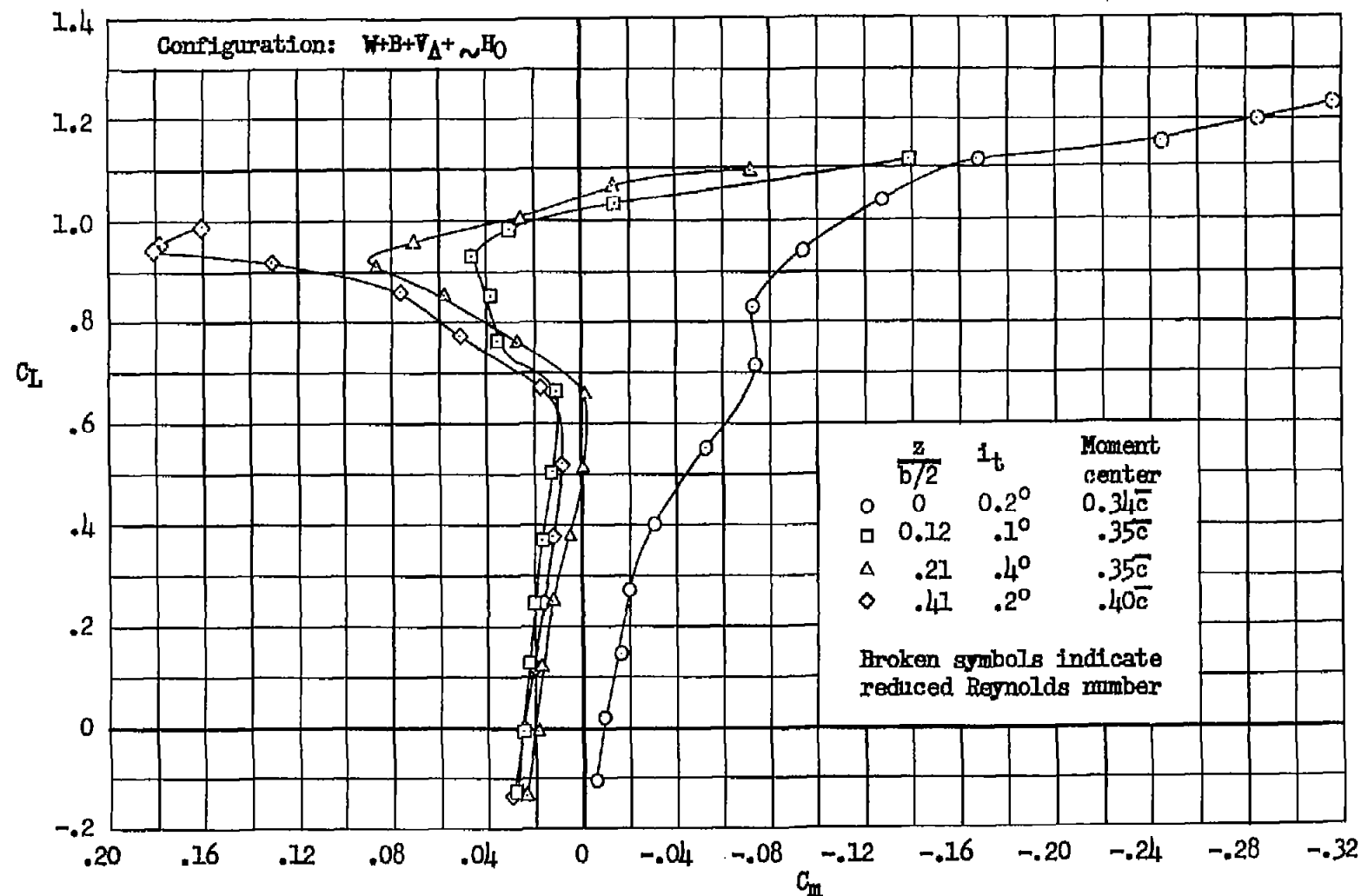


Figure 17.- Basic wing; effect of the position of the horizontal tail, in conjunction with the triangular vertical tail, on the pitching moment of the model; Reynolds numbers 10 and 8×10^6 .

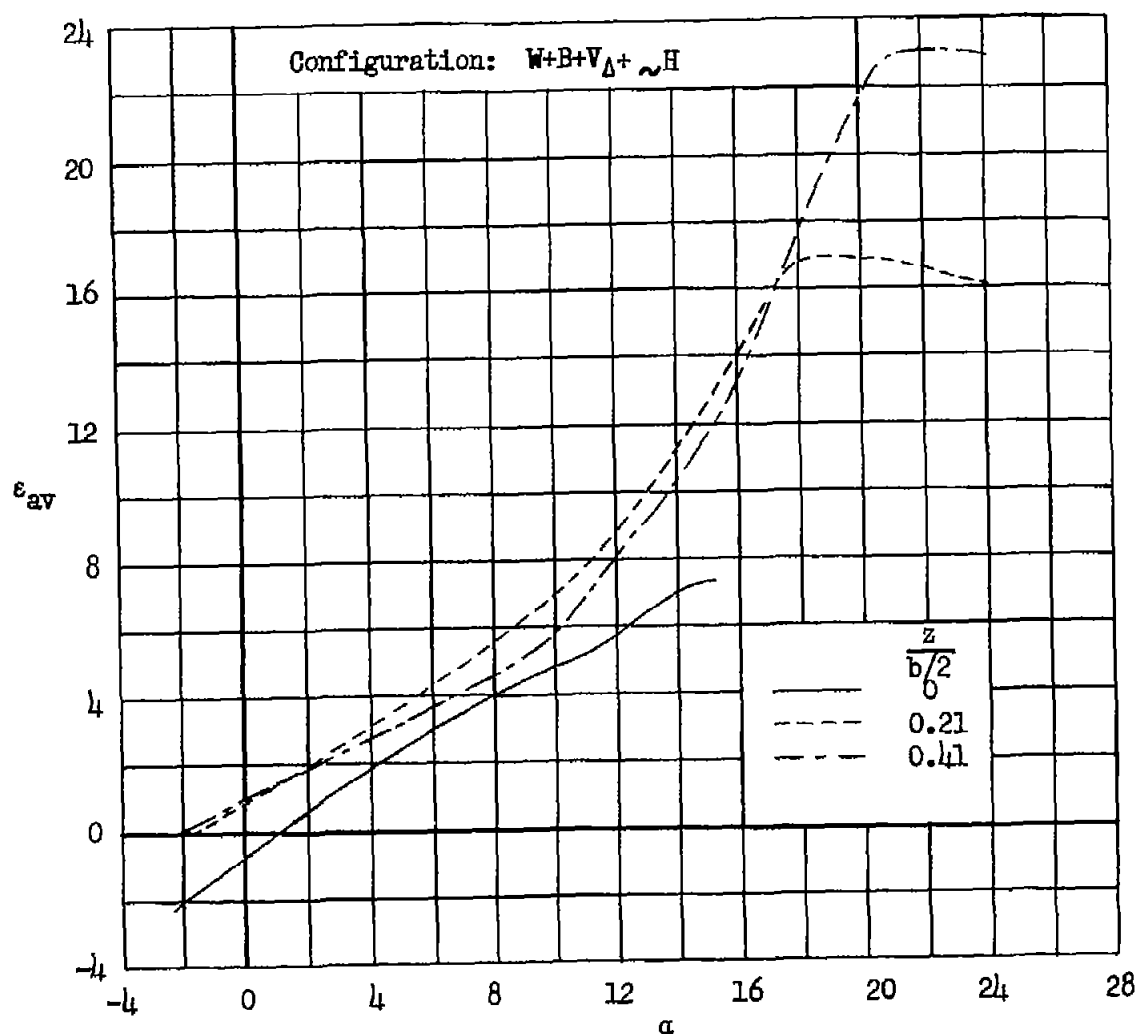


Figure 18.- Basic wing; average effective downwash at the three positions of the horizontal tail in conjunction with the triangular vertical tail; determined at Reynolds numbers 10 and 8×10^6 .

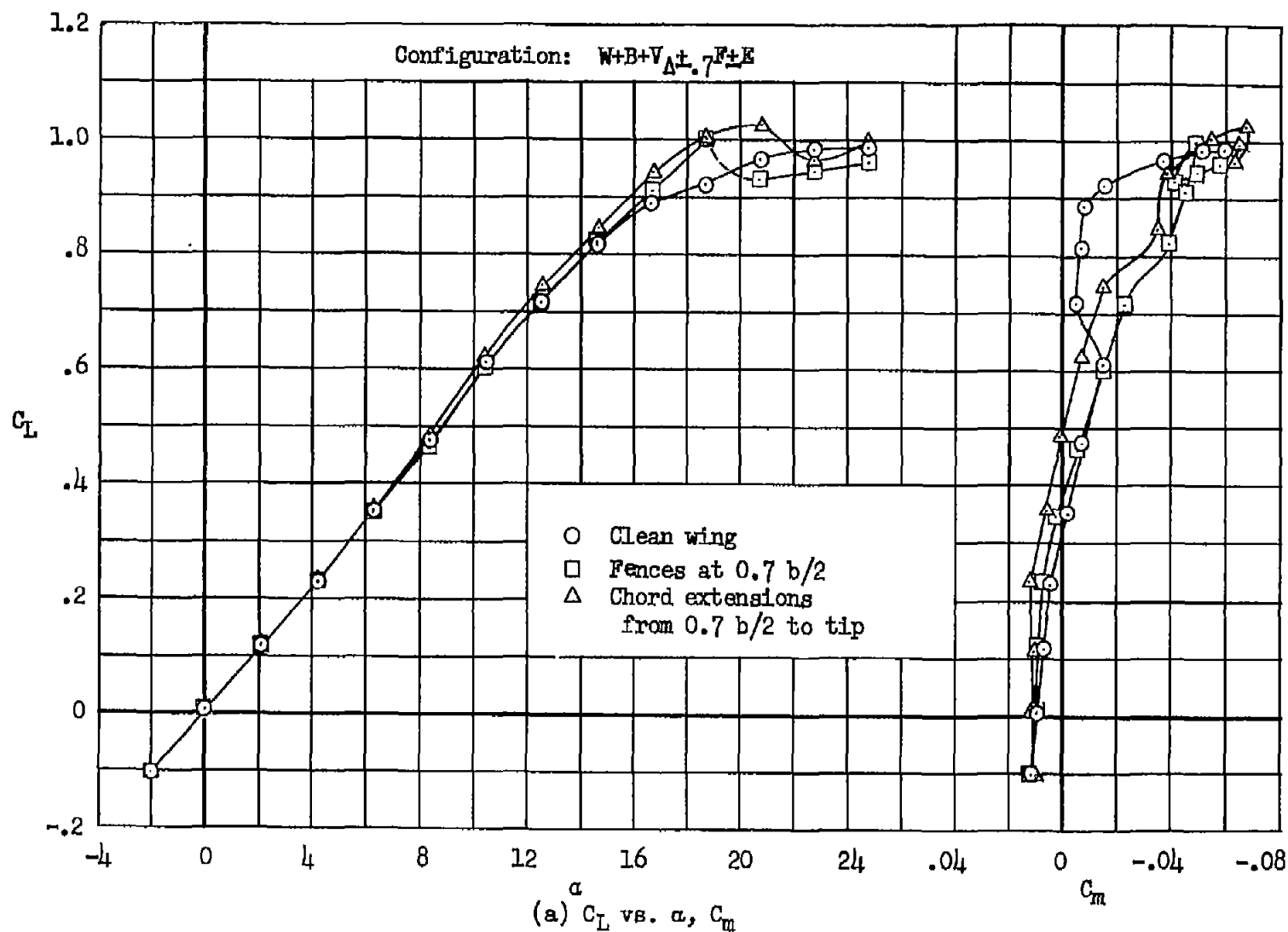


Figure 19.- Basic wing; effect of fences and chord extensions on the longitudinal characteristics of the model without the horizontal tail, Reynolds number 10×10^6 .

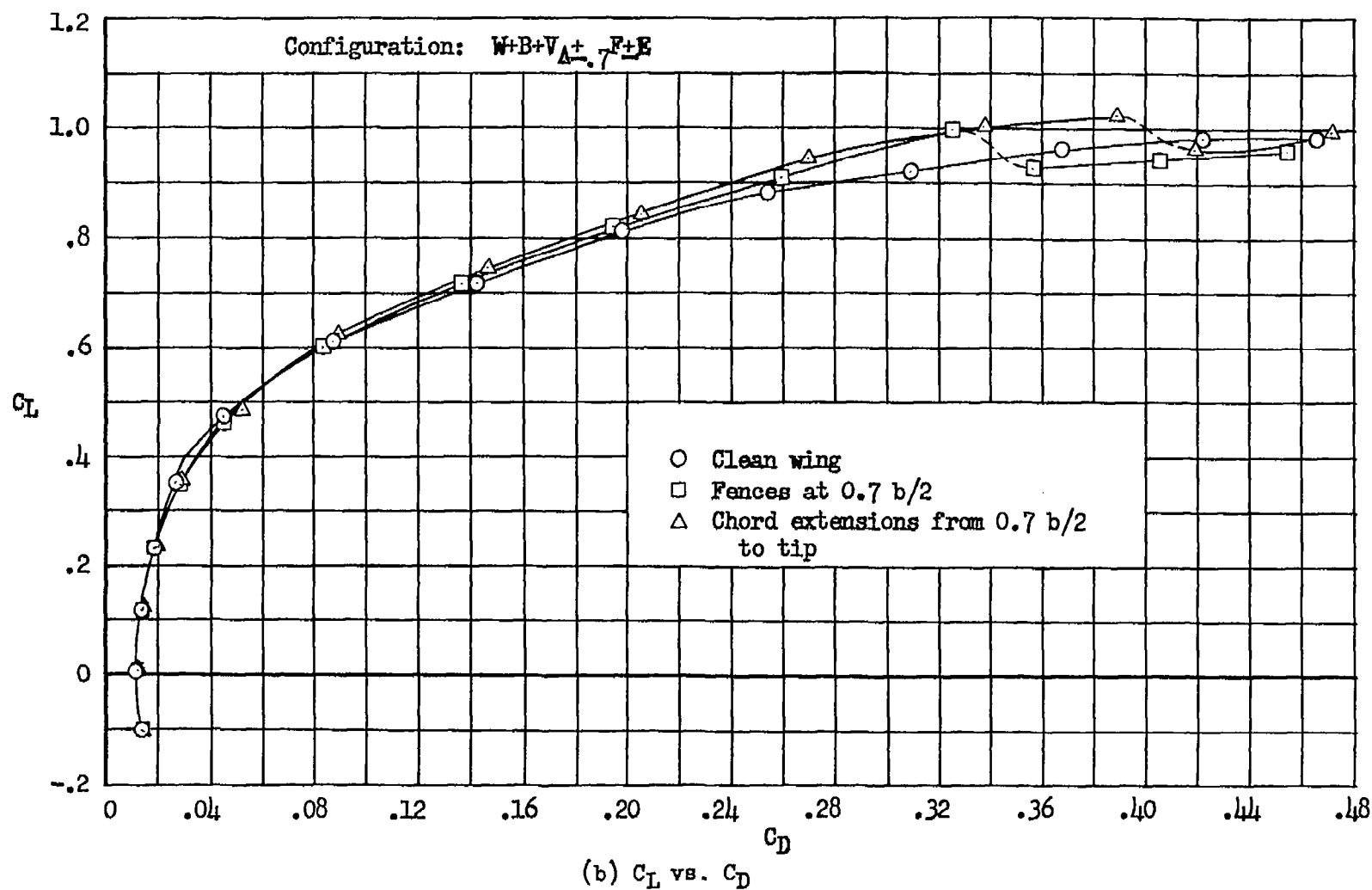


Figure 19.- Concluded.

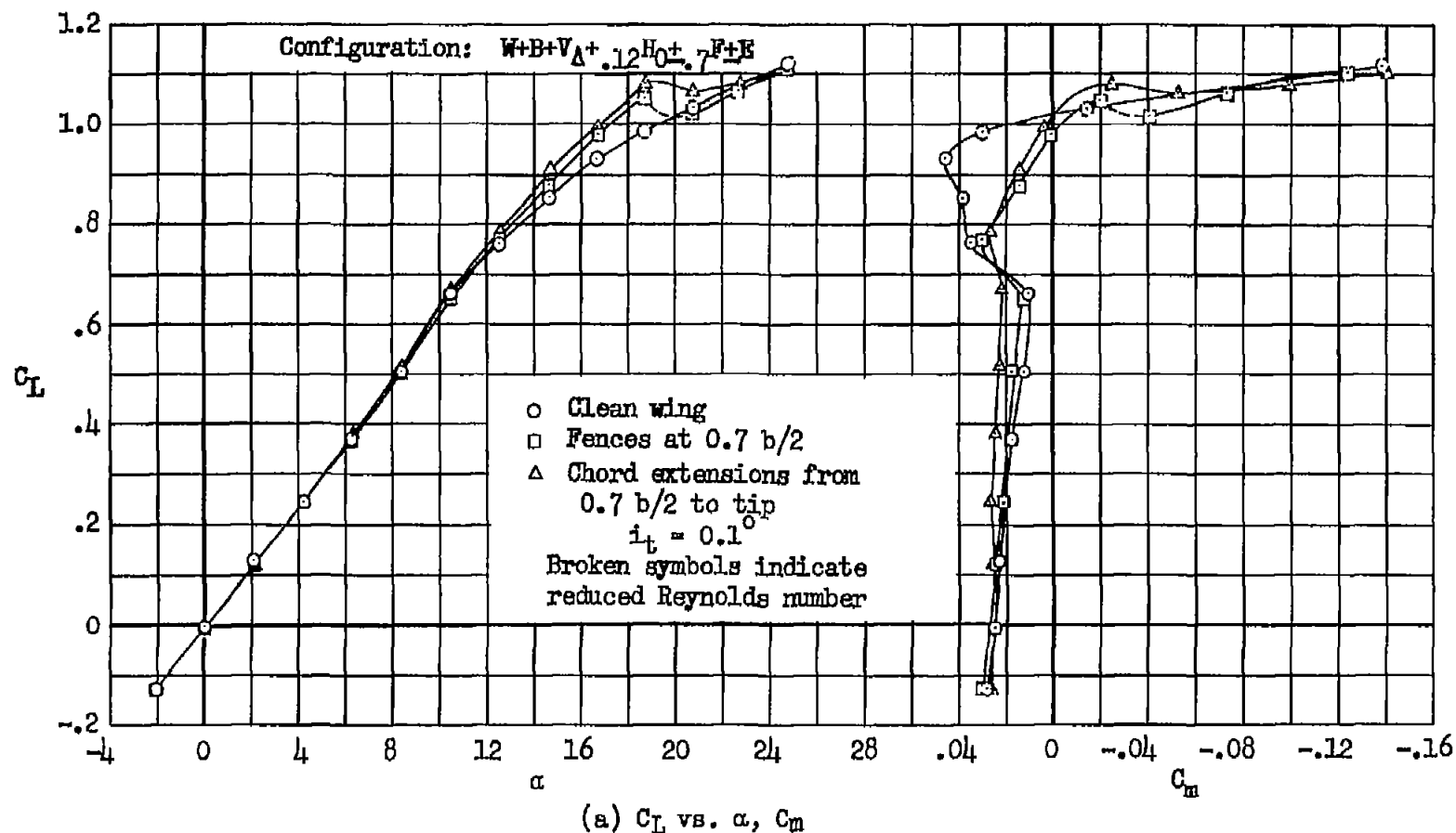


Figure 20.- Basic wing; effect of fences and chord extensions on the longitudinal characteristics of the model with the horizontal tail mounted on the triangular vertical tail at $z/(b/2) = 0.12$, moment center at $0.35\bar{c}$, Reynolds numbers 10 and 8×10^6 .

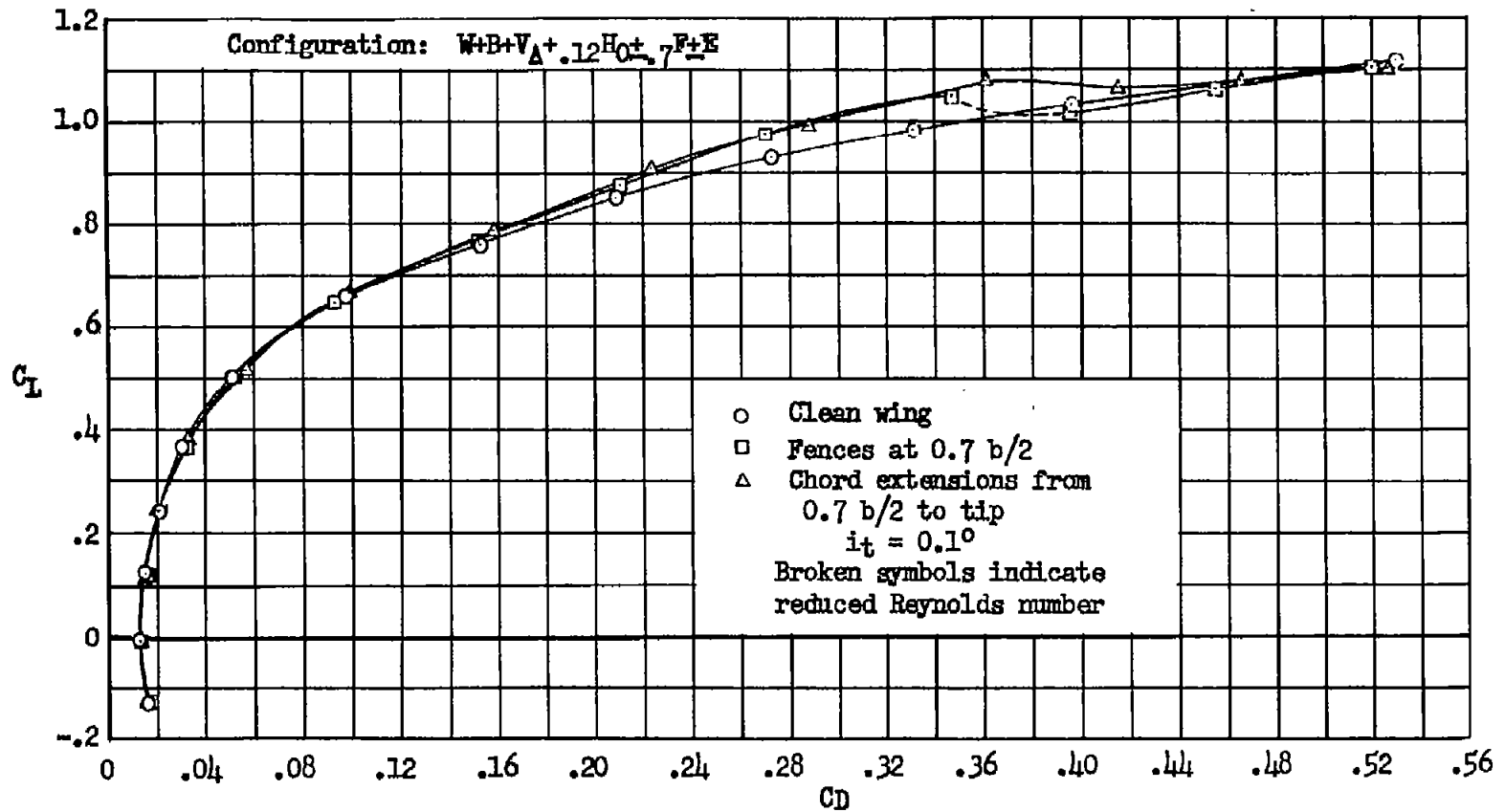
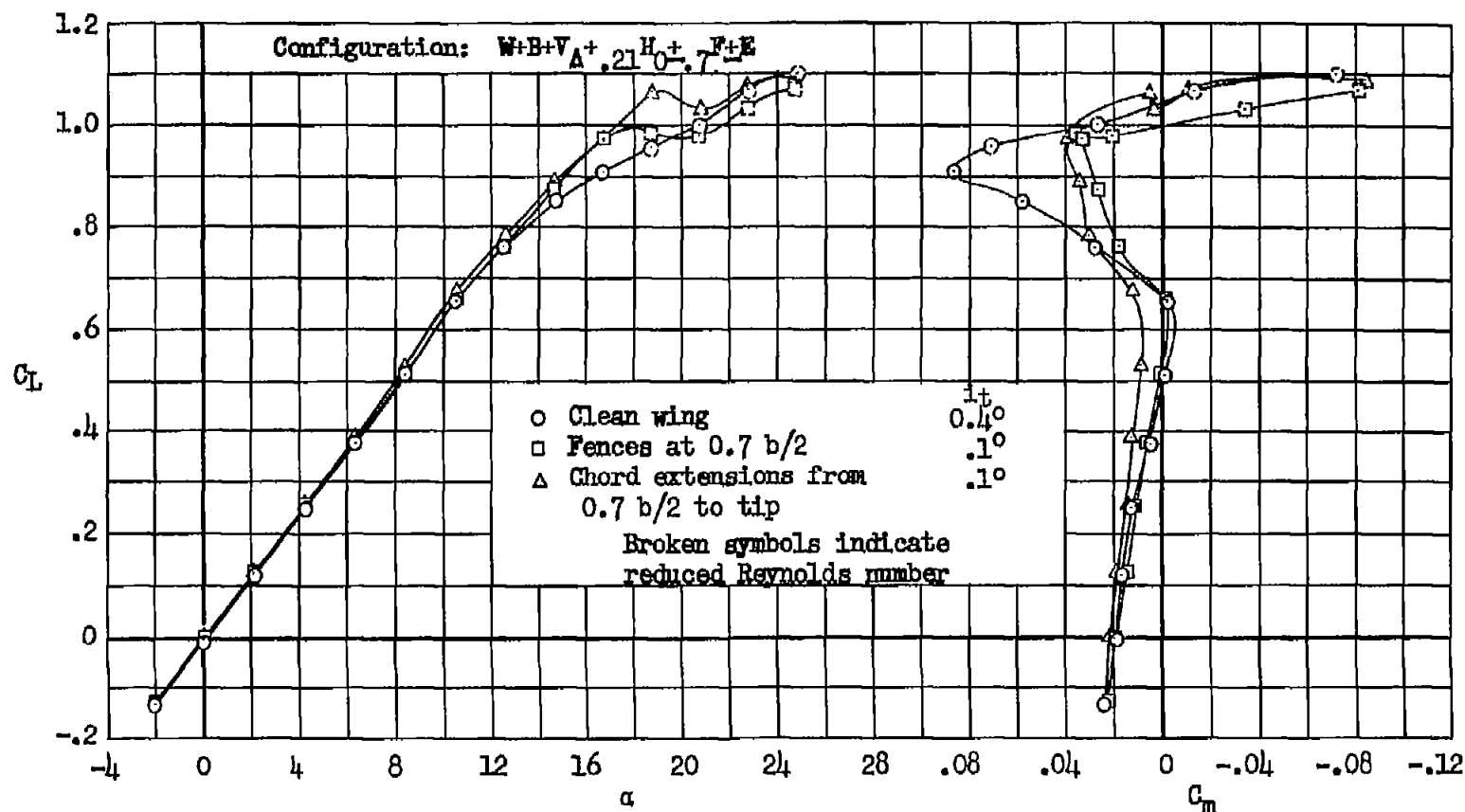
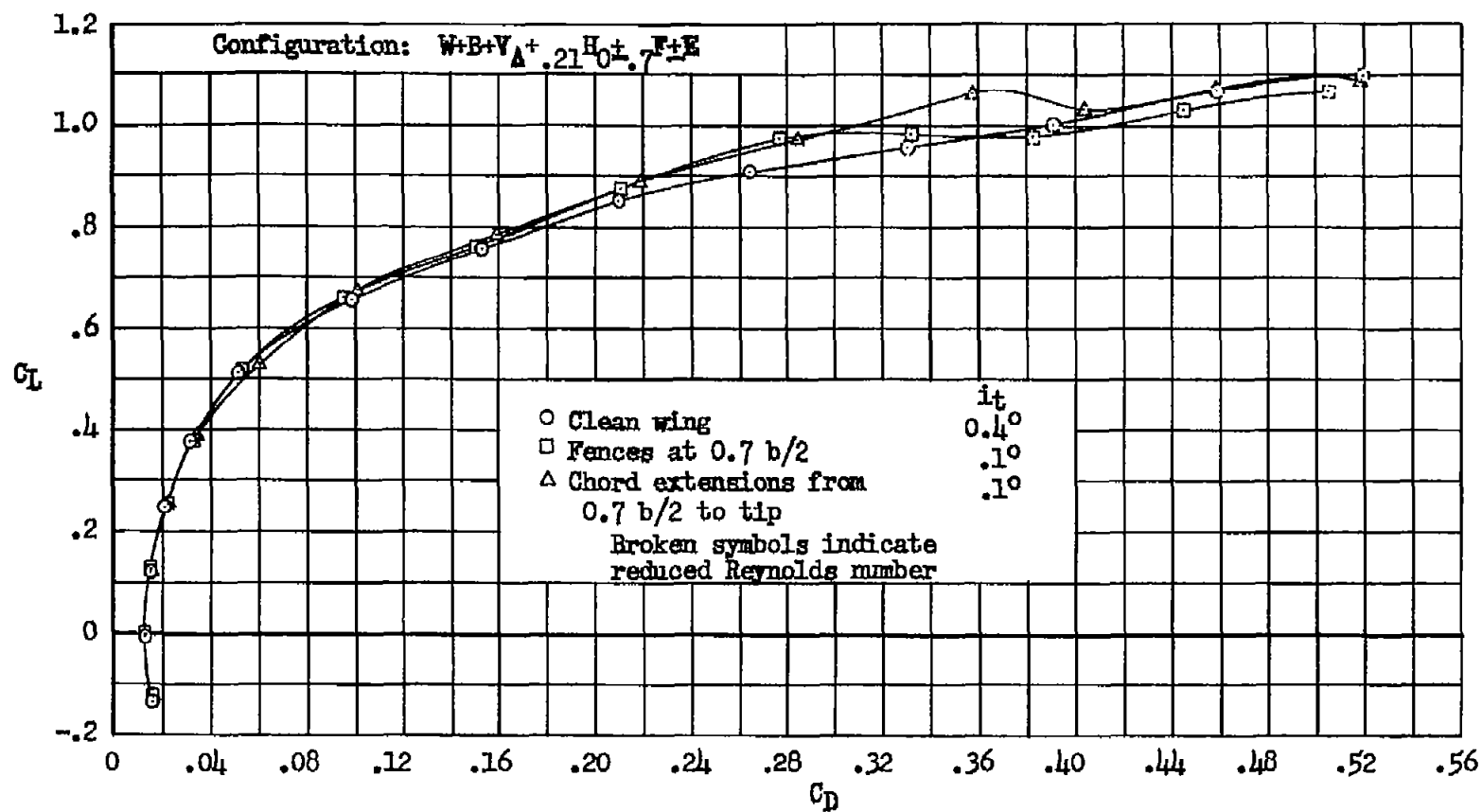
(b) C_L vs. C_D

Figure 20.- Concluded.



(a) C_L vs. α , C_m

Figure 21.- Basic wing; effect of fences and chord extensions on the longitudinal characteristics of the model with the horizontal tail mounted on the triangular vertical tail at $z/(b/2) = 0.21$, moment center at $0.35\bar{c}$, Reynolds numbers 10 and 8×10^6 .



(b) C_L vs. C_D

Figure 21.- Concluded.

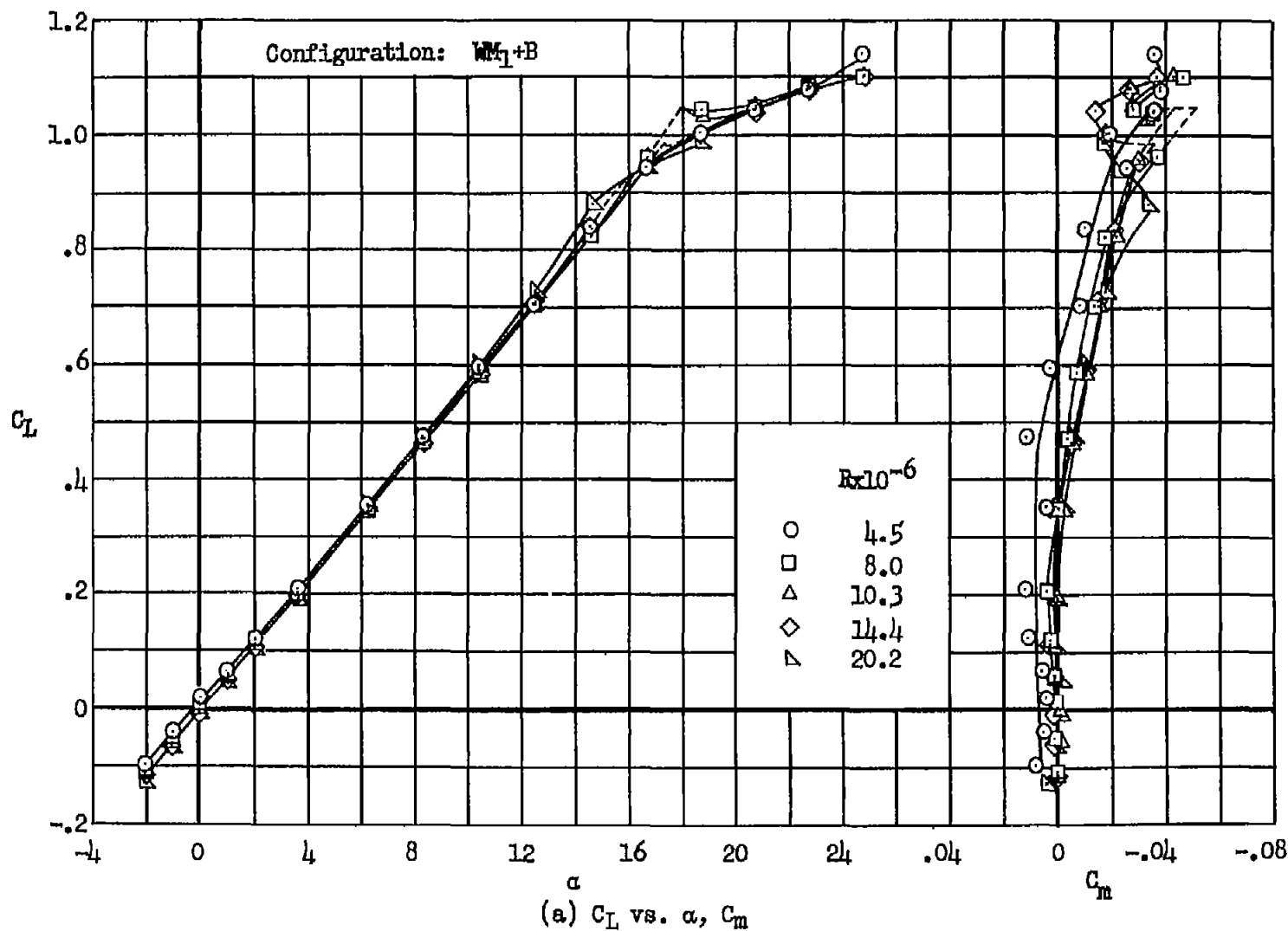


Figure 22.- Wing modification 1; longitudinal characteristics of the wing and body at several Reynolds numbers.

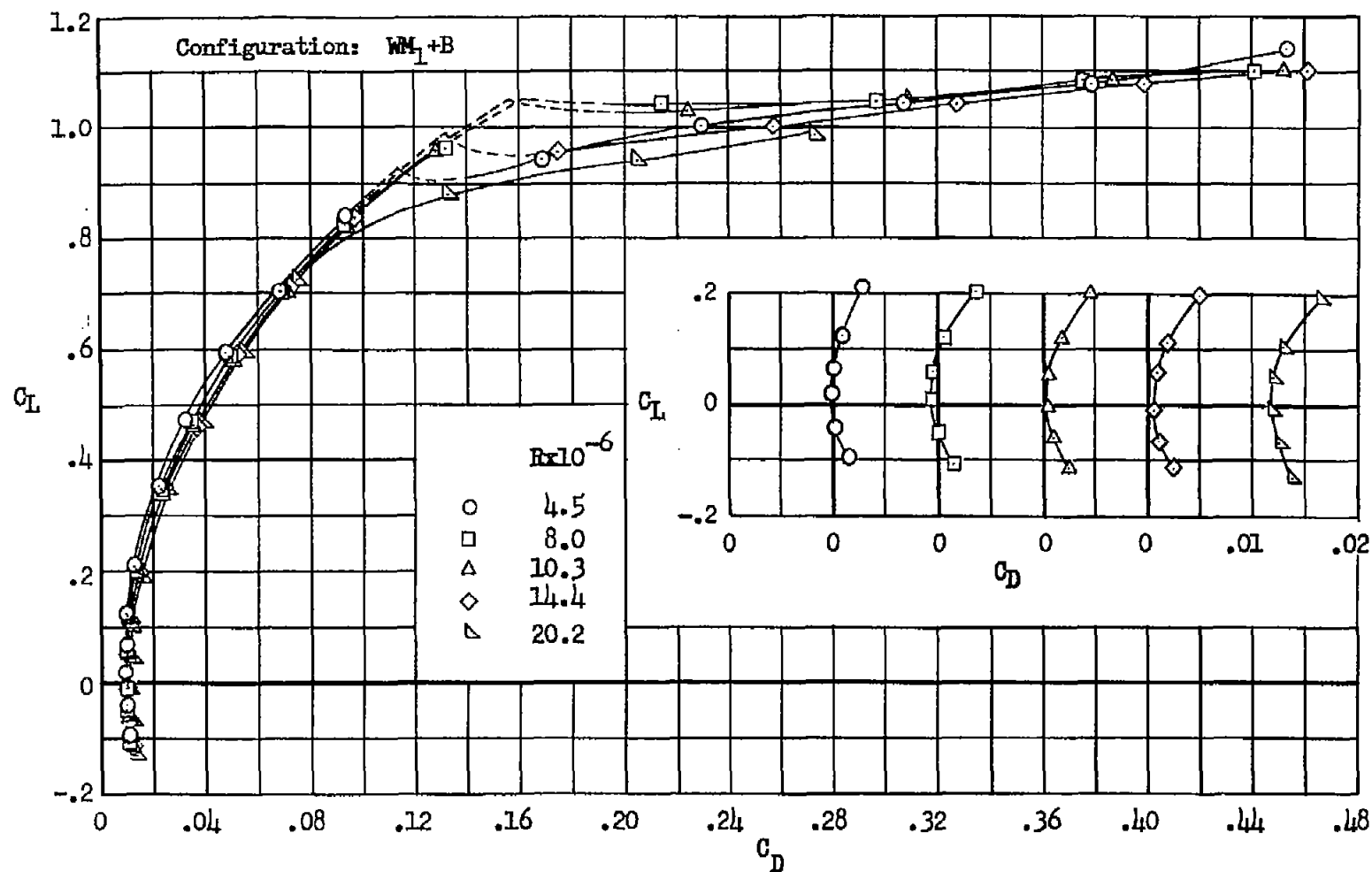
(b) C_L vs. C_D

Figure 22.- Concluded.

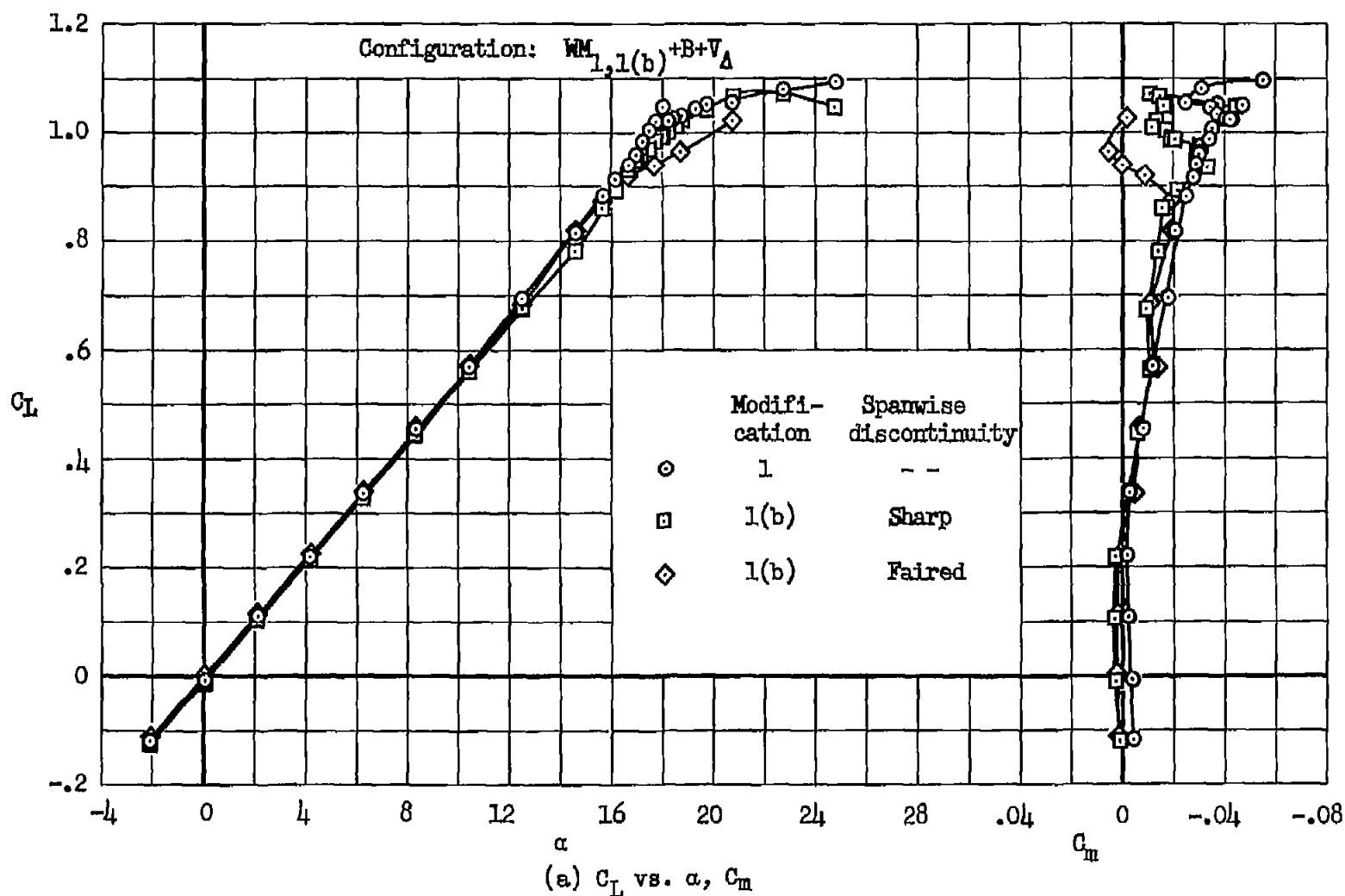


Figure 23.- Wing modifications 1 and 1(b); comparison of the longitudinal characteristics of the model with the two modifications, Reynolds number 10×10^6 .

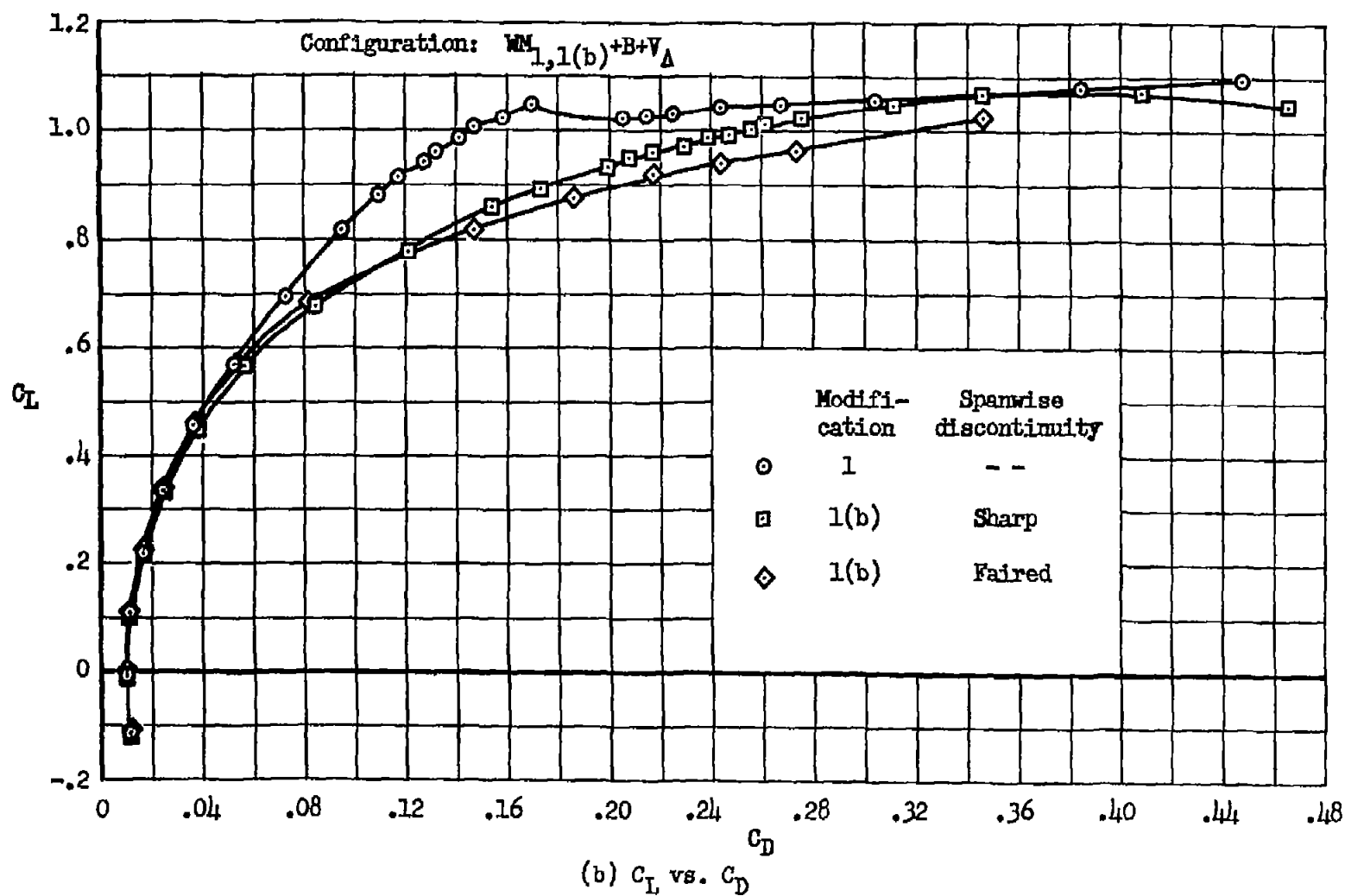


Figure 23.- Concluded.

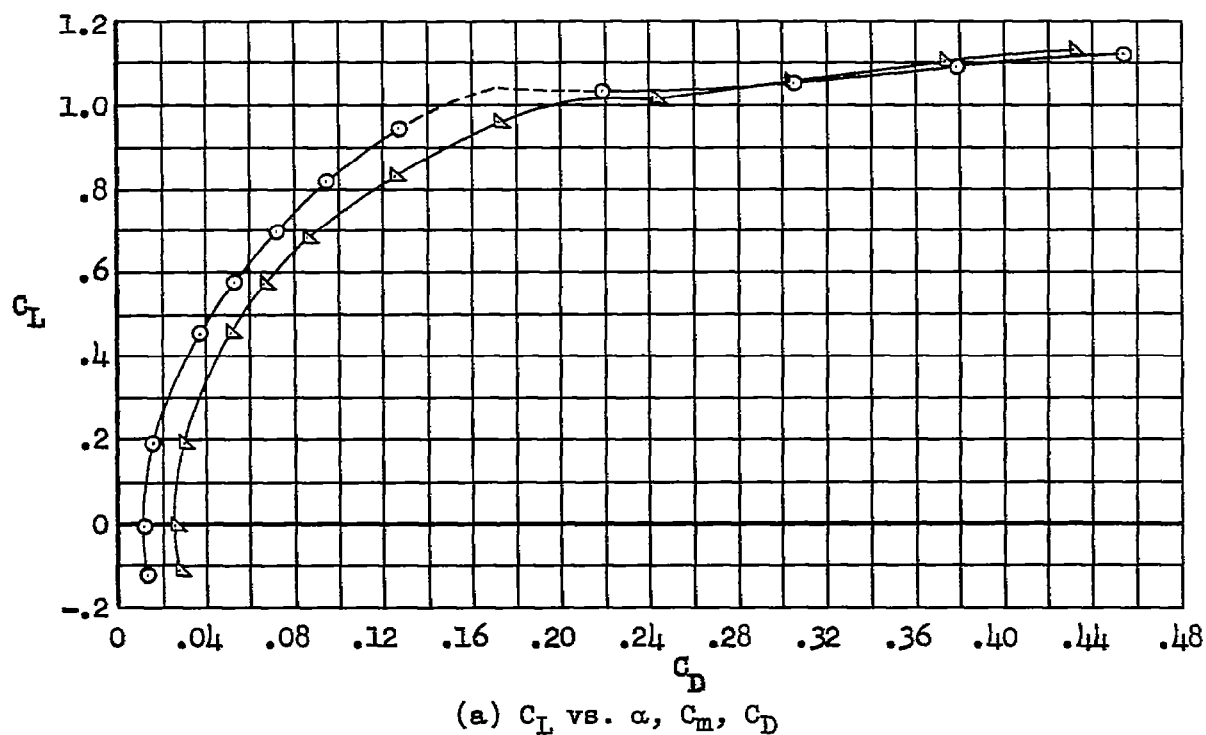
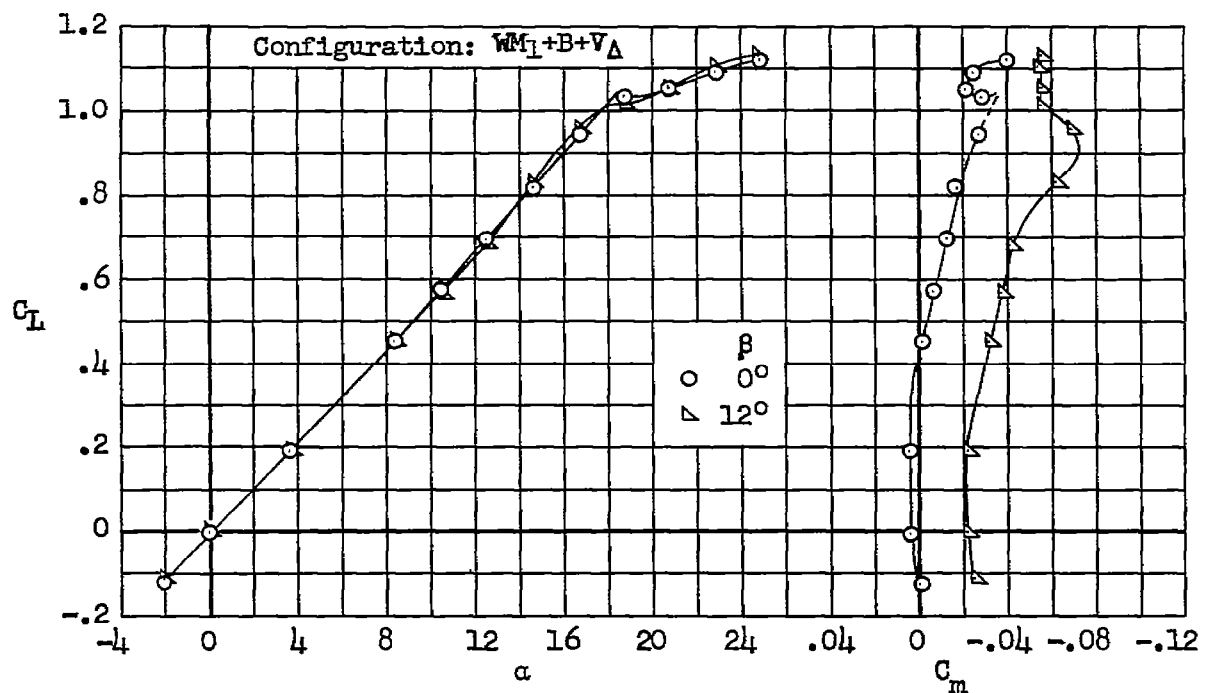
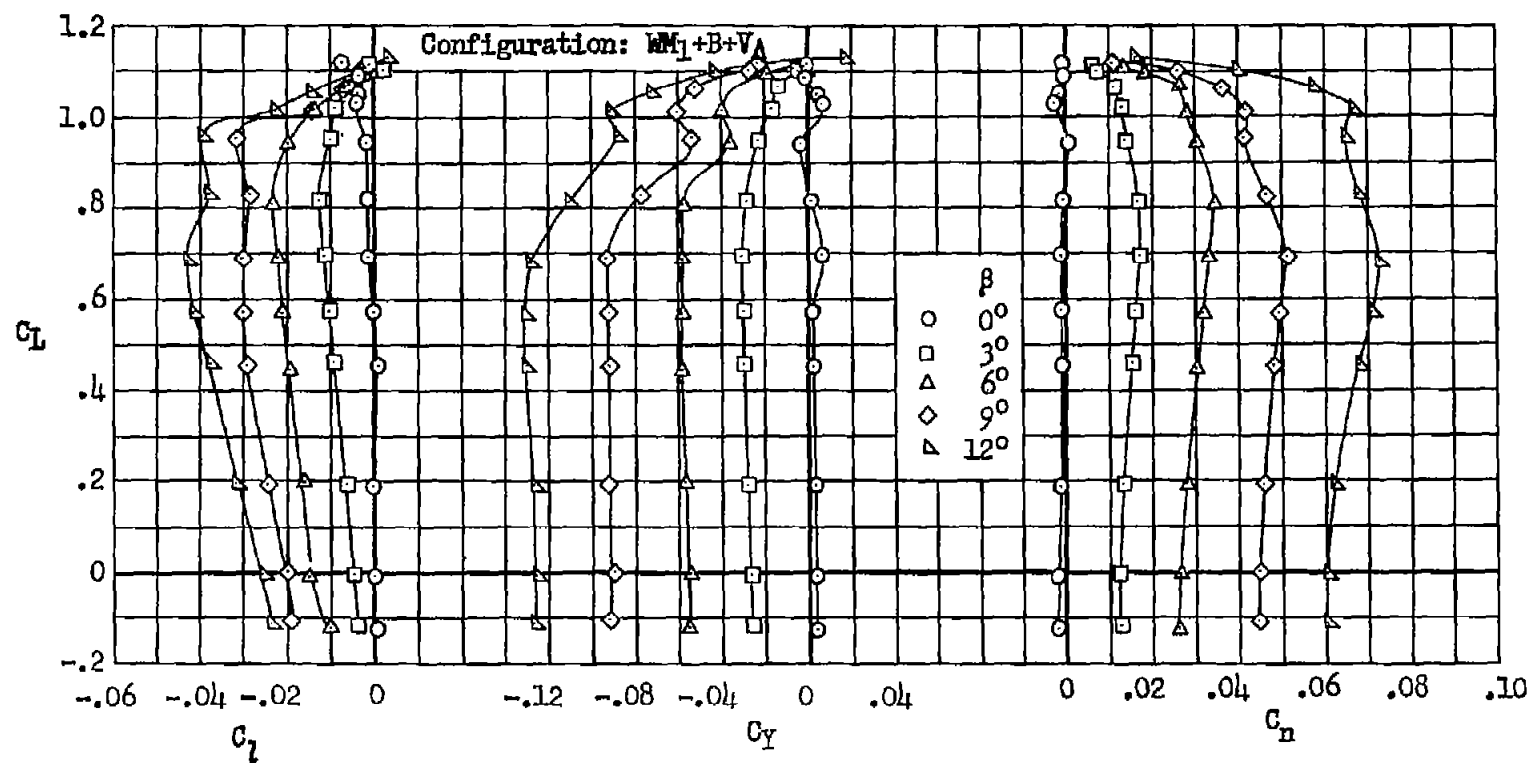


Figure 24.- Wing modification 1; characteristics in sideslip of the model with the triangular vertical tail, without the horizontal tail, Reynolds number 10×10^6 .



(b) C_L vs. C_D , C_Y , C_N

Figure 24.- Concluded.

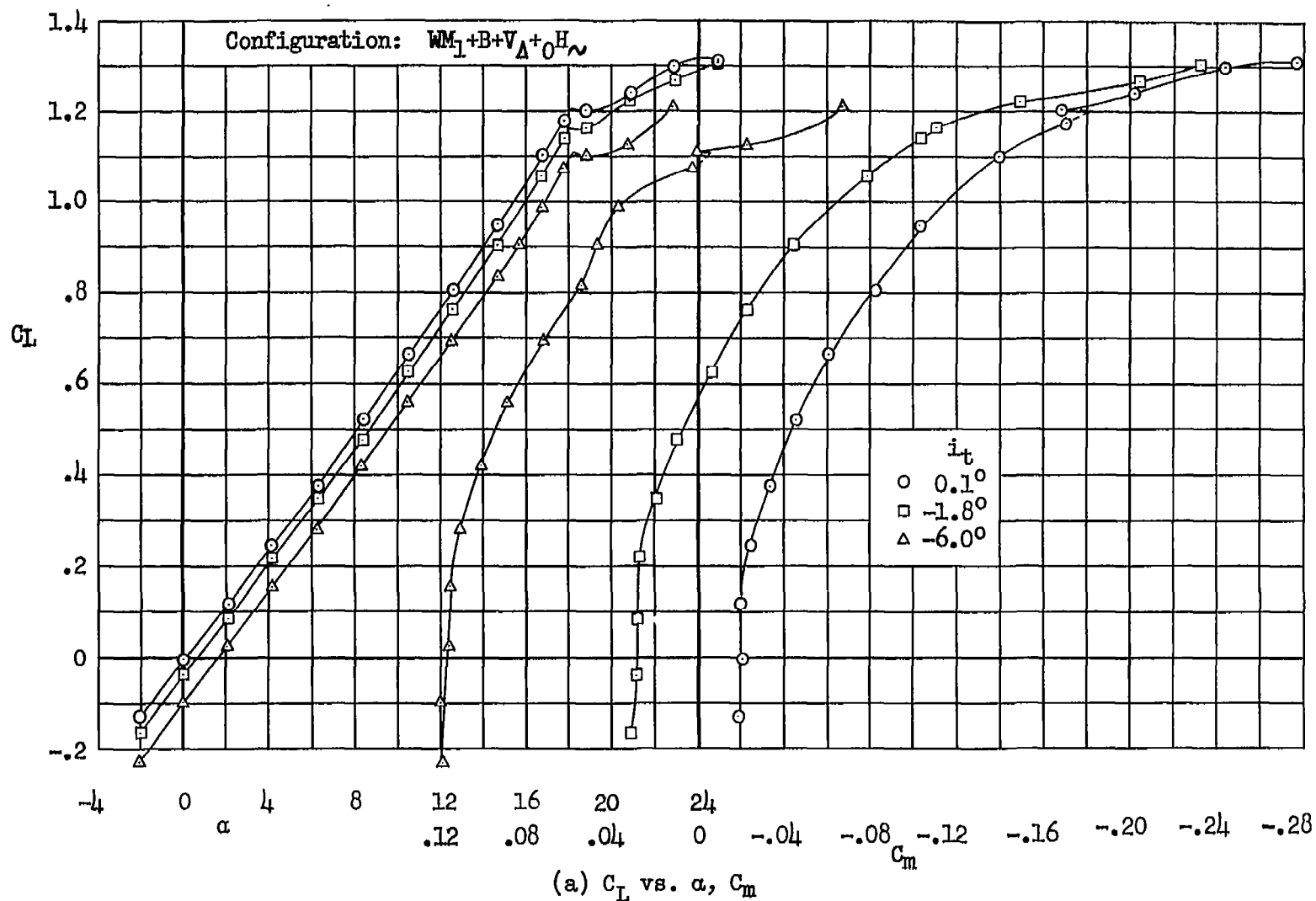


Figure 25.- Wing modification 1; longitudinal characteristics of the model with the horizontal tail in the wing chord plane, moment center at $0.34\bar{c}$, Reynolds number 10×10^6 .

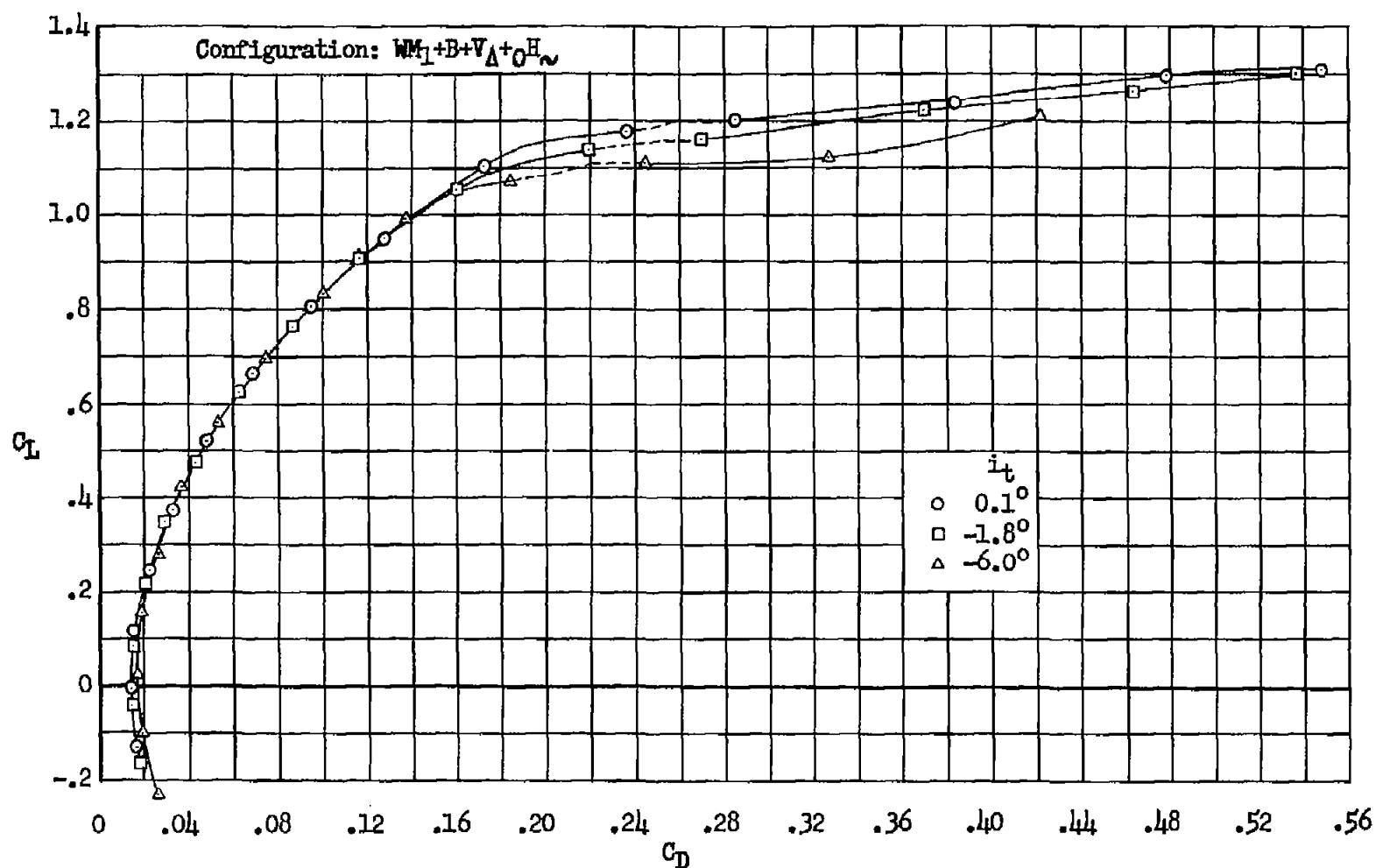
(b) C_L vs. C_D

Figure 25.- Concluded.

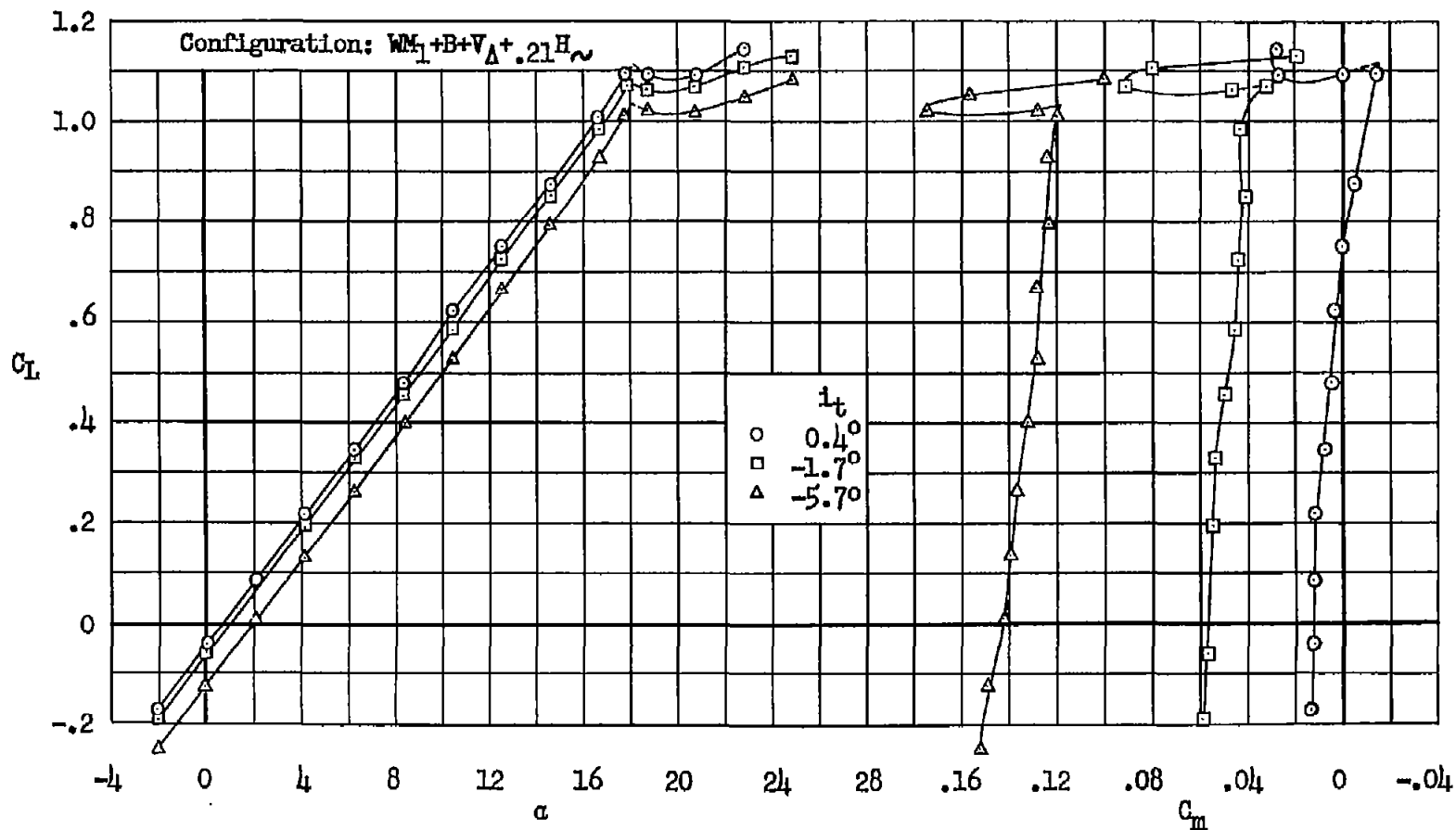
(a) C_L vs. α , C_m

Figure 26.- Wing modification 1; longitudinal characteristics of the model with the horizontal tail mounted on the triangular vertical tail at $z/(b/2) = 0.21$, moment center at $0.35\bar{c}$, Reynolds number 10×10^6 .

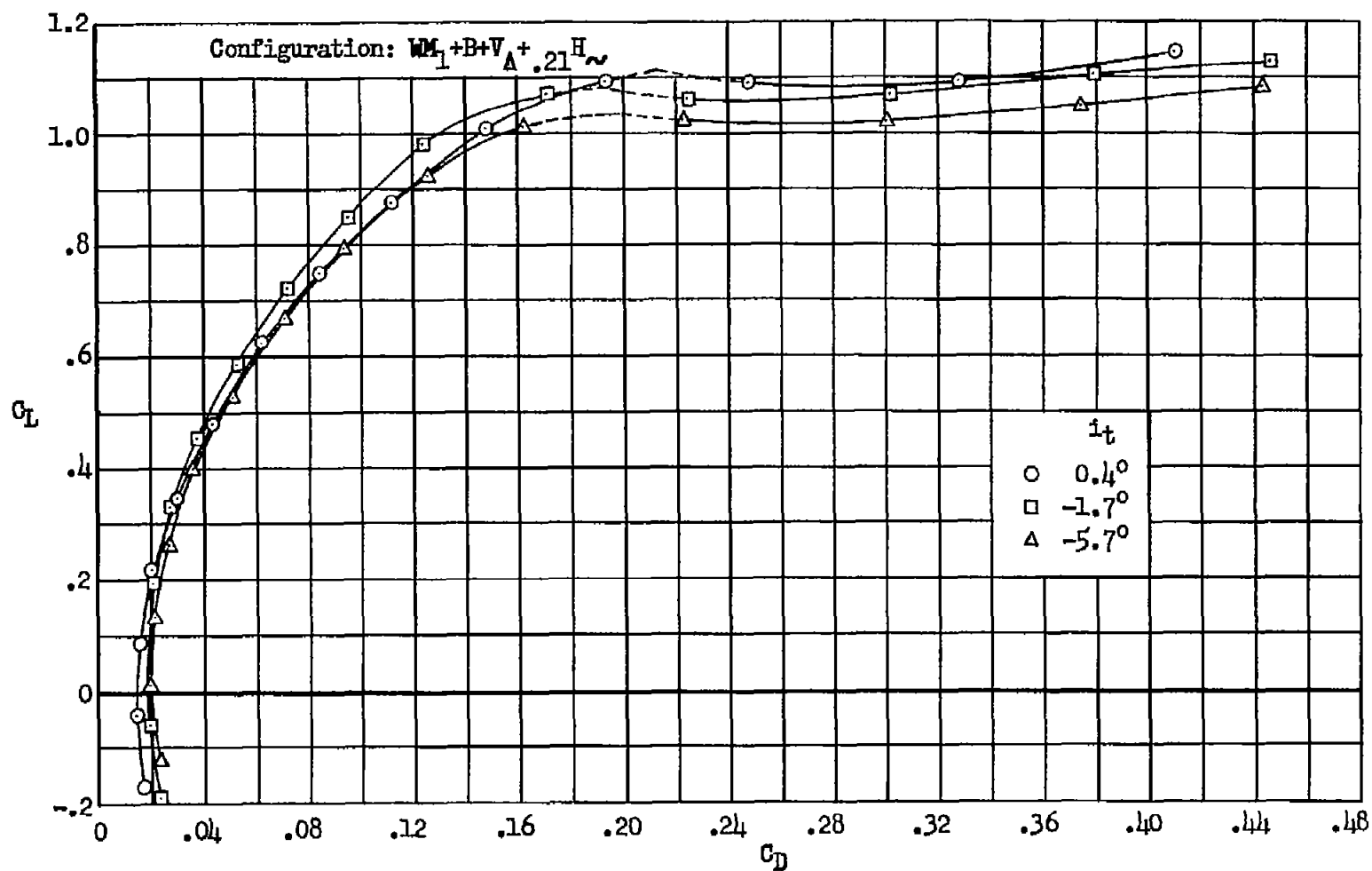
(b) C_L vs. C_D

Figure 26.- Concluded.

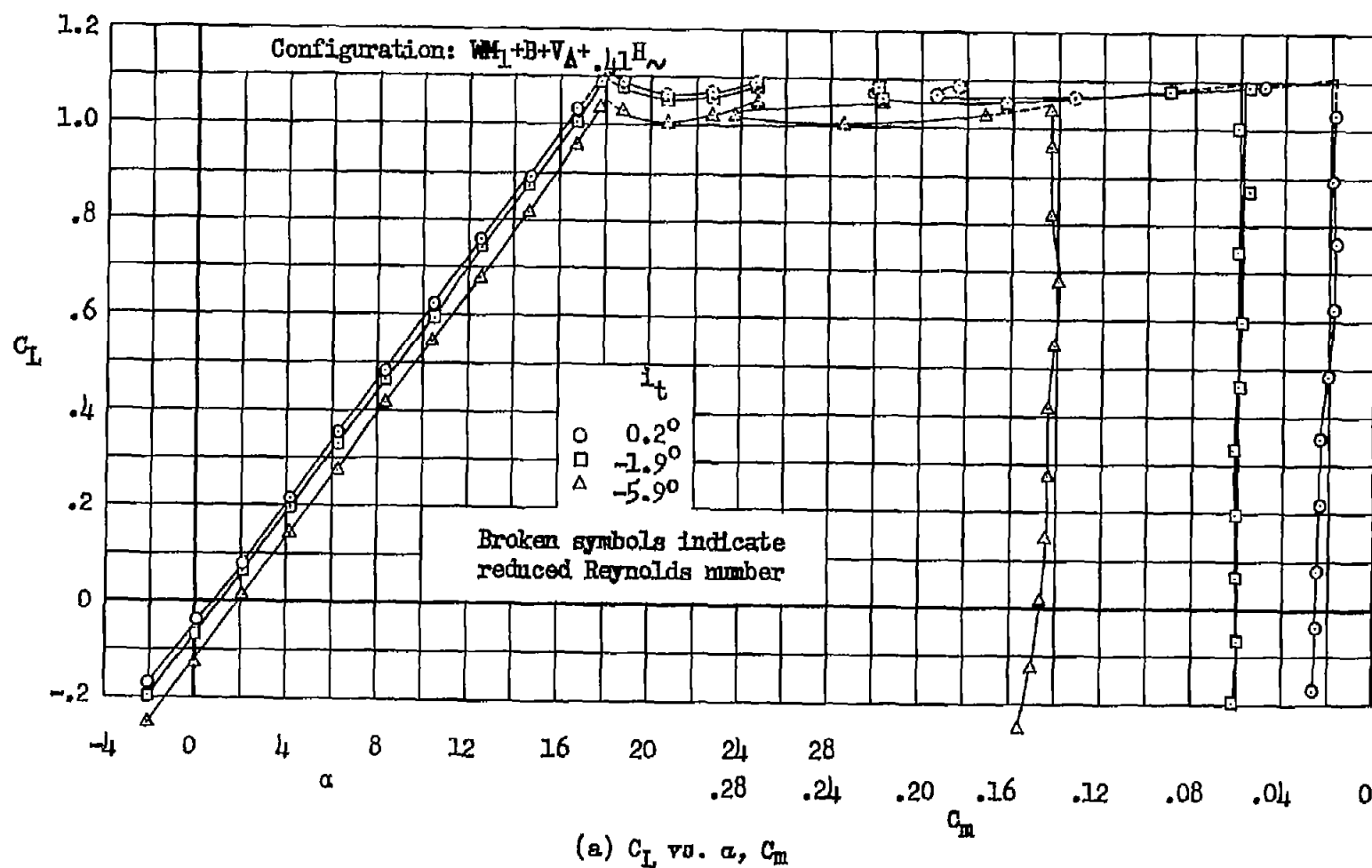


Figure 27.- Wing modification 1; longitudinal characteristics of the model with the horizontal tail mounted on the triangular vertical tail at $z/(b/2) = 0.41$, moment center at $0.40\bar{c}$, Reynolds numbers 10 and 8×10^6 .

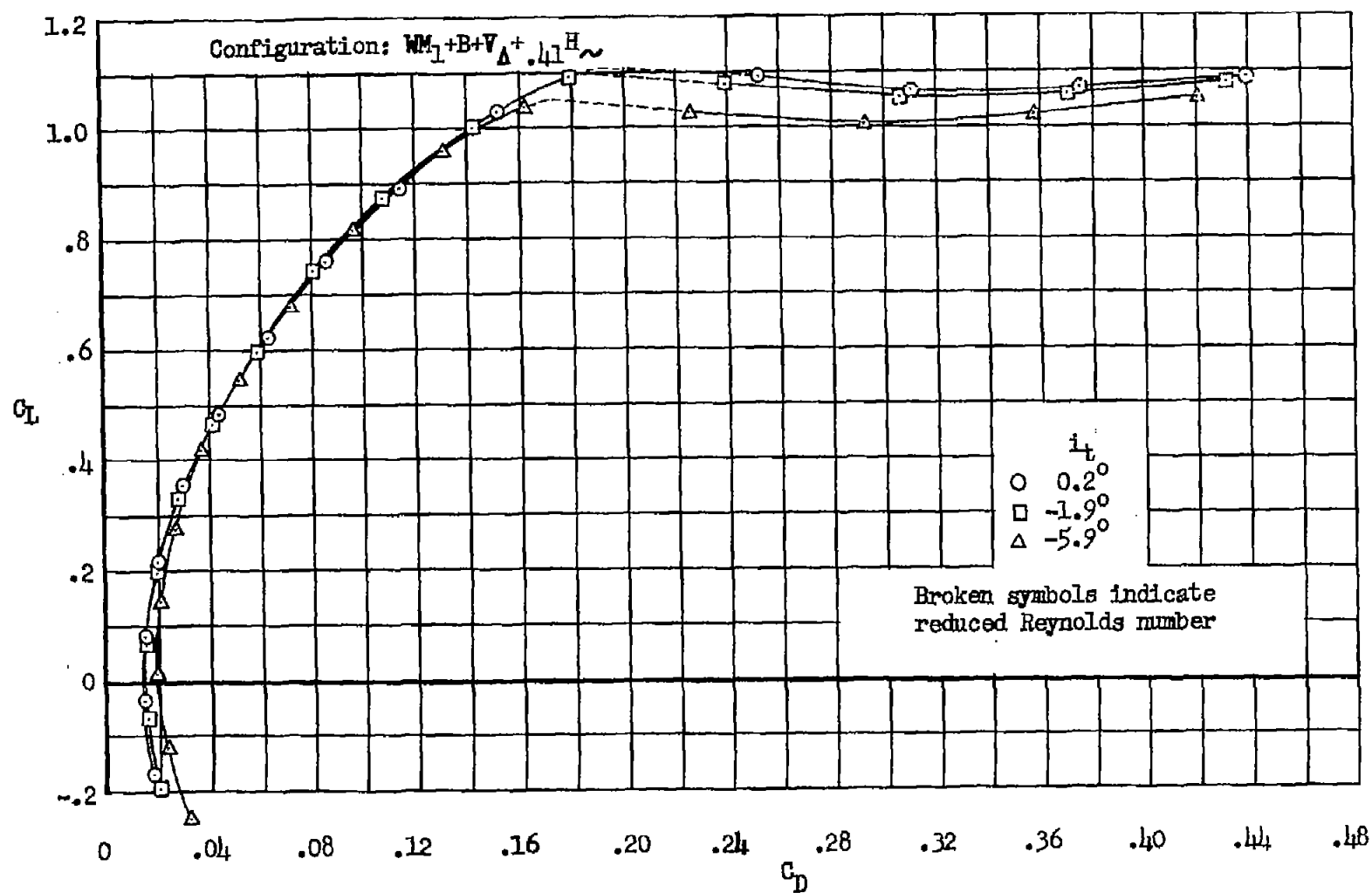
(b) C_L vs. C_D

Figure 27.- Concluded.

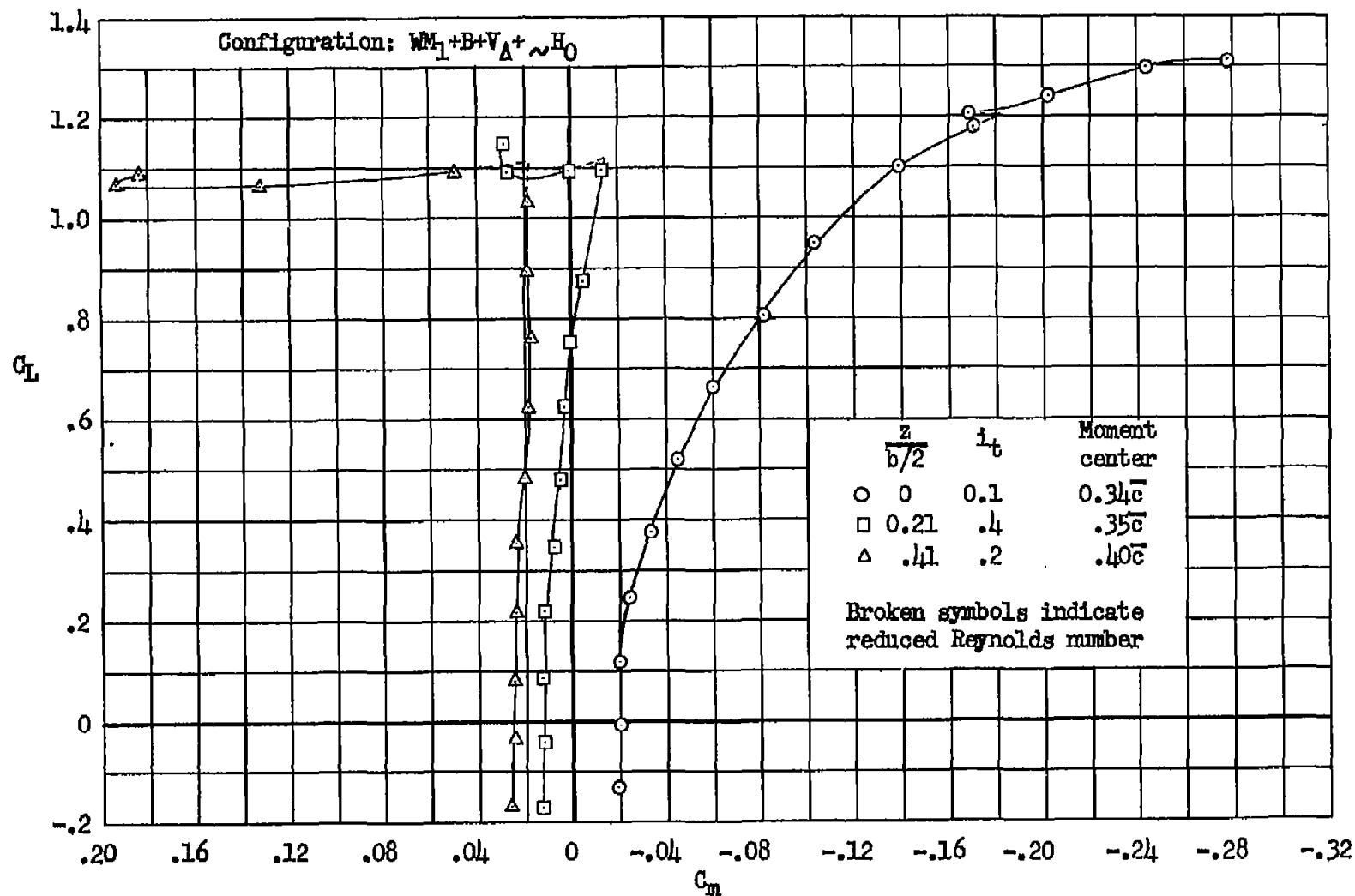


Figure 28.- Wing modification 1; effect of the position of the horizontal tail, in conjunction with the triangular vertical tail on the pitching moment of the model; Reynolds numbers 10 and 8×10^5 .

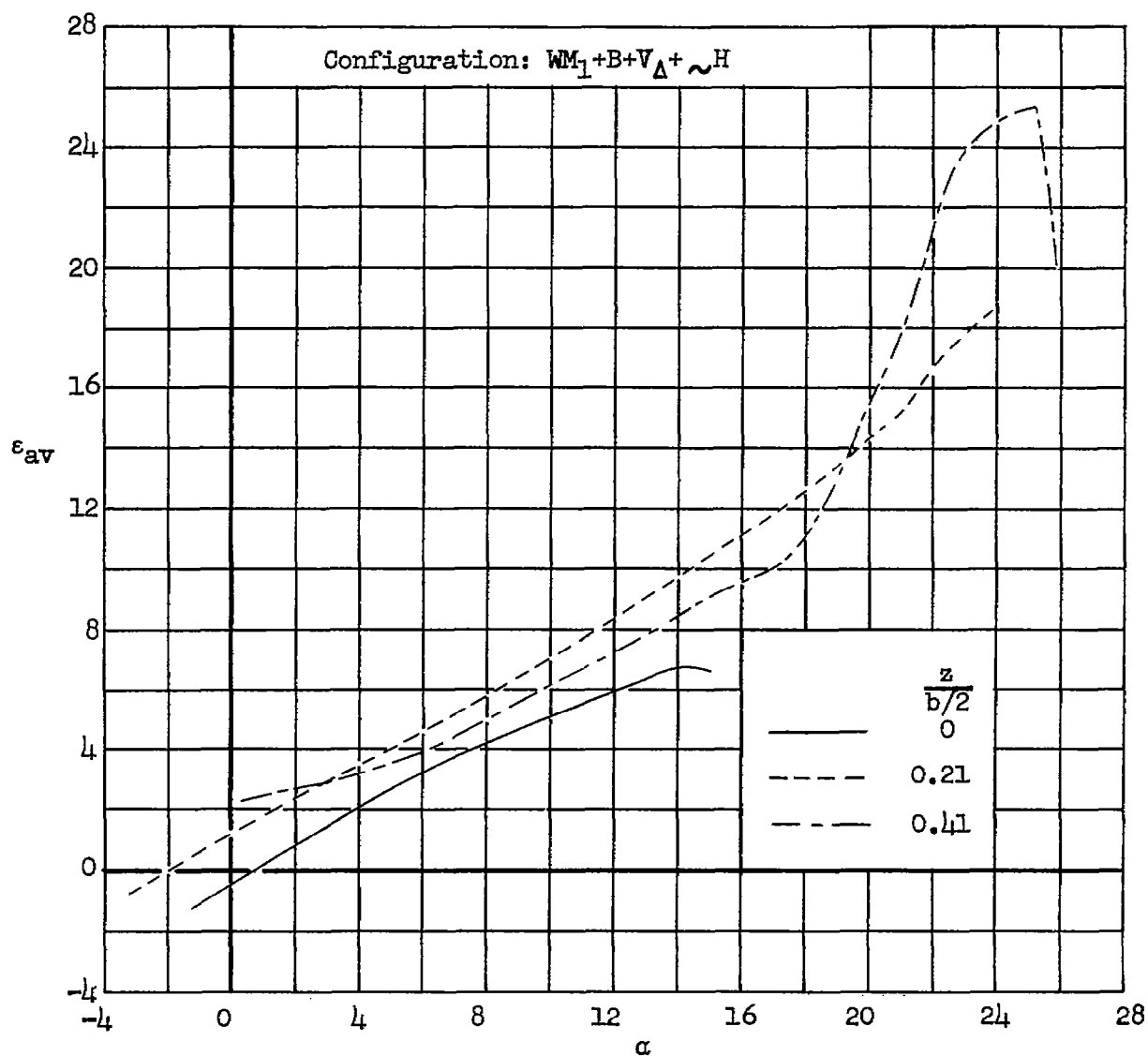
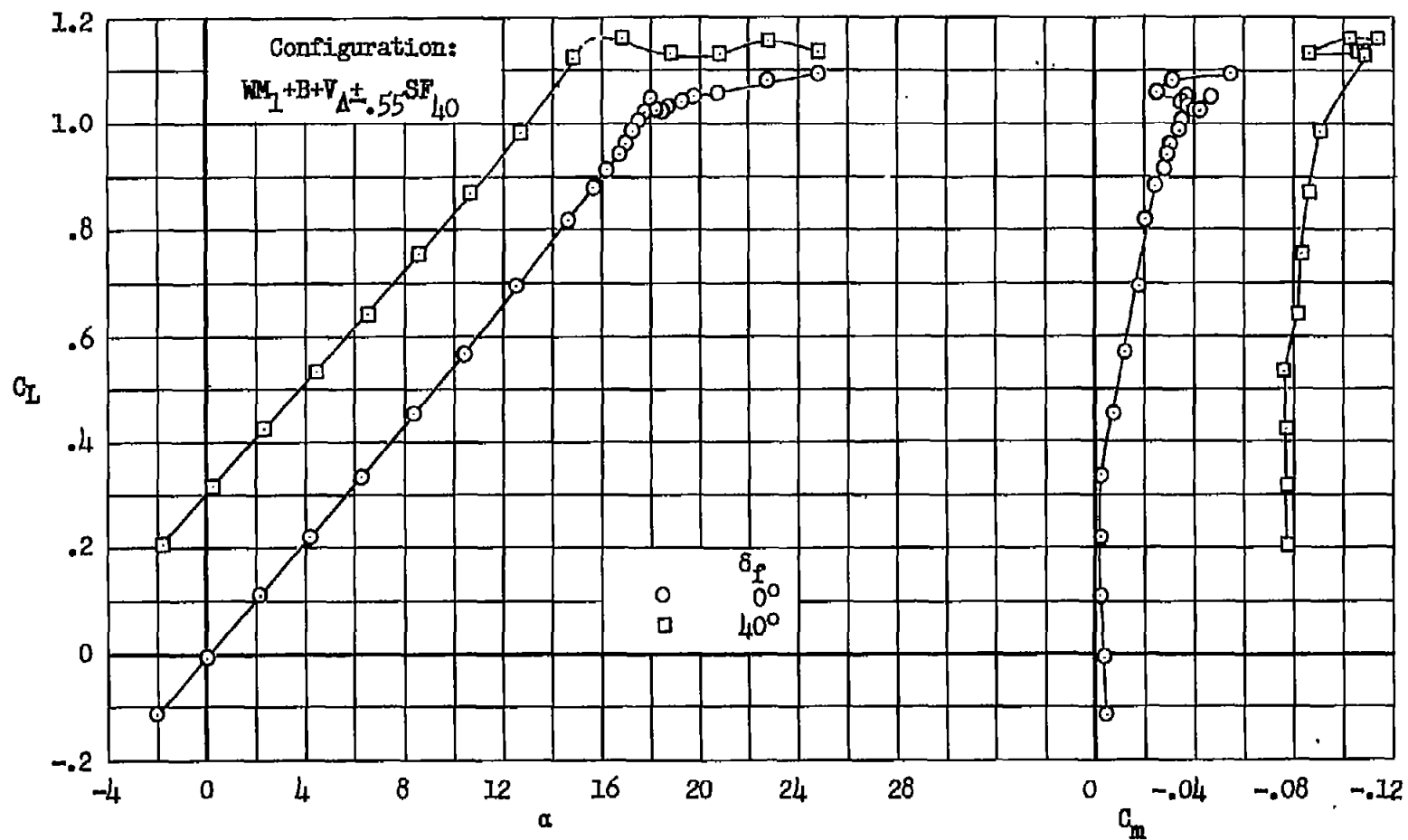


Figure 29.- Wing modification 1; average effective downwash at three positions of the horizontal tail in conjunction with the triangular vertical tail, determined at Reynolds numbers of 10 and 8×10^6 .



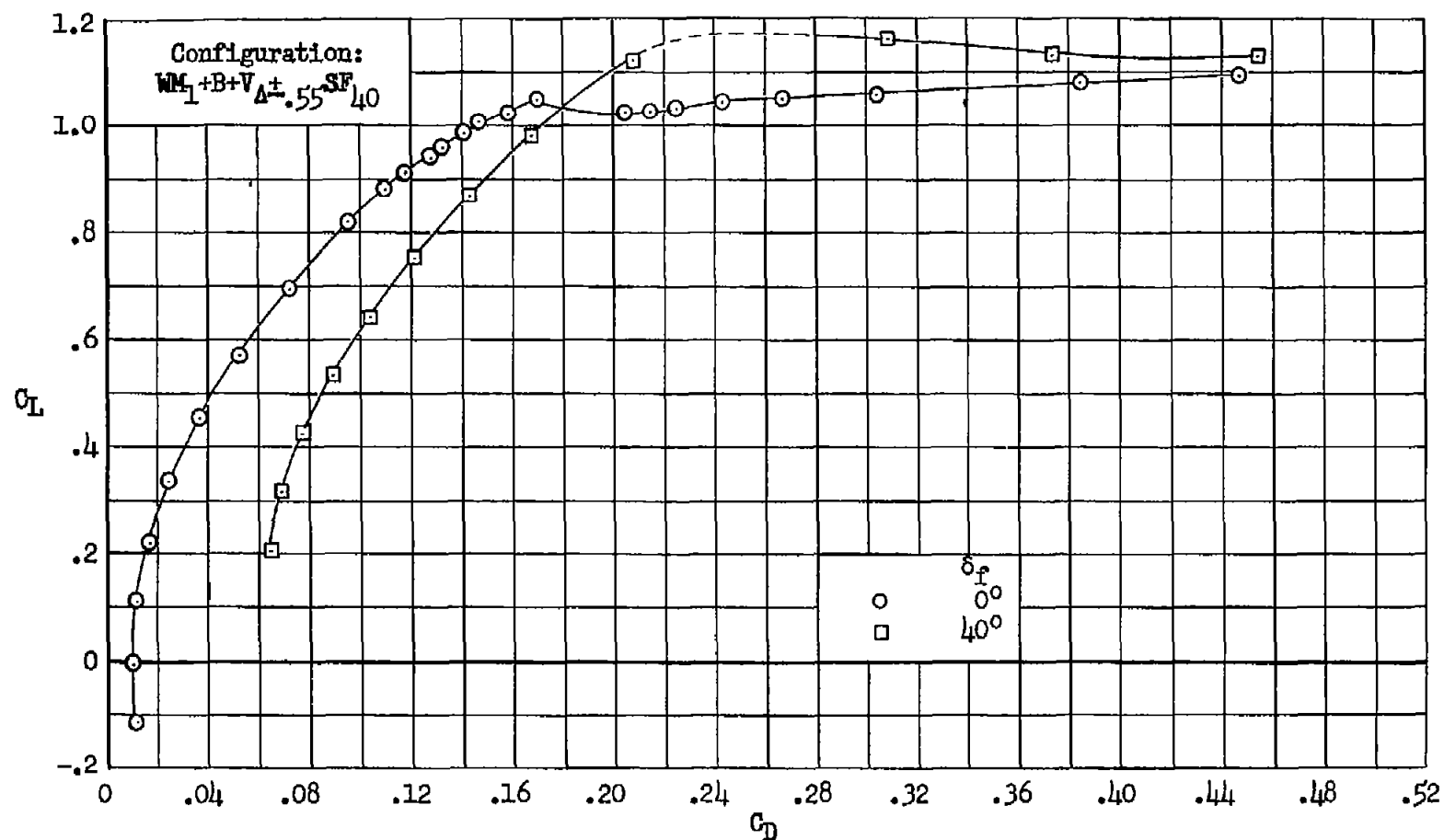
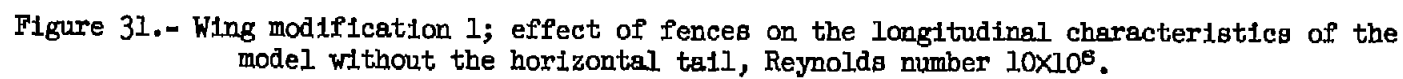
(b) C_L vs. C_D

Figure 30.- Concluded.



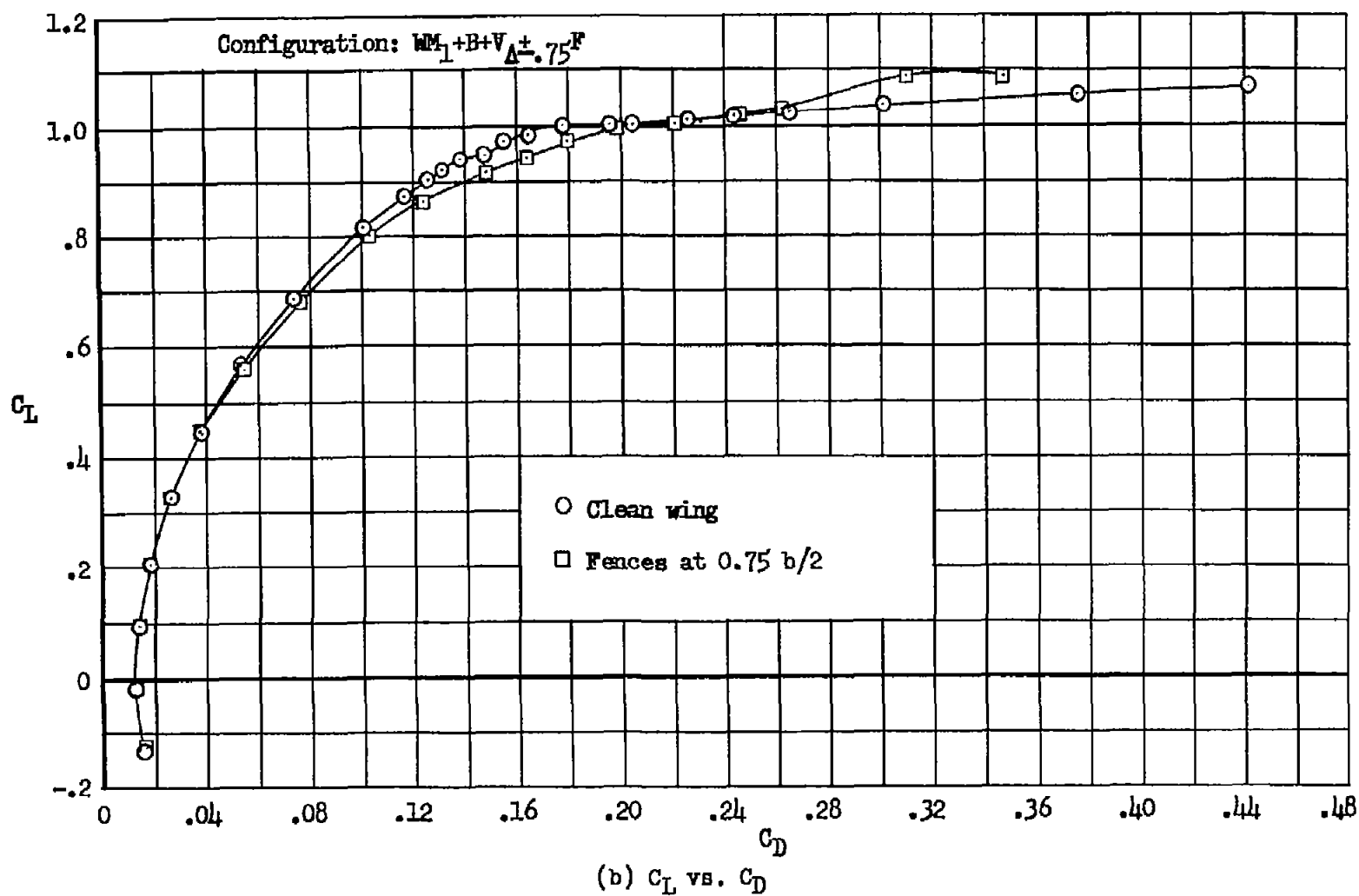


Figure 31.- Concluded.

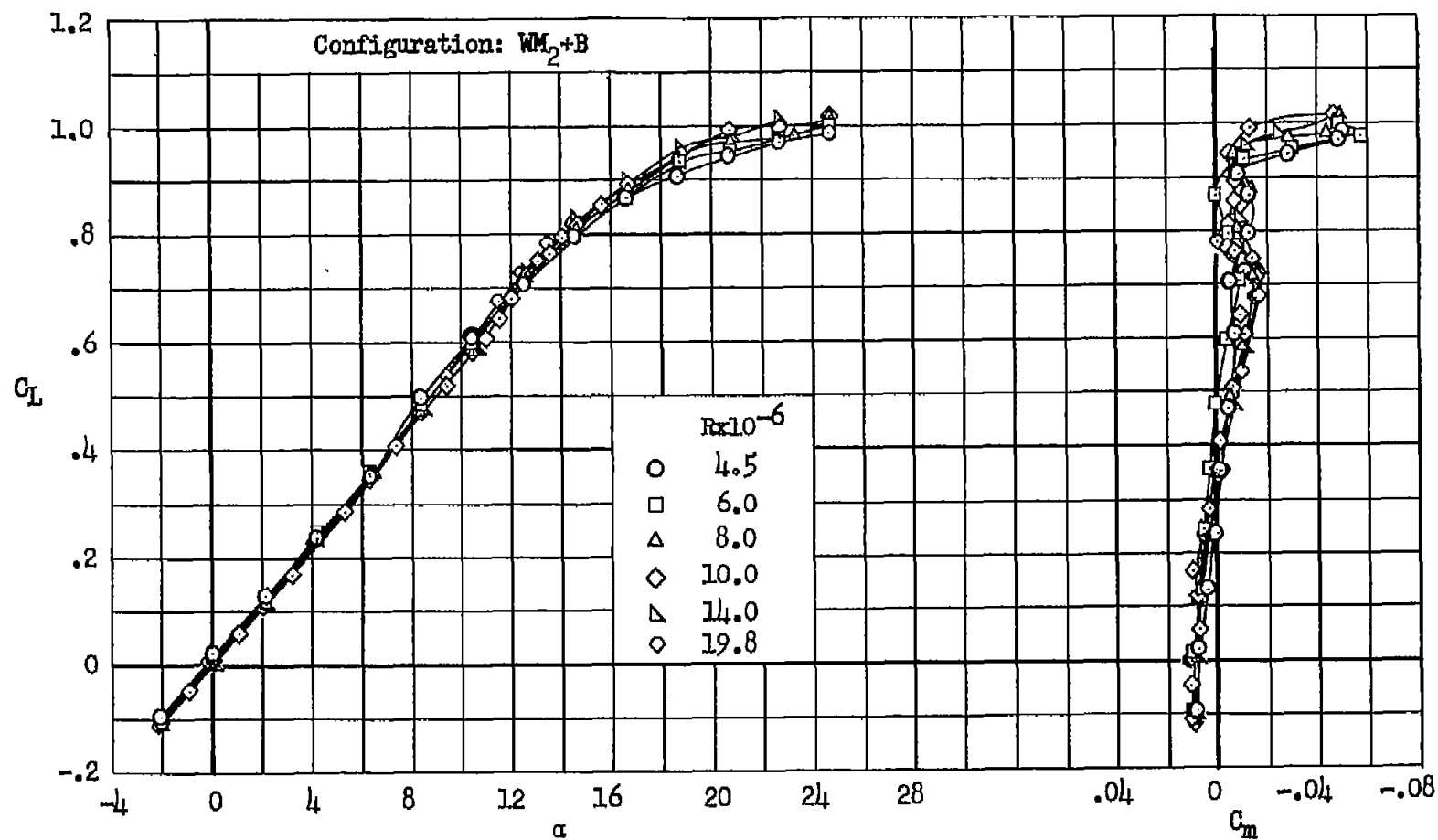
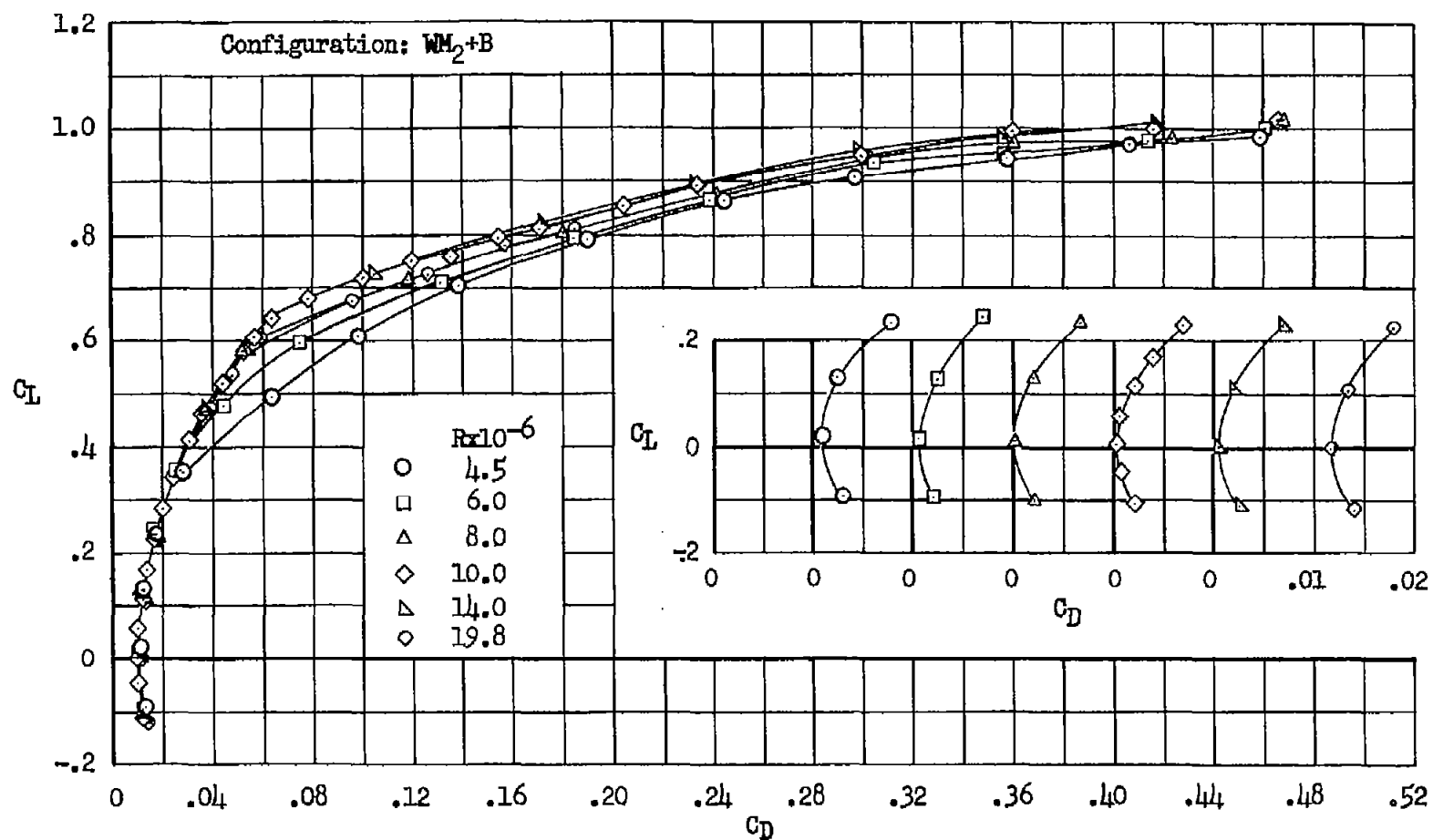
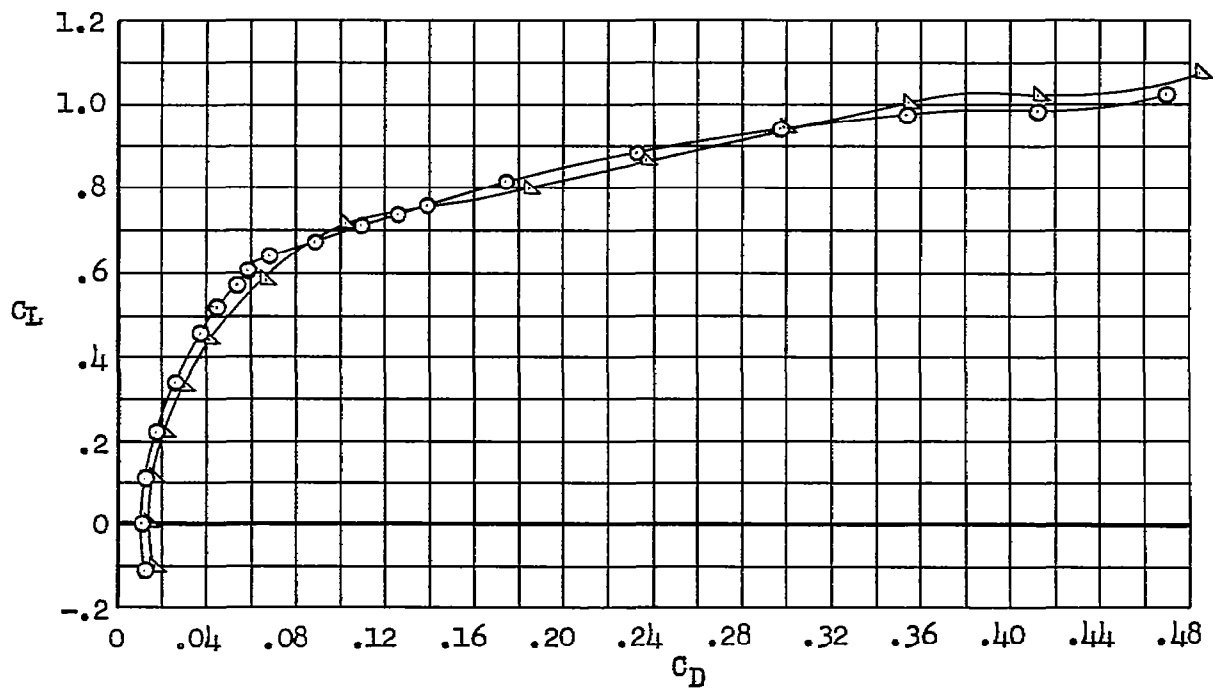
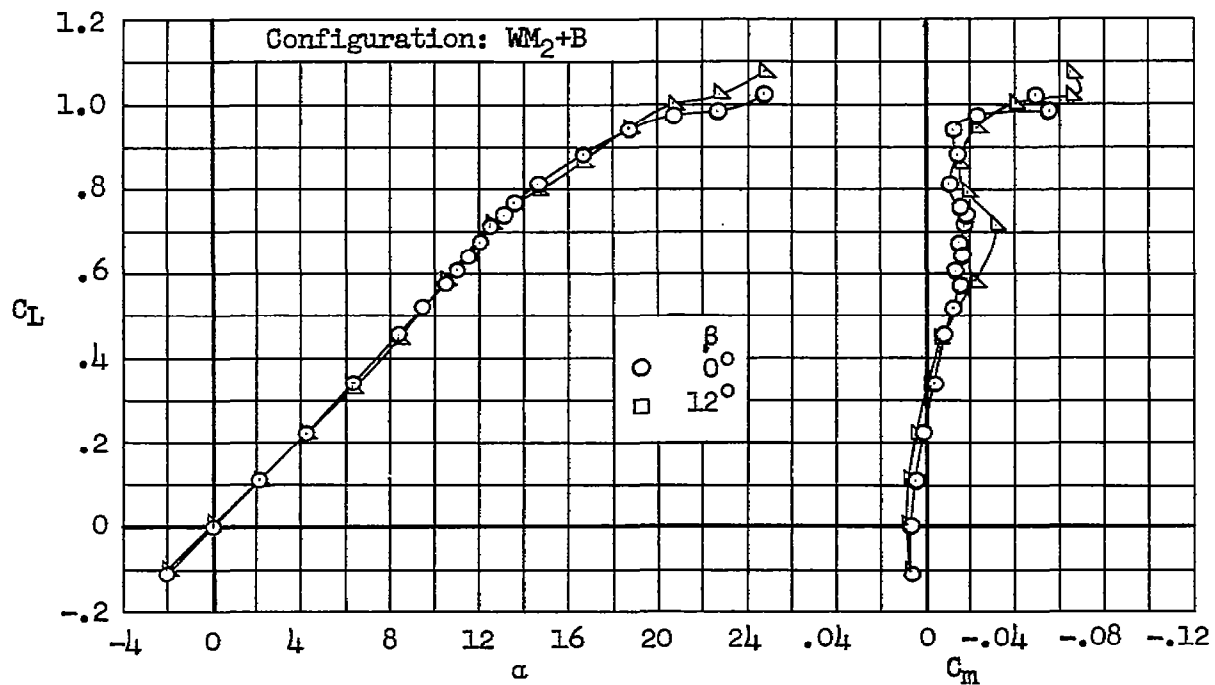
(a) C_L vs. α , C_m

Figure 32.- Wing modification 2; longitudinal characteristics of the wing and body at several Reynolds numbers.



(b) C_L vs. C_D

Figure 32.- Concluded.

(a) C_L vs. α , C_m , C_D Figure 33.- Wing modification 2; characteristics in sideslip of the wing and body, Reynolds number 10×10^6 .

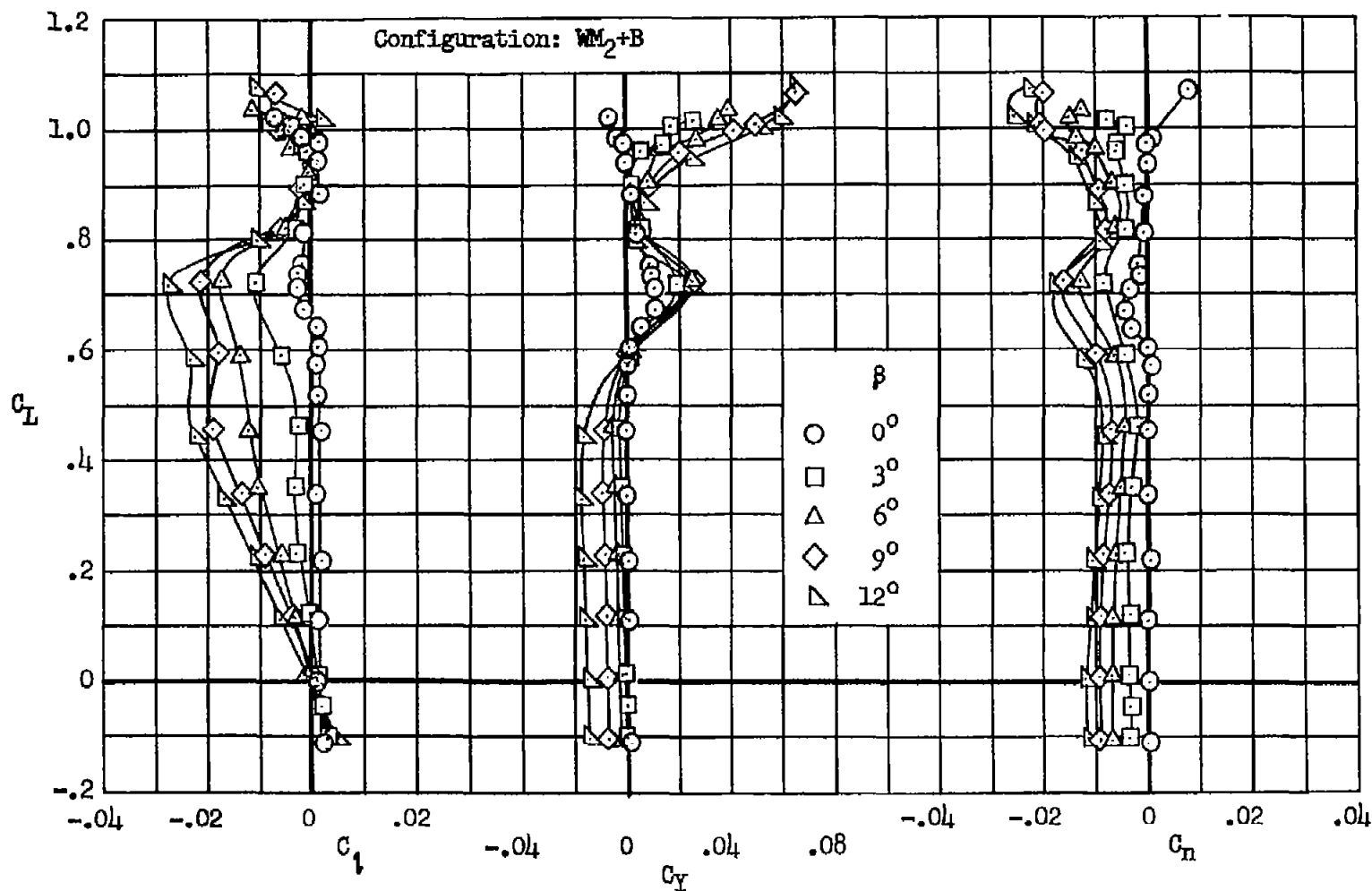
(b) C_L vs. C_D , C_Y , C_N

Figure 33.- Concluded.

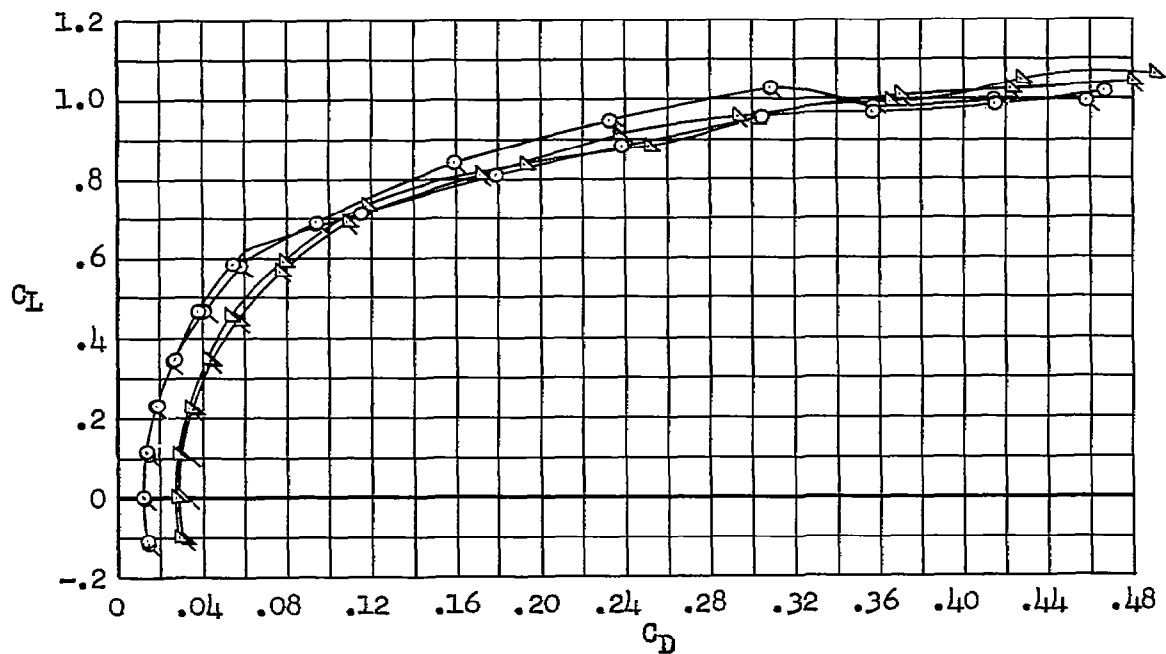
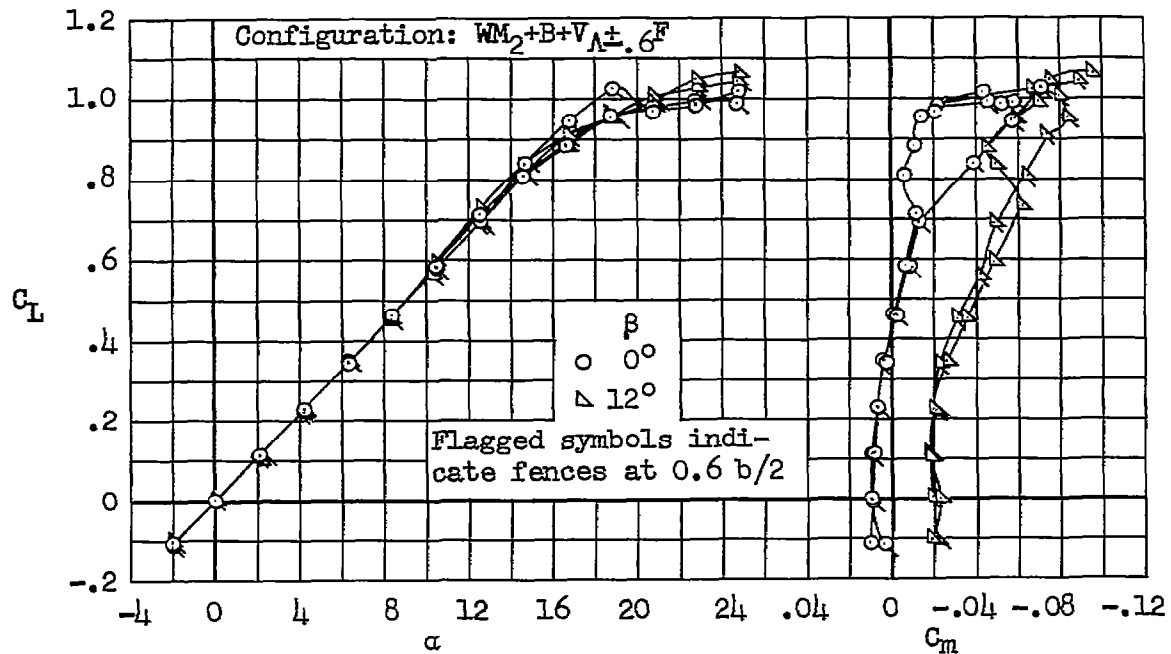
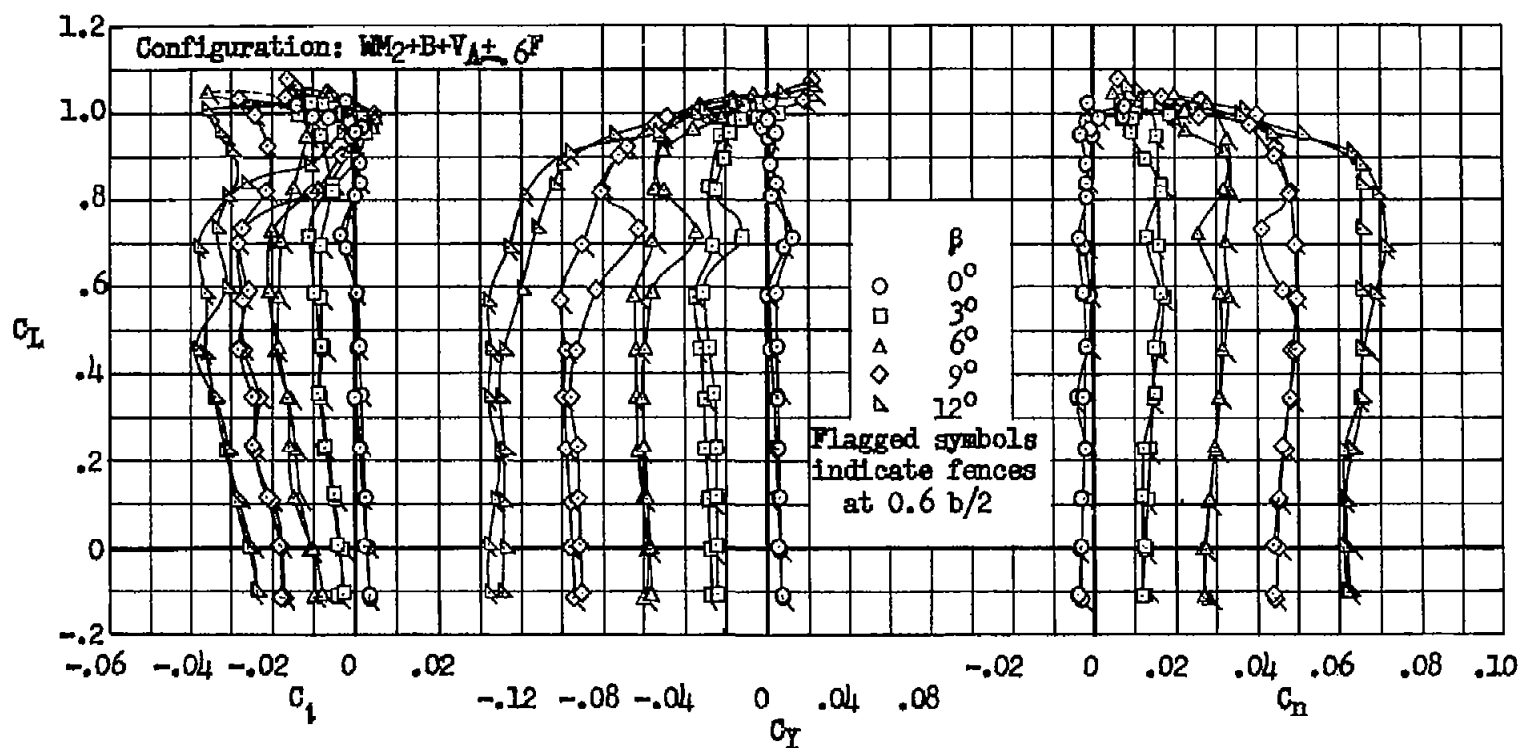
(a) C_L vs. α , C_m , C_D

Figure 34.- Wing modification 2; effect of fences on the characteristics in sideslip of the model with the swept vertical tail, without the horizontal tail; Reynolds number 10×10^6 .



(b) C_L vs. C_D , C_Y , C_N

Figure 34.- Concluded.

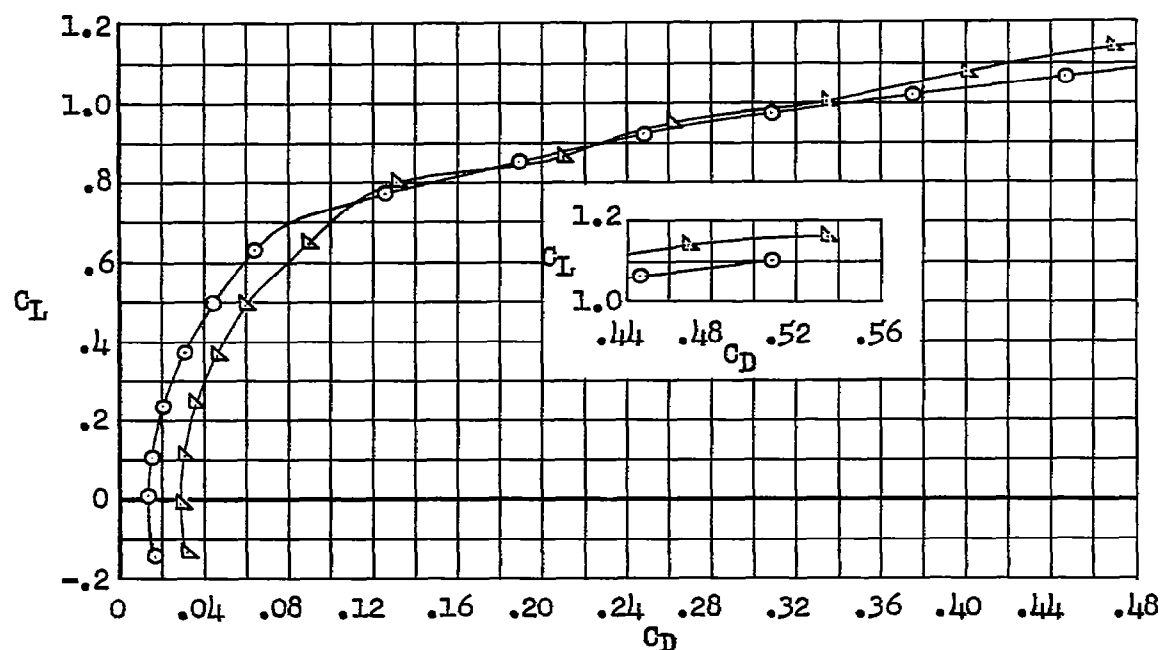
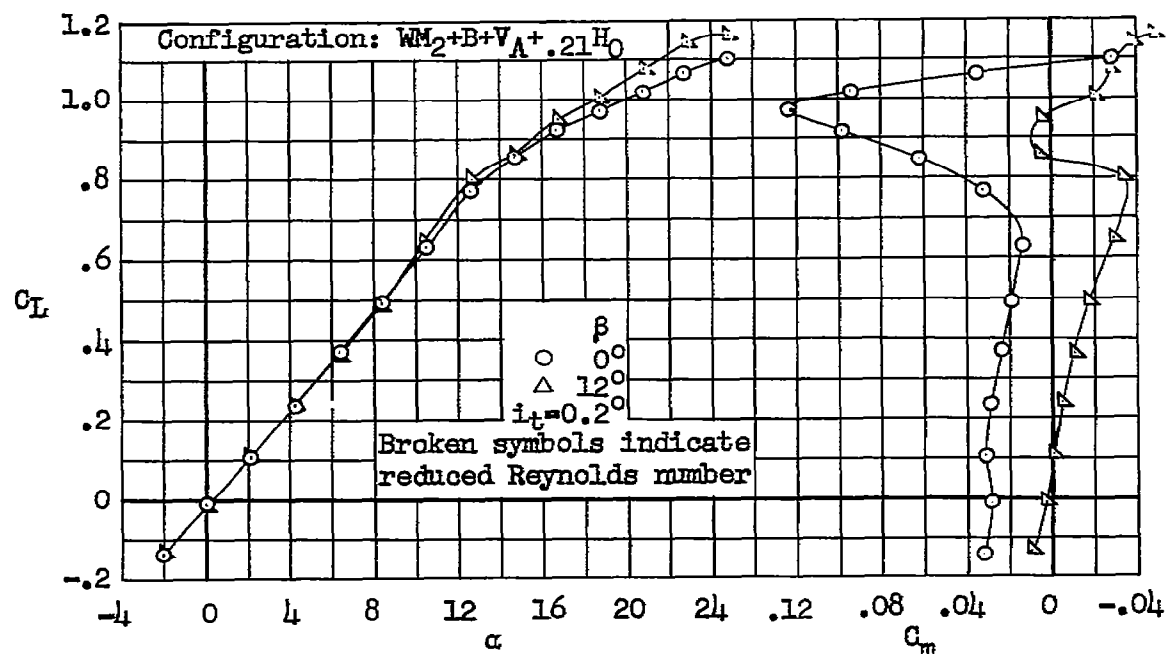
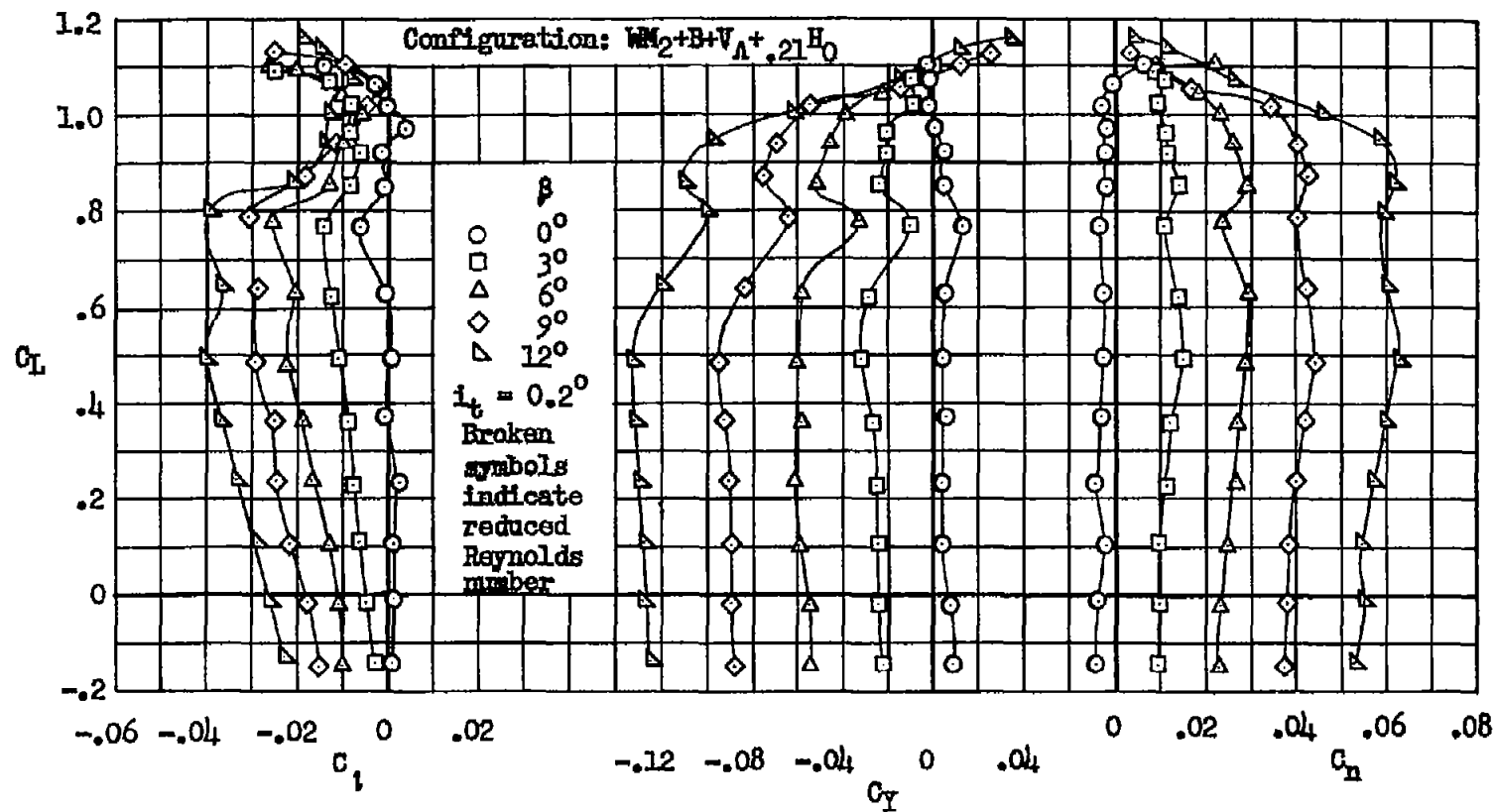
(a) C_L vs. α , C_m , C_D

Figure 35.- Wing modification 2; characteristics in sideslip of the model with the horizontal tail mounted on the swept vertical tail at $z/(b/2) = 0.21$, moment center at $0.35\bar{c}$, Reynolds numbers 10 and 8×10^6 .



(b) C_L vs. C_D , C_Y , C_N

Figure 35.- Concluded.

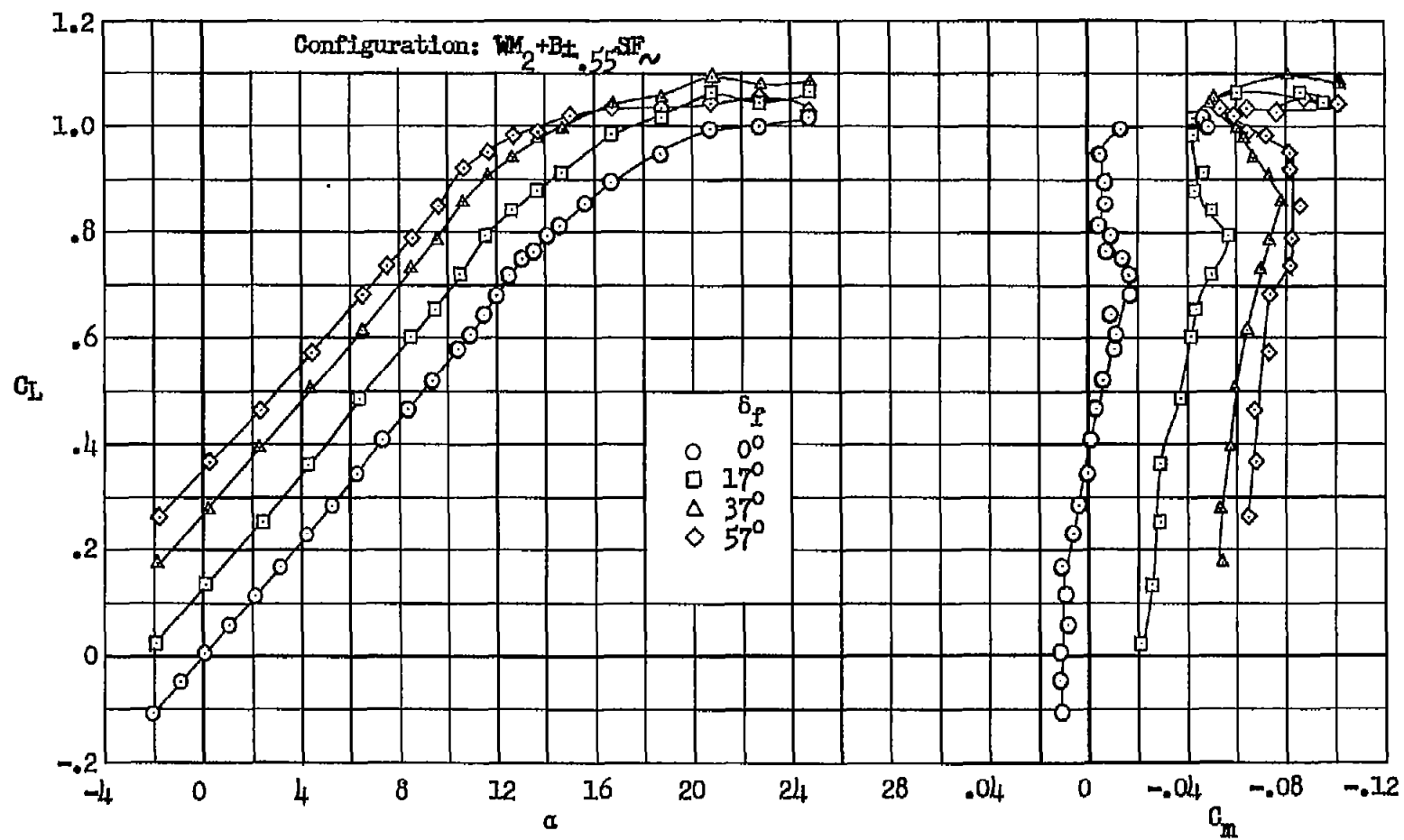
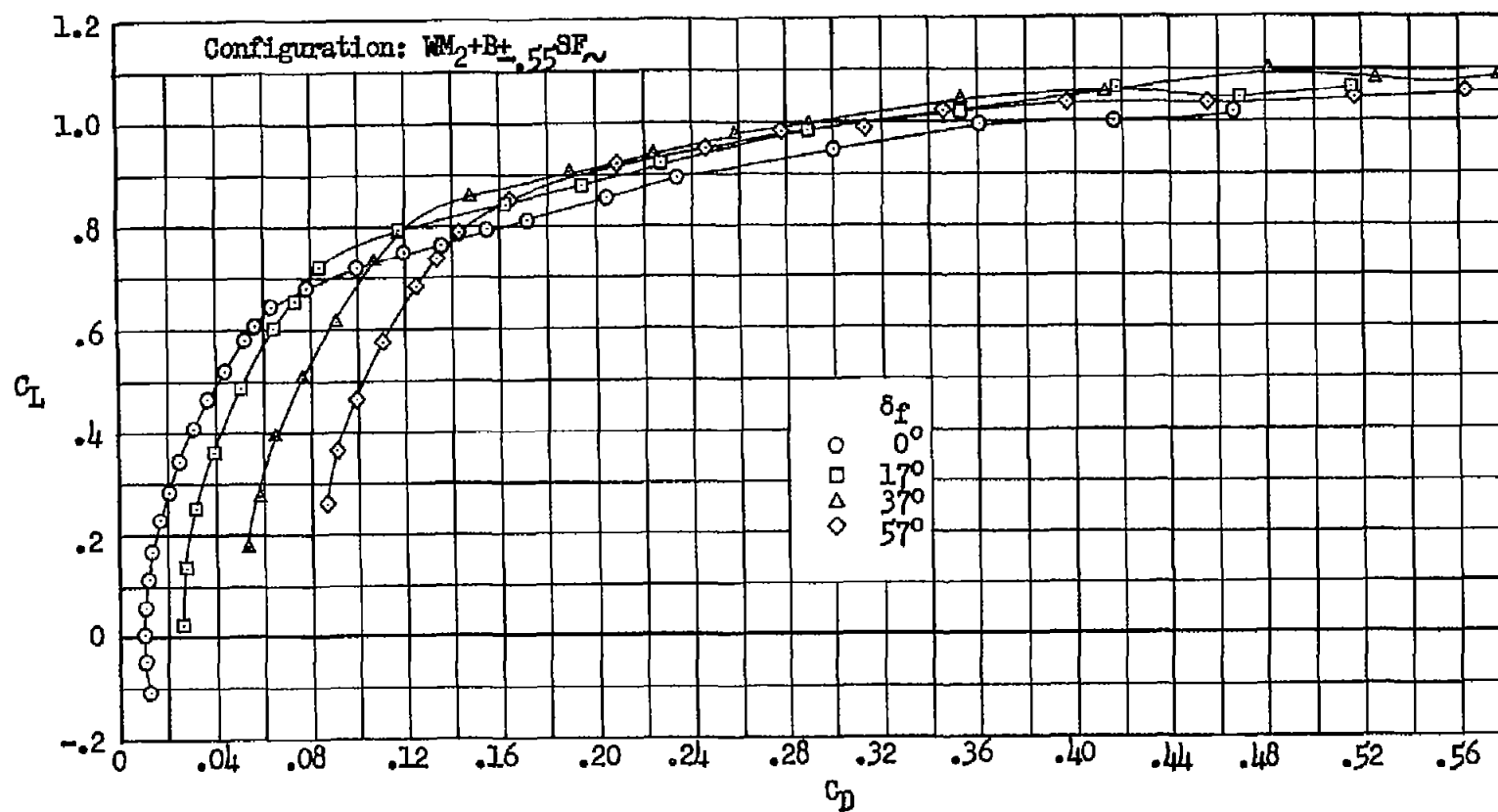
(a) C_L vs. α , C_m

Figure 36.- Wing modification 2; effect of split flaps of span $0.55 b/2$ on the longitudinal characteristics of the wing and body, Reynolds number 10×10^6 .



(b) C_L vs. C_D

Figure 36.- Concluded.

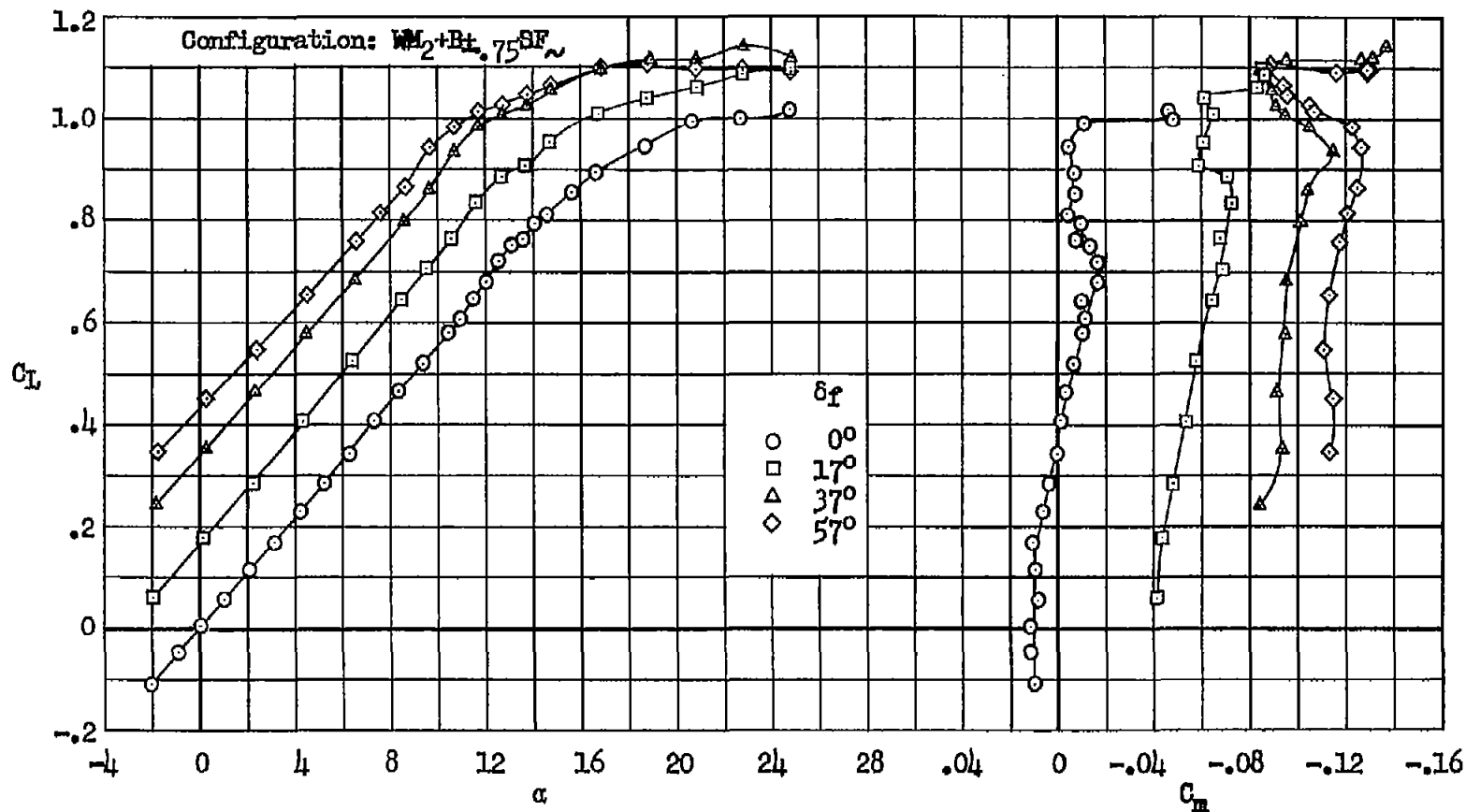
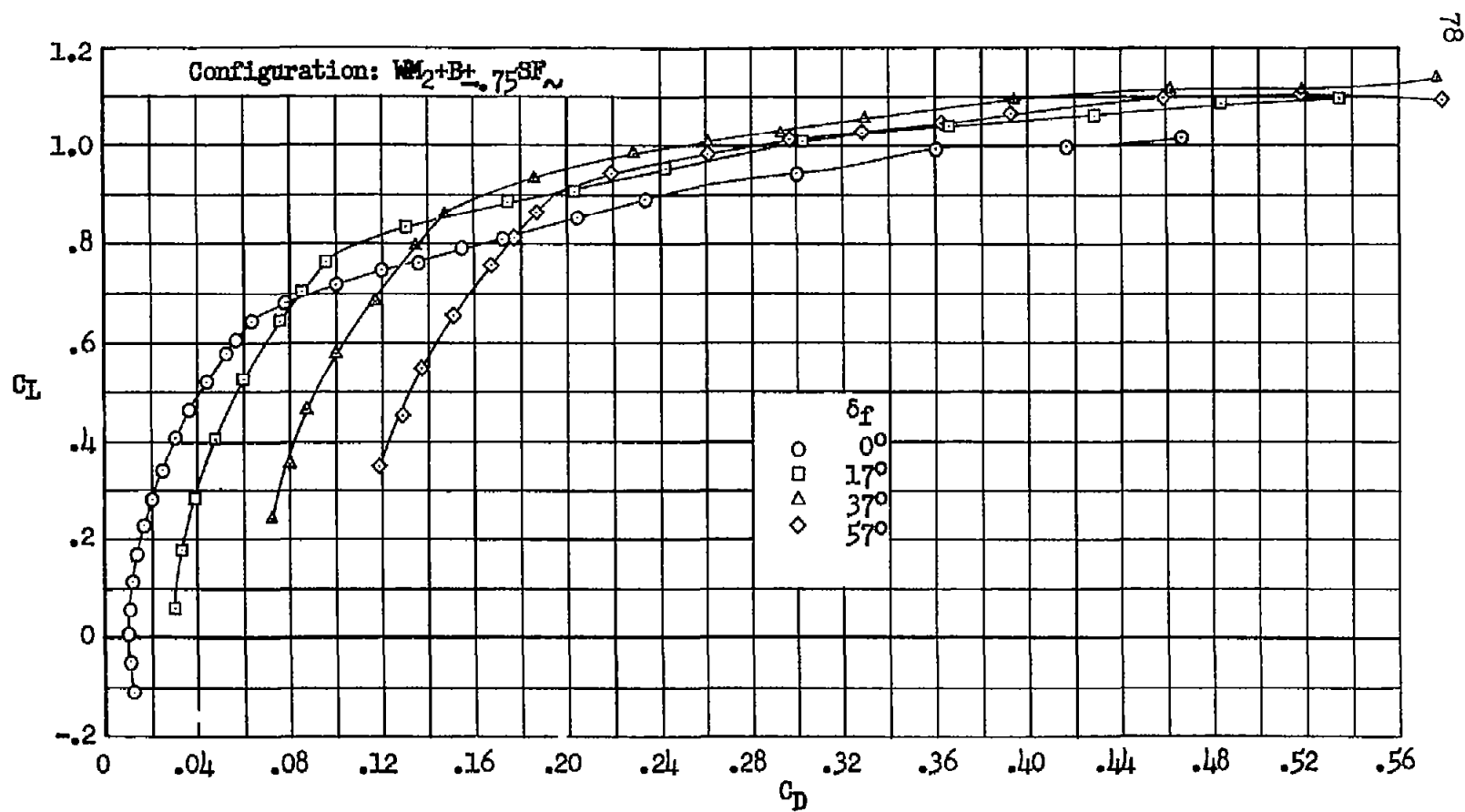
(a) C_L vs. α , C_m

Figure 37.- Wing modification 2; effect of split flaps of span $0.75 b/2$ on the longitudinal characteristics of the wing and body, Reynolds number 10×10^6 .



(b) C_L vs. C_D

Figure 37.- Concluded.

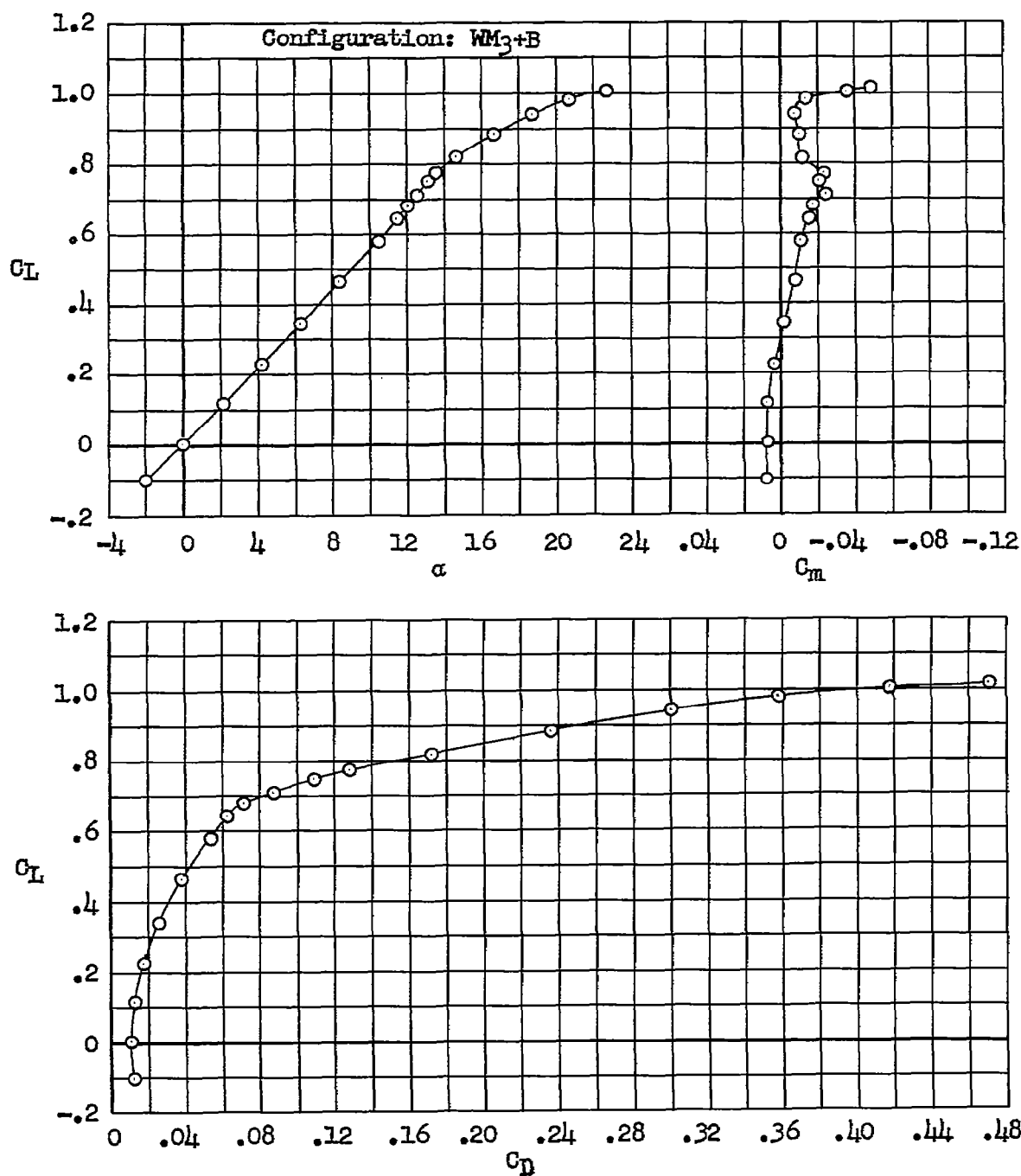


Figure 38.- Wing modification 3; longitudinal characteristics of the wing and body at a Reynolds number of 10×10^6 .

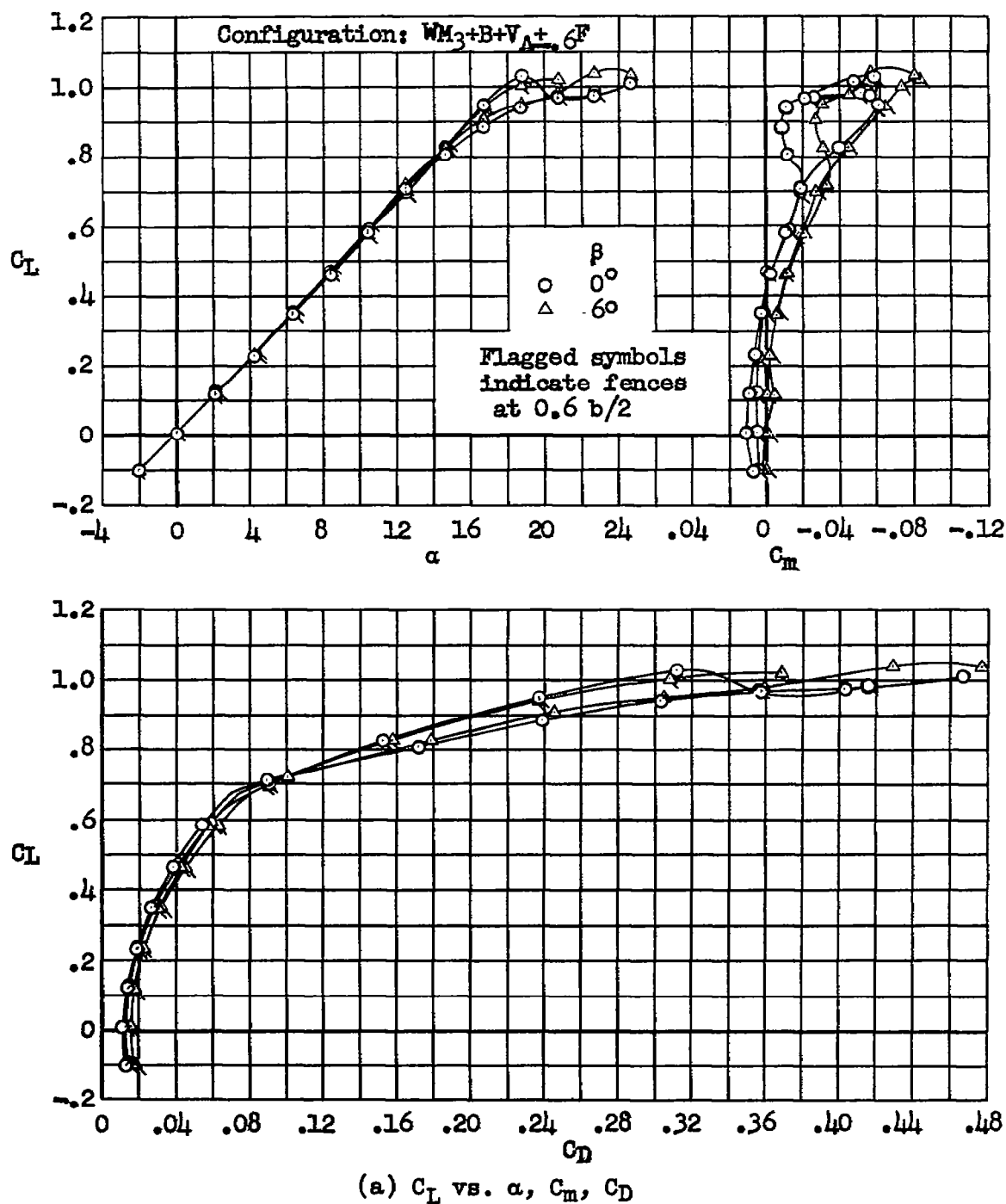


Figure 39.- Wing modification 3; effect of fences on the characteristics in sideslip of the model with the swept vertical tail, without the horizontal tail; Reynolds number 10×10^6 .

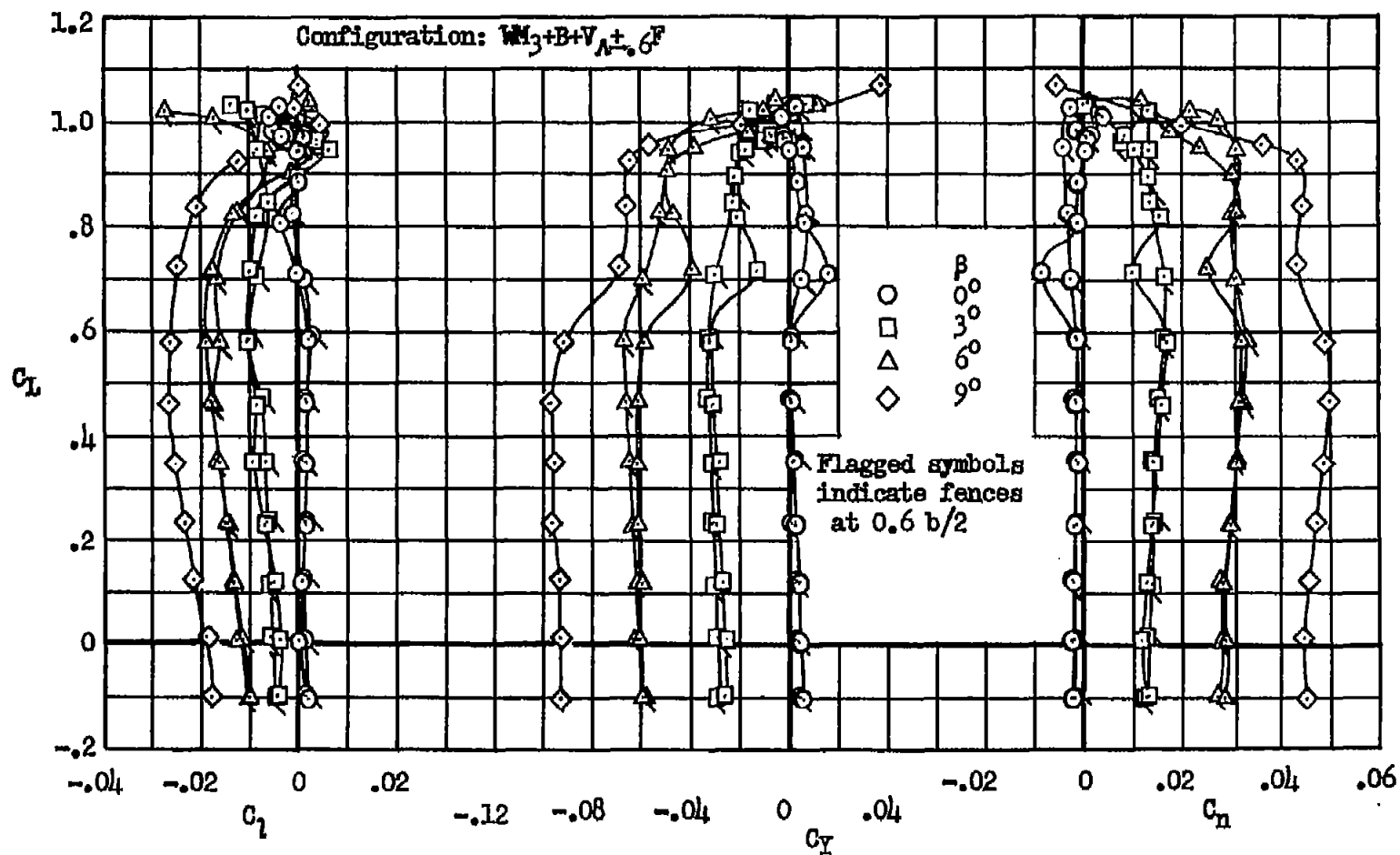
(b) C_L vs. C_D , C_Y , C_N

Figure 39.- Concluded.

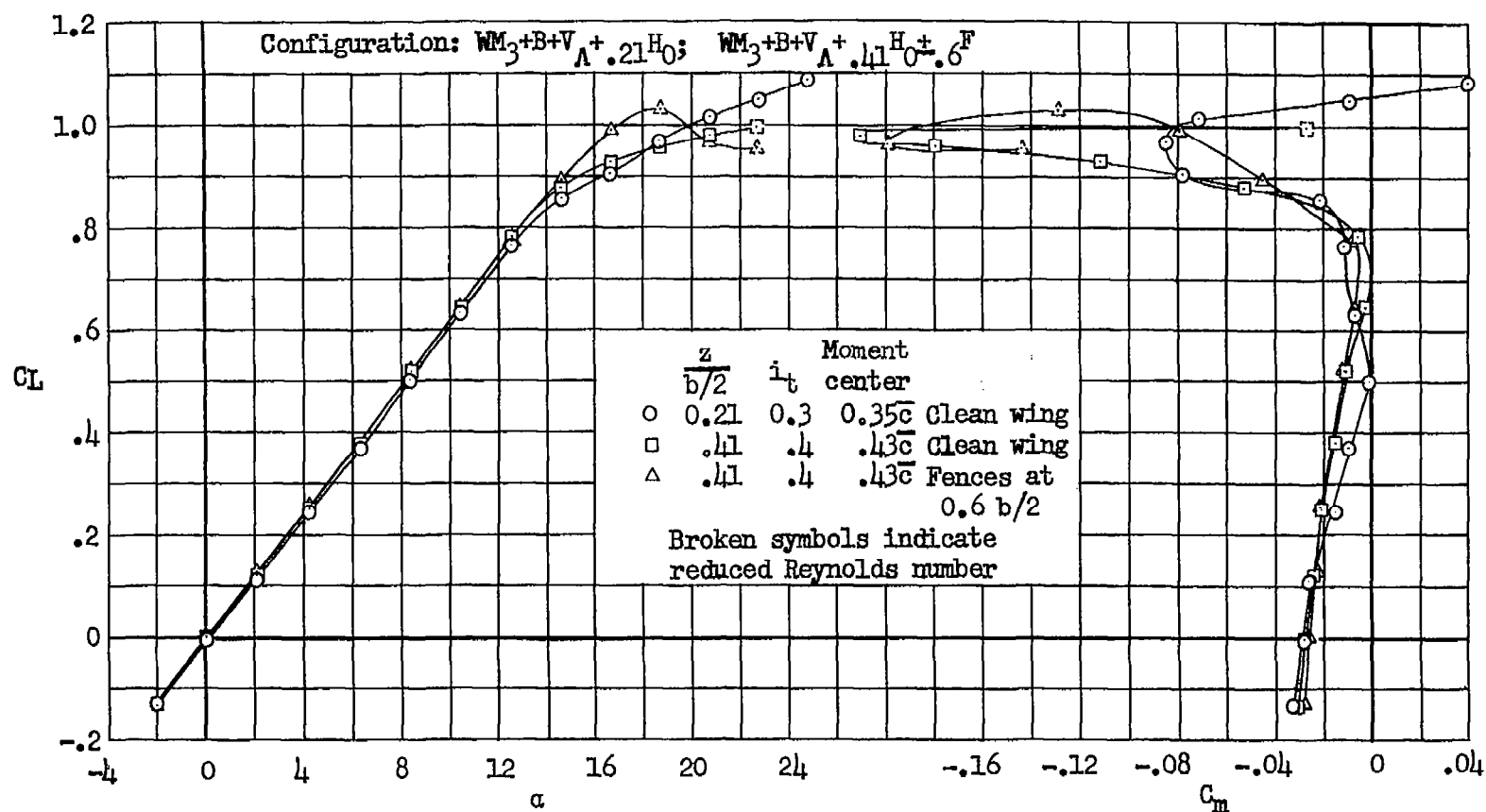
(a) C_L vs. α , C_m

Figure 40.- Wing modification 3; effect of two positions of the horizontal tail, in conjunction with the swept vertical tail, on the longitudinal characteristics of the model, and effect of fences for the higher position of the horizontal tail; Reynolds numbers 10 and 8×10^6 .

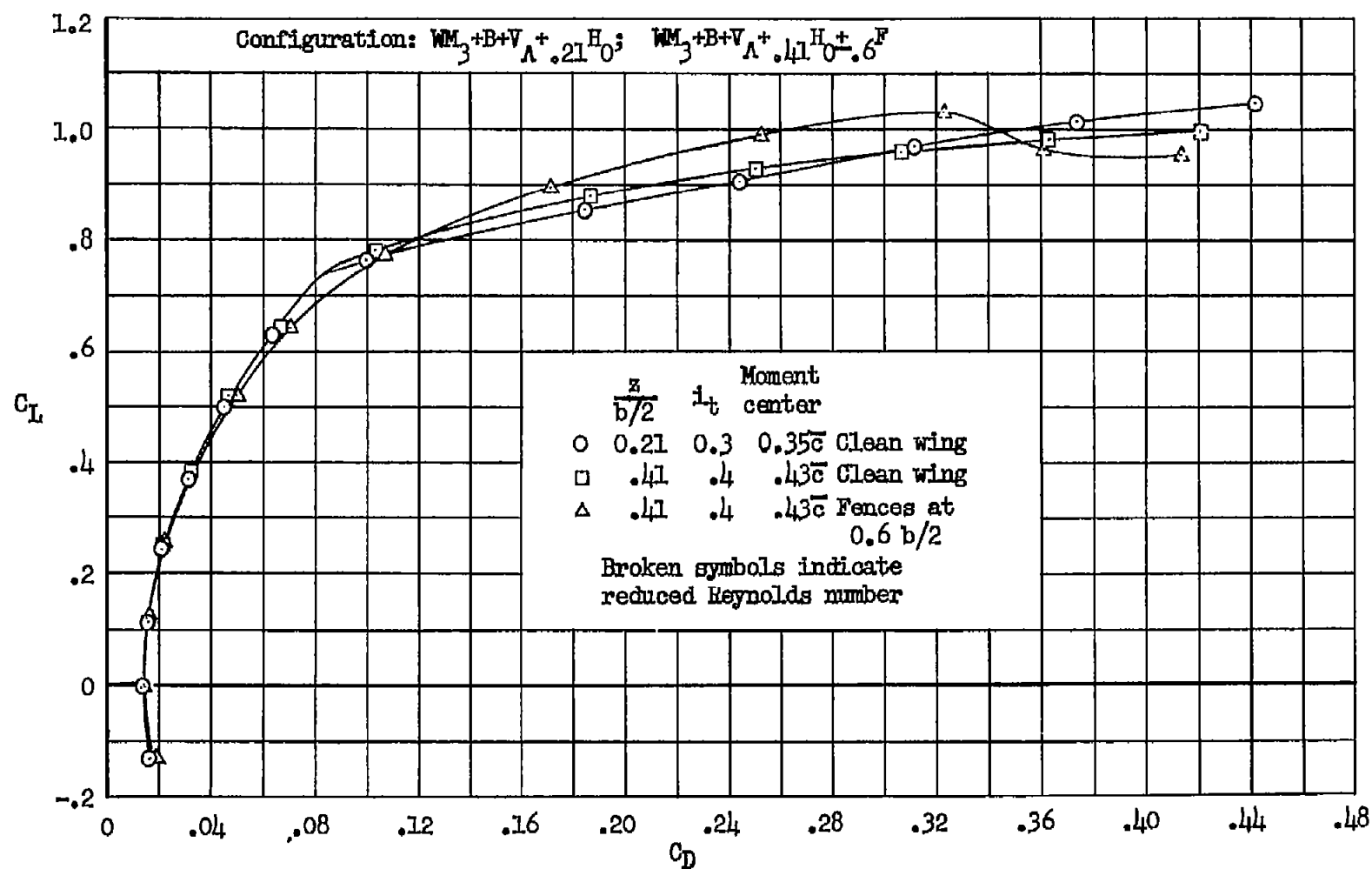
(b) C_L vs. C_D

Figure 40.- Concluded.

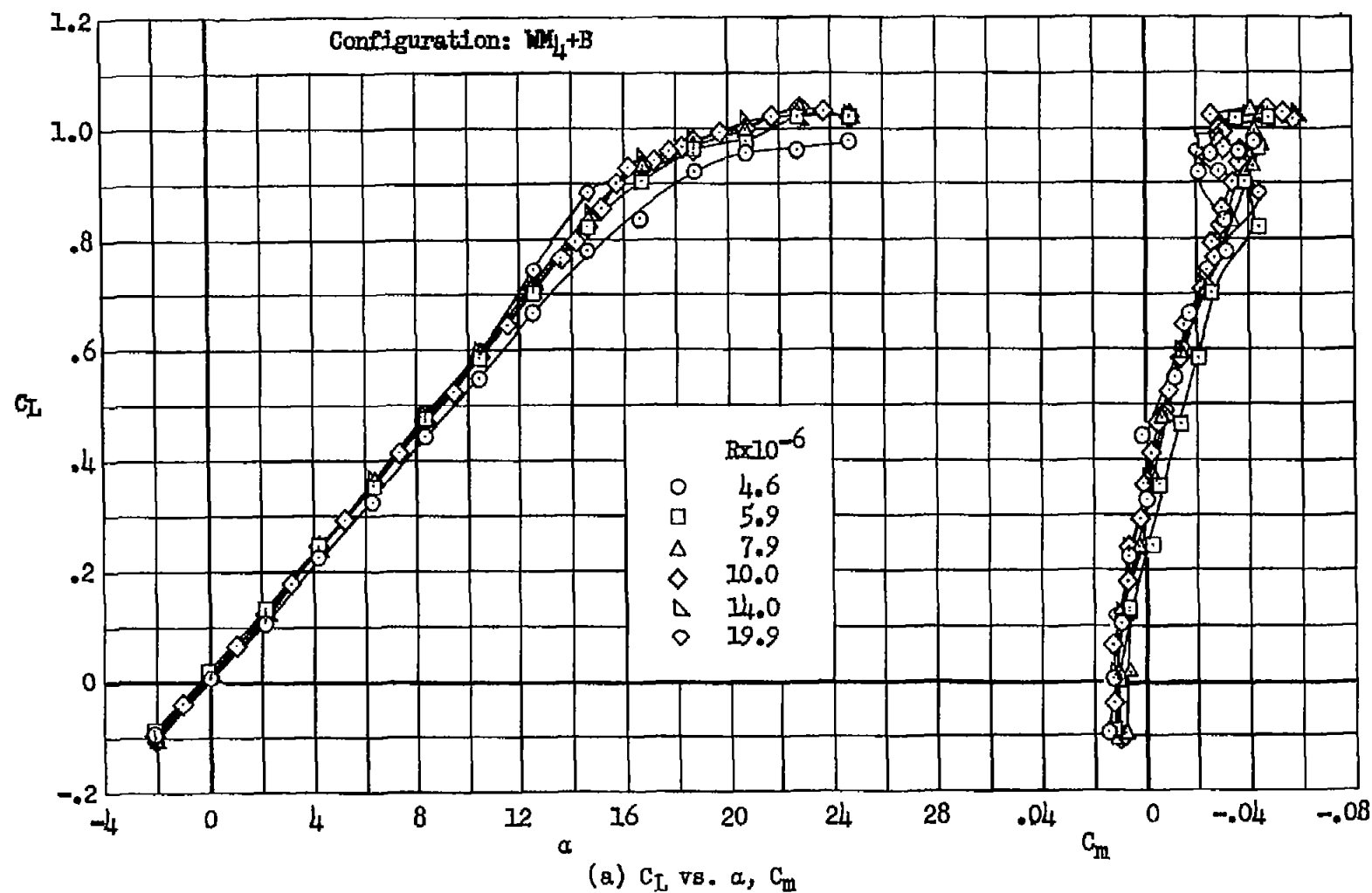
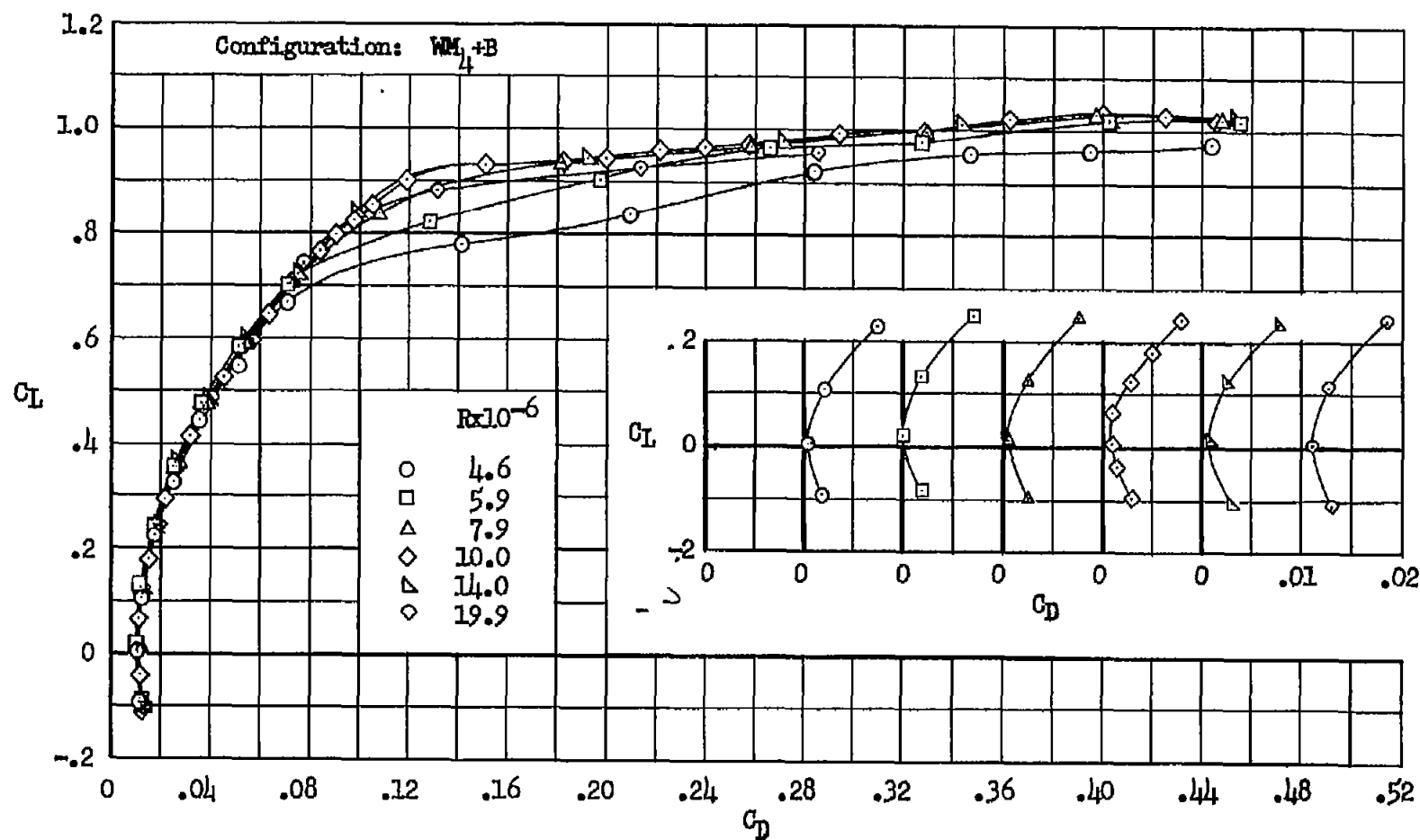


Figure 41.- Wing modification 4; longitudinal characteristics of the wing and body at several Reynolds numbers.



(b) C_L vs. C_D

Figure 41.- Concluded.

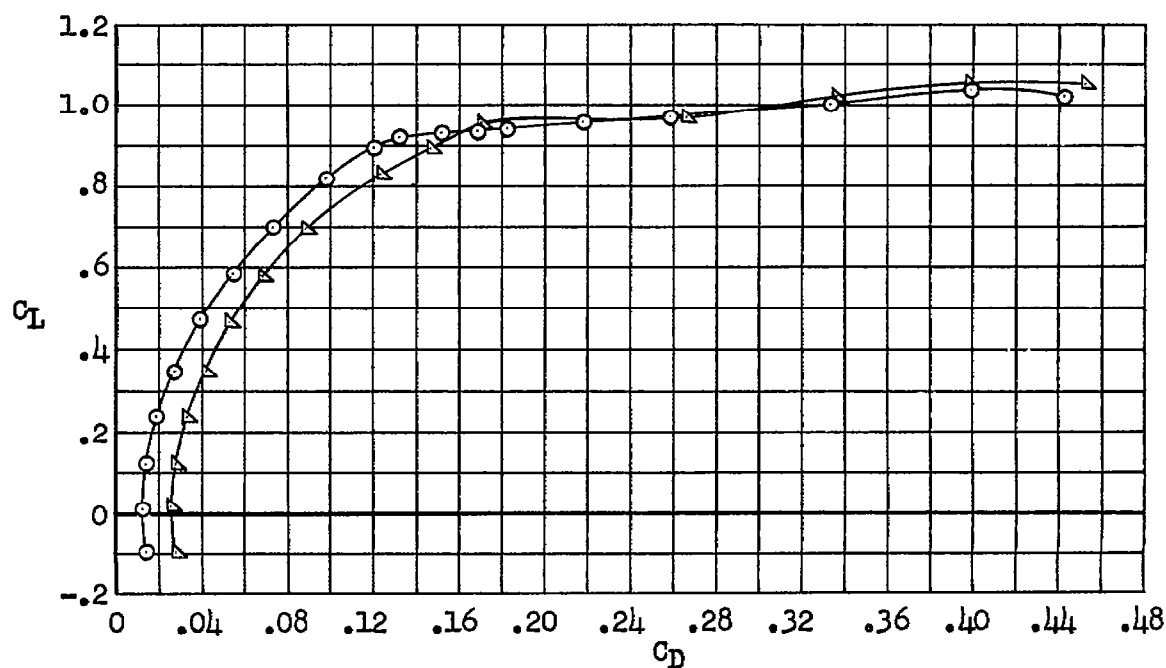
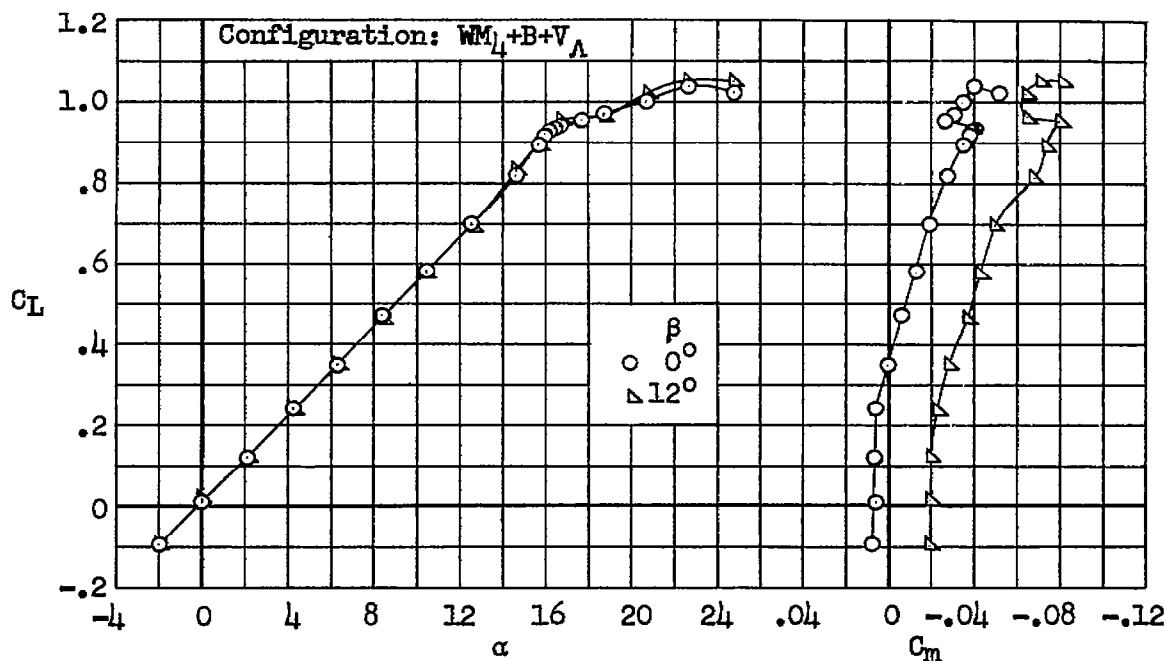
(a) C_L vs. α , C_m , C_D

Figure 42.- Wing modification 4; characteristics in sideslip of the model with the swept vertical tail, without the horizontal tail; Reynolds number 10×10^6 .

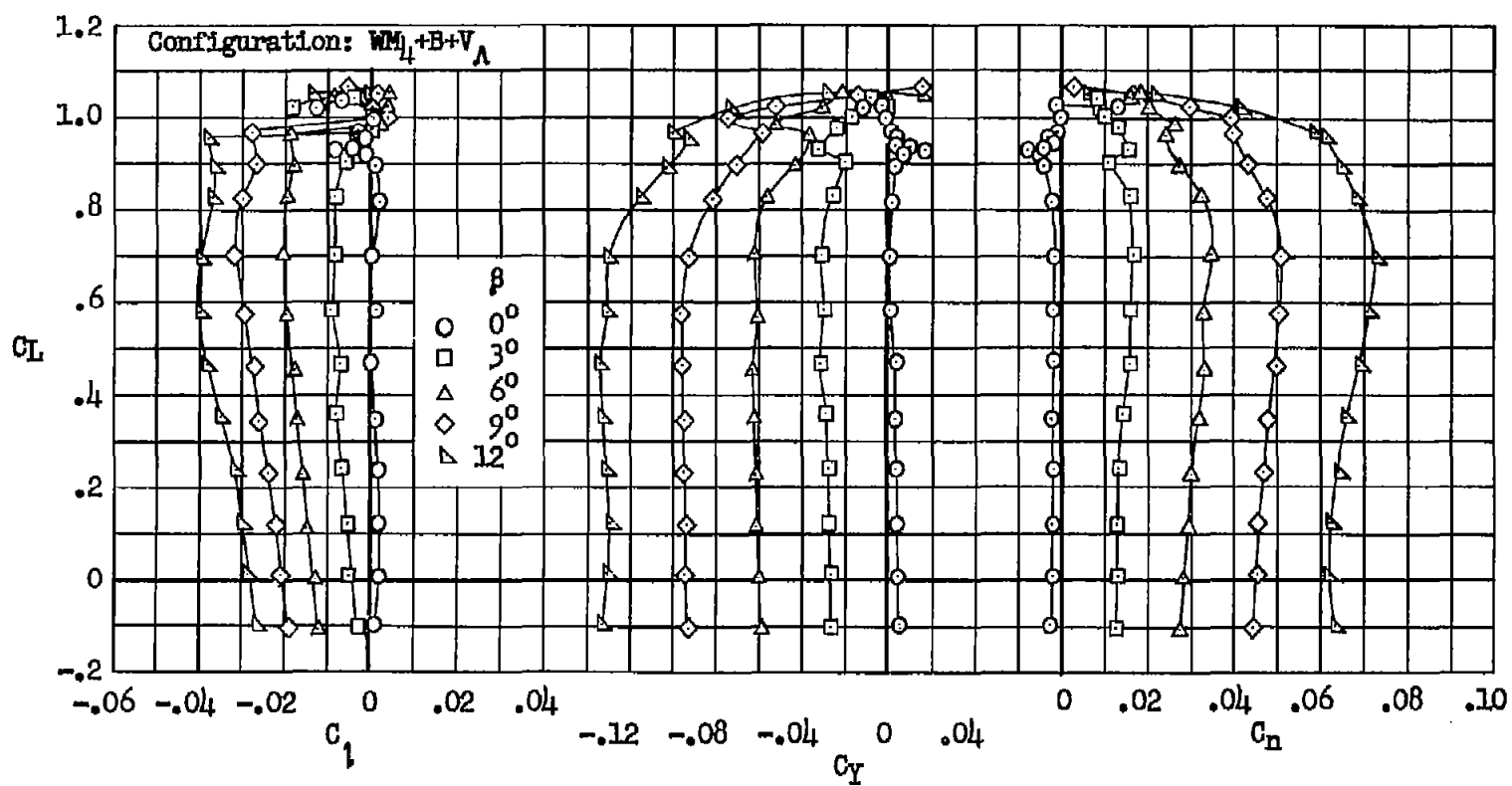
(b) C_L vs. C_1 , C_Y , C_N

Figure 42.- Concluded.

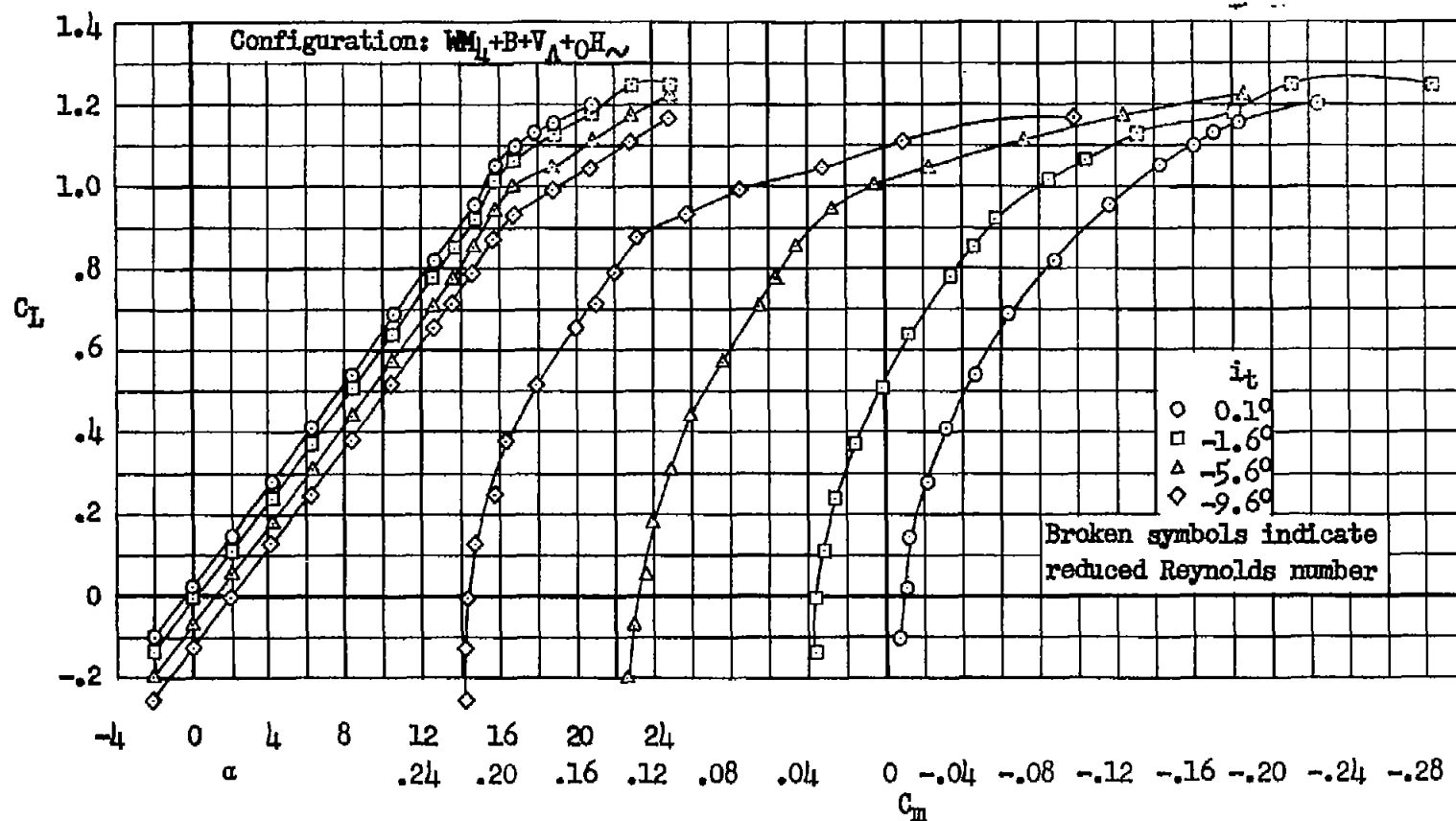
(a) C_L vs. α , C_m

Figure 43.- Wing modification 4; longitudinal characteristics of the model with the horizontal tail in the wing chord plane, moment center at $0.34\bar{c}$, Reynolds numbers 10 and 8×10^6 .

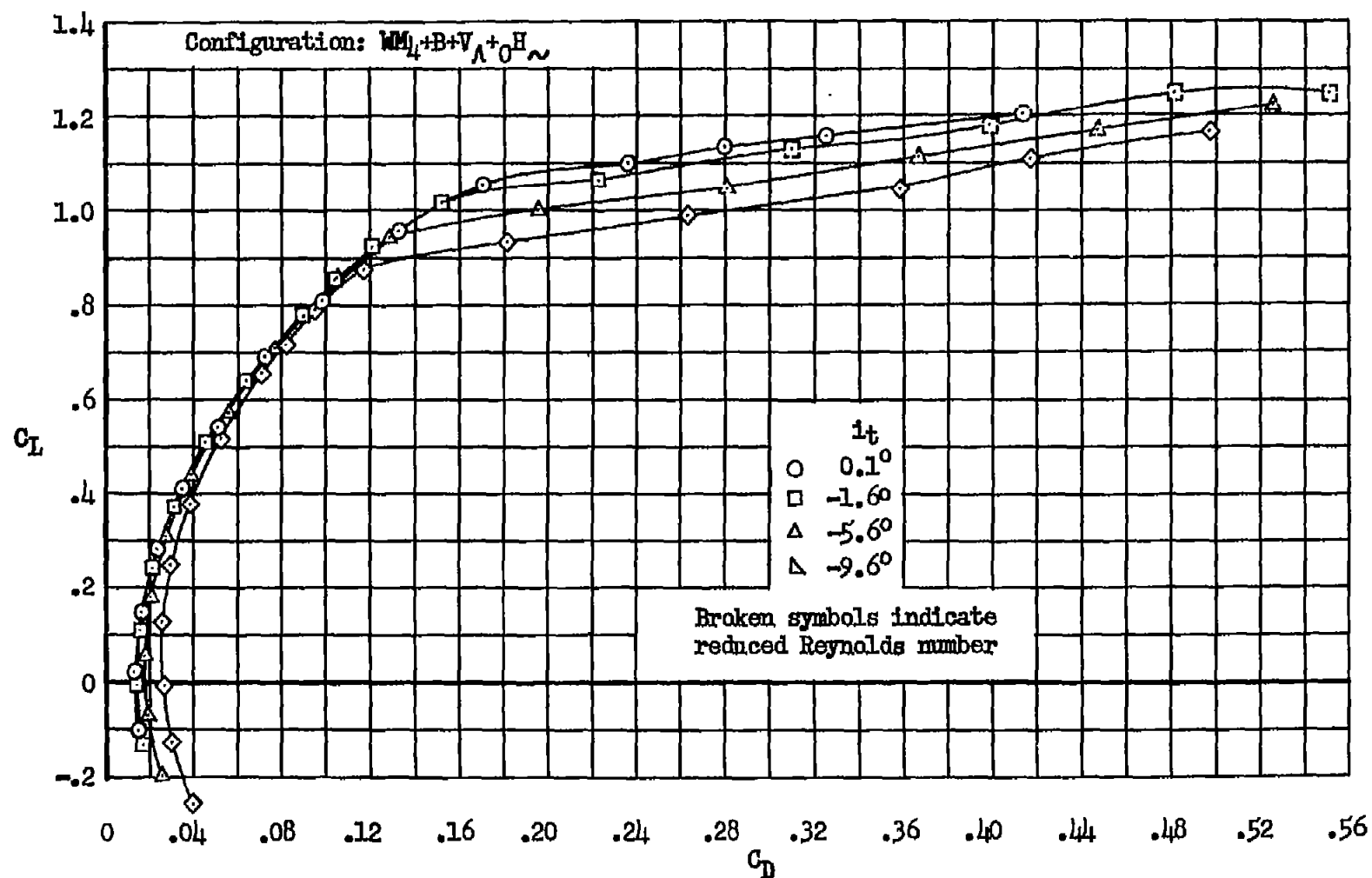
(b) C_L vs. C_D

Figure 43.- Concluded.

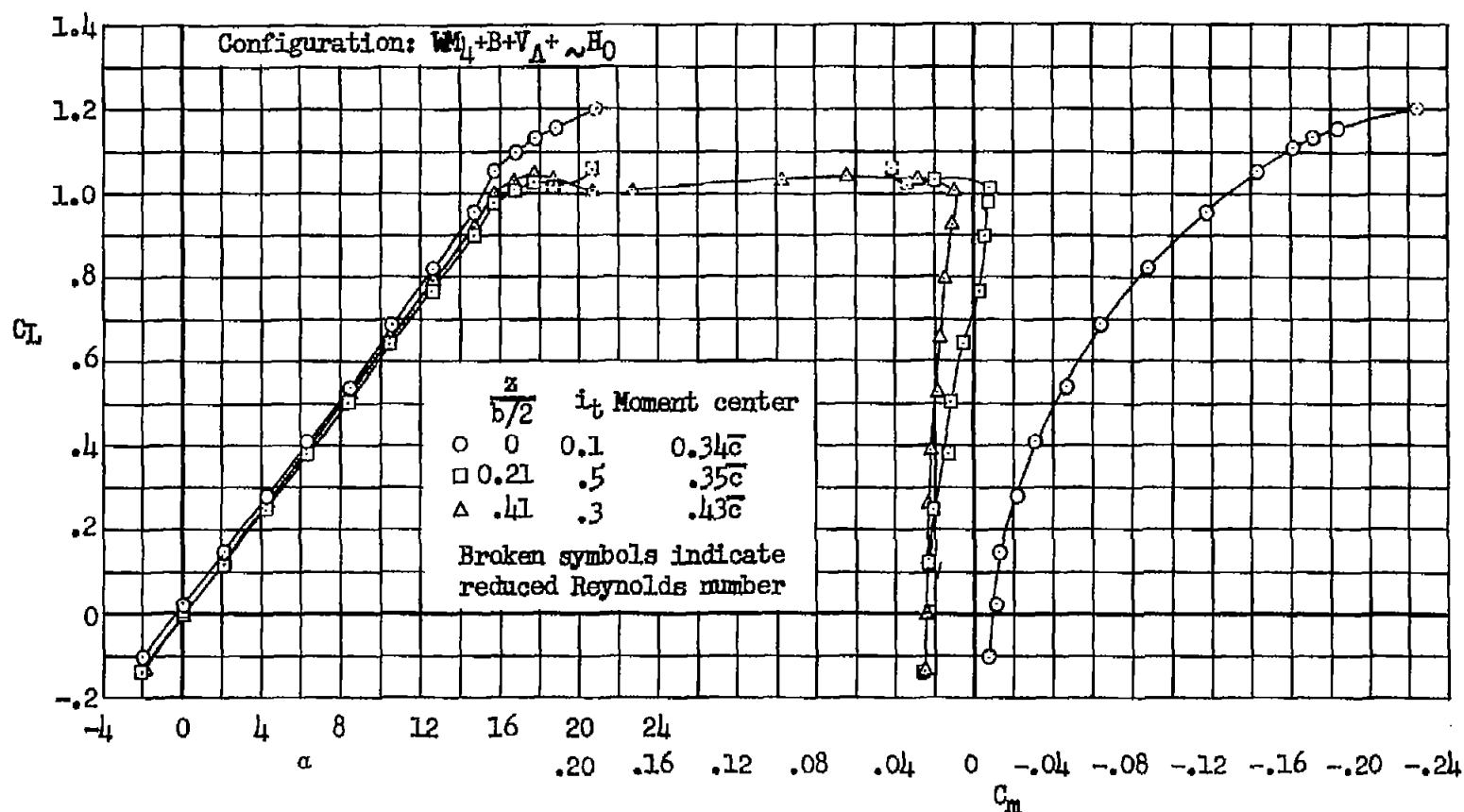
(a) C_L vs. α , C_m

Figure 44.- Wing modification 4; effect of the position of the horizontal tail, in conjunction with the swept vertical tail, on the longitudinal characteristics of the model; Reynolds numbers 10 and 8×10^6 .

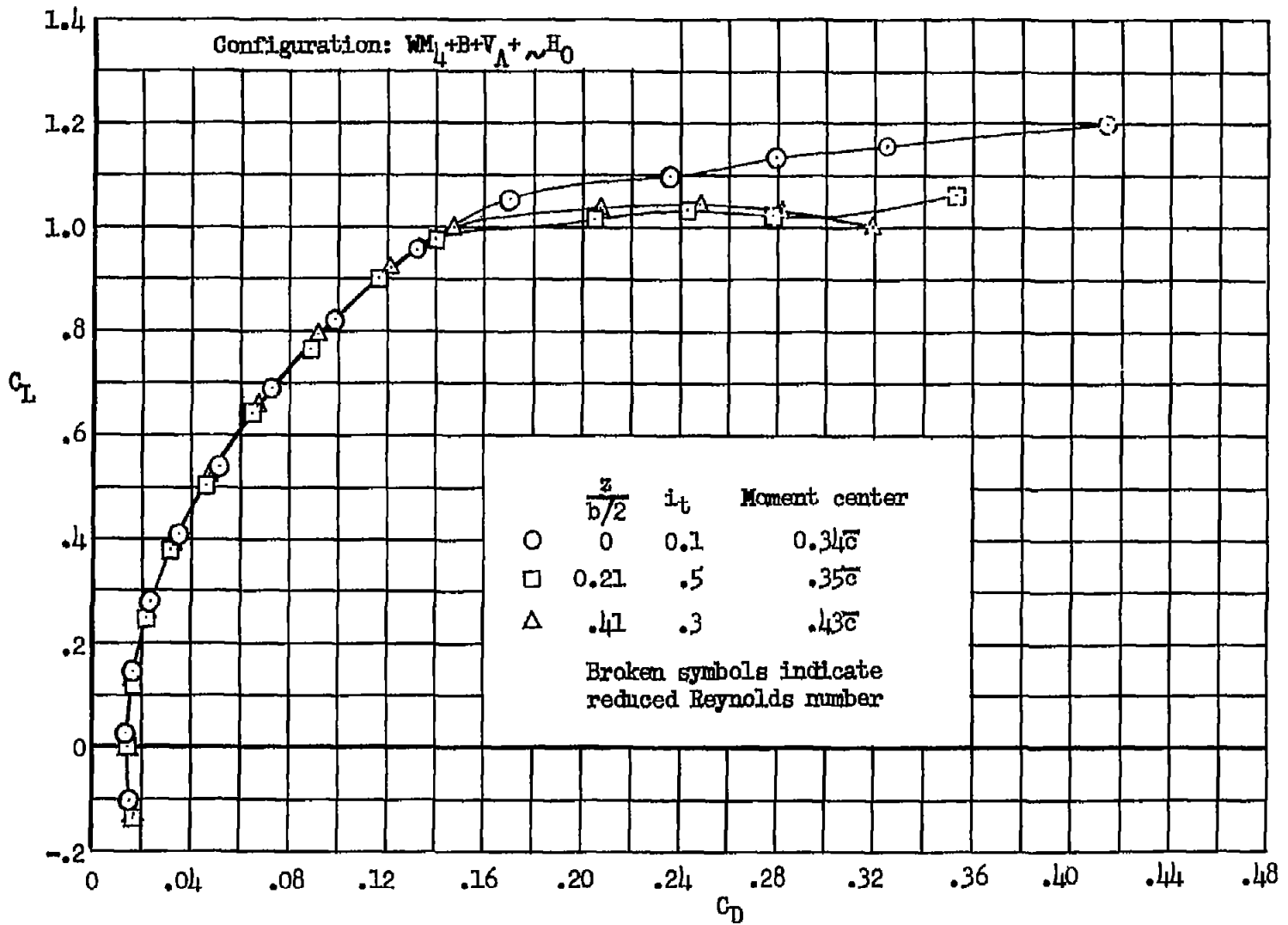
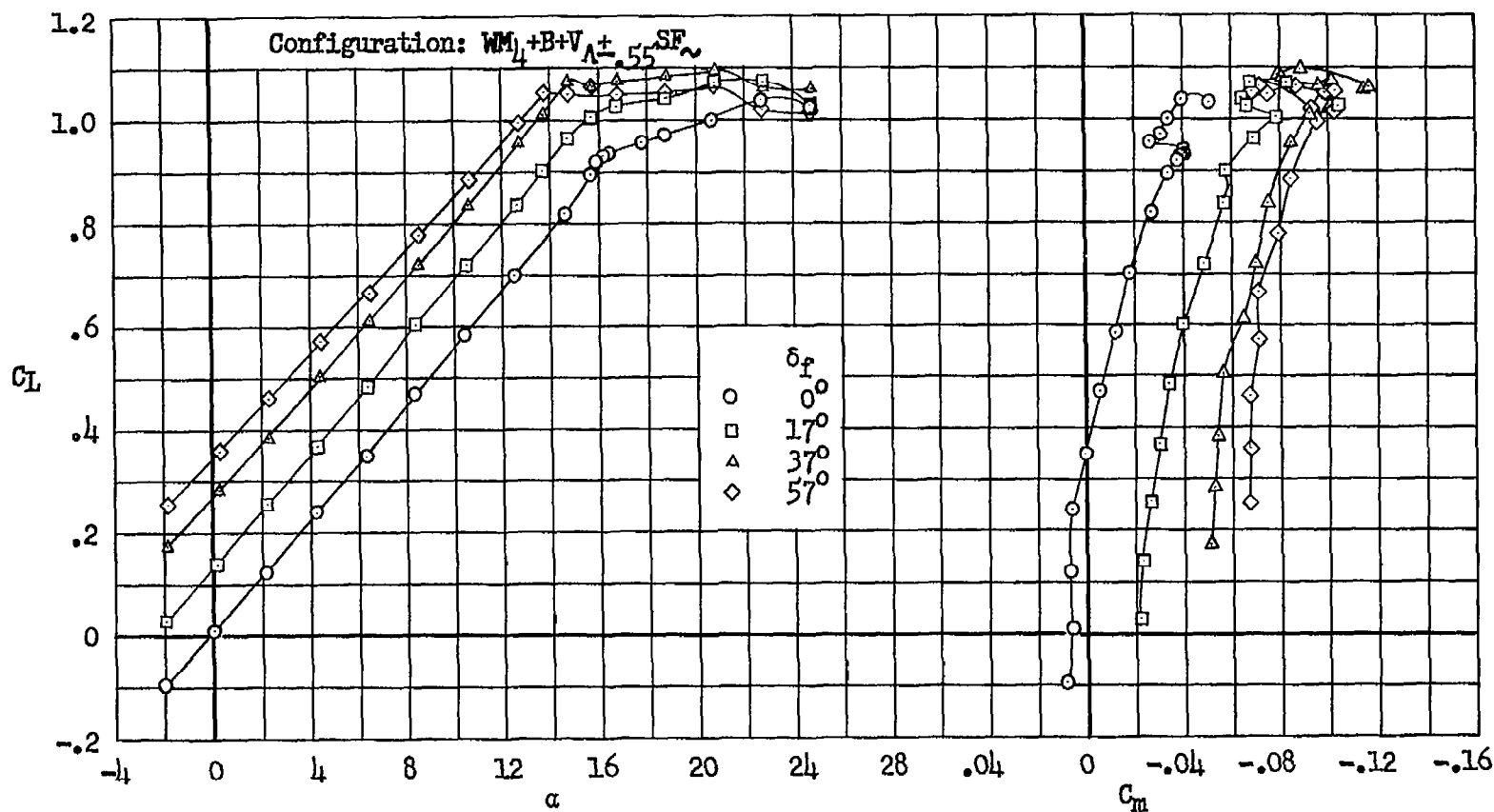
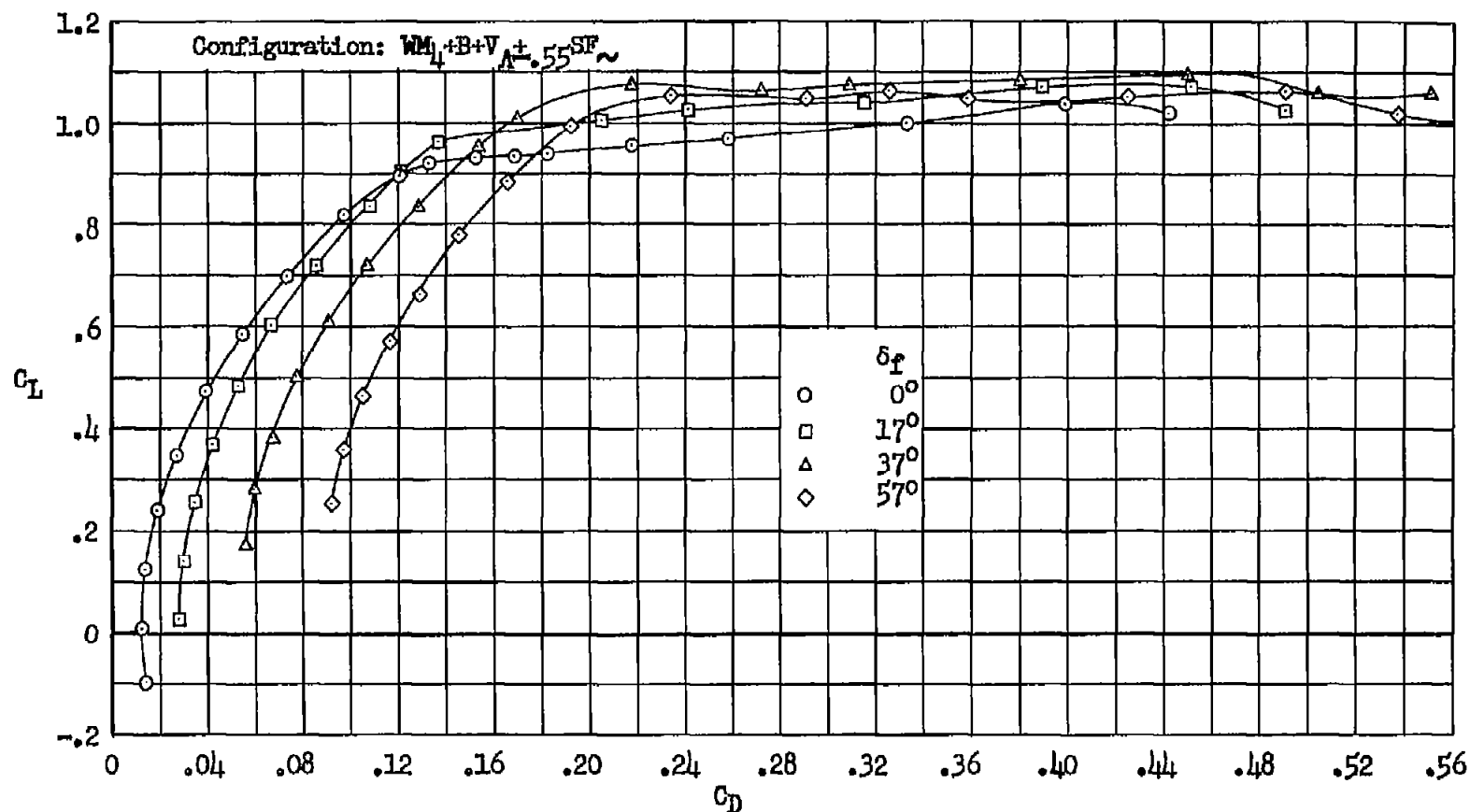
(b) C_L vs. C_D

Figure 44.- Concluded.



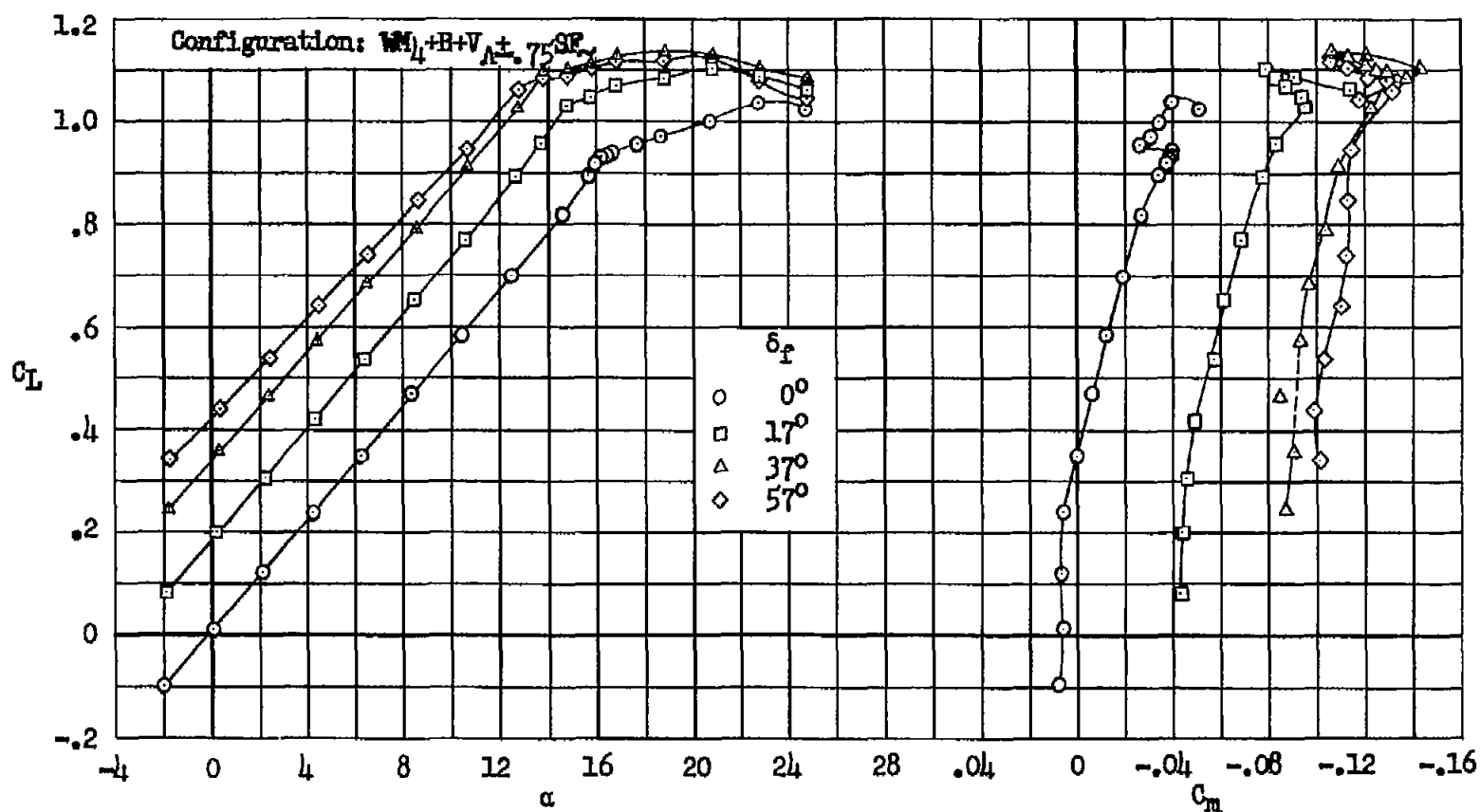
(a) C_L vs. α , C_m

Figure 45.- Wing modification 4; effect of split flaps of span $0.55 b/2$ on the longitudinal characteristics of the model without the horizontal tail, Reynolds number 10×10^6 .



(b) C_L vs. C_D

Figure 45.- Concluded.



(a) C_L vs. α , C_m

Figure 46.- Wing modification 4; effect of split flaps of span $0.75 b/2$ on the longitudinal characteristics of the model without the horizontal tail, Reynolds number 10×10^6 .

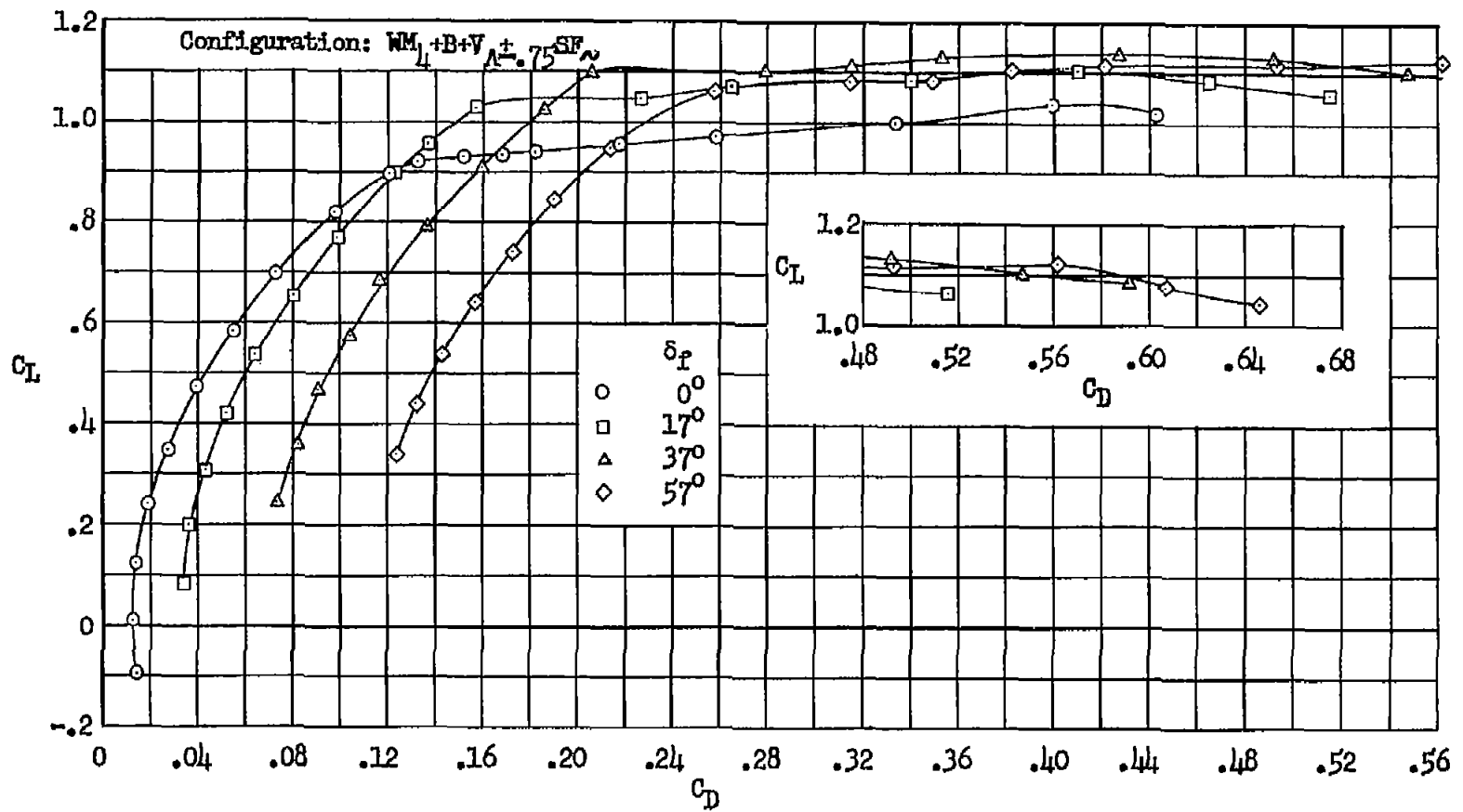
(b) C_L vs. C_D

Figure 46.- Concluded.

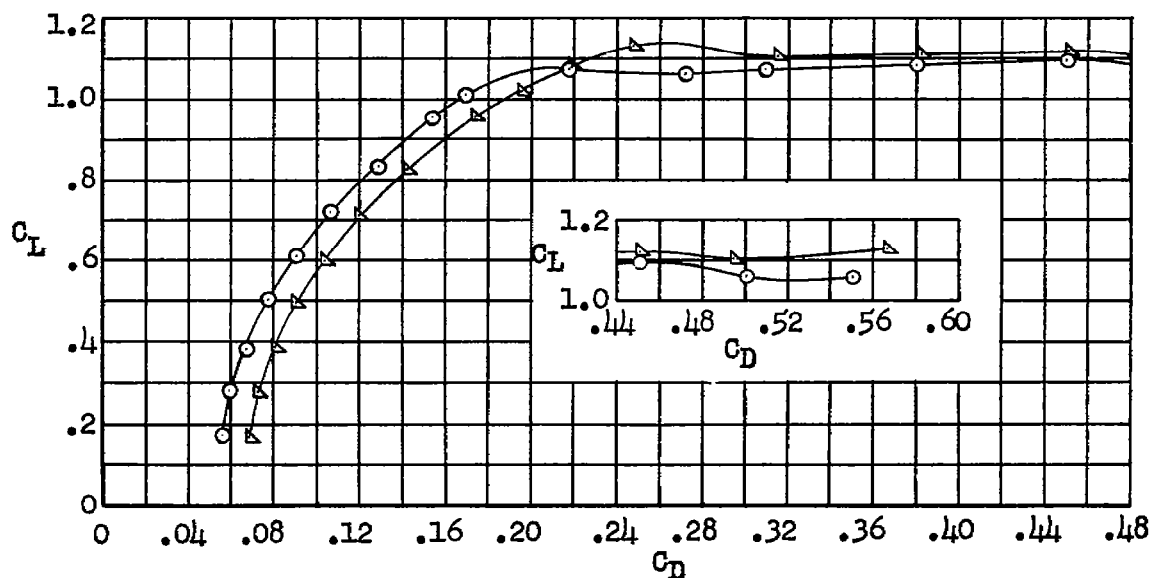
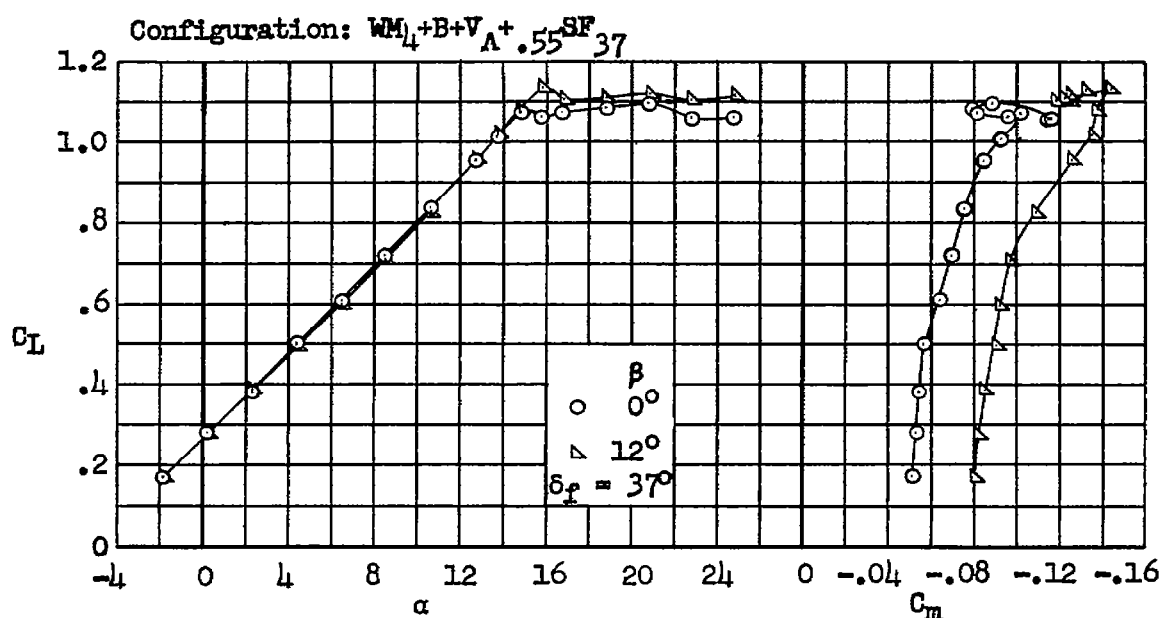
(a) C_L vs. α , C_m , C_D

Figure 47.- Wing modification 4; characteristics in sideslip of the model with split flaps of span $0.55 b/2$, with the swept vertical tail, without the horizontal tail; Reynolds number 10×10^6 .

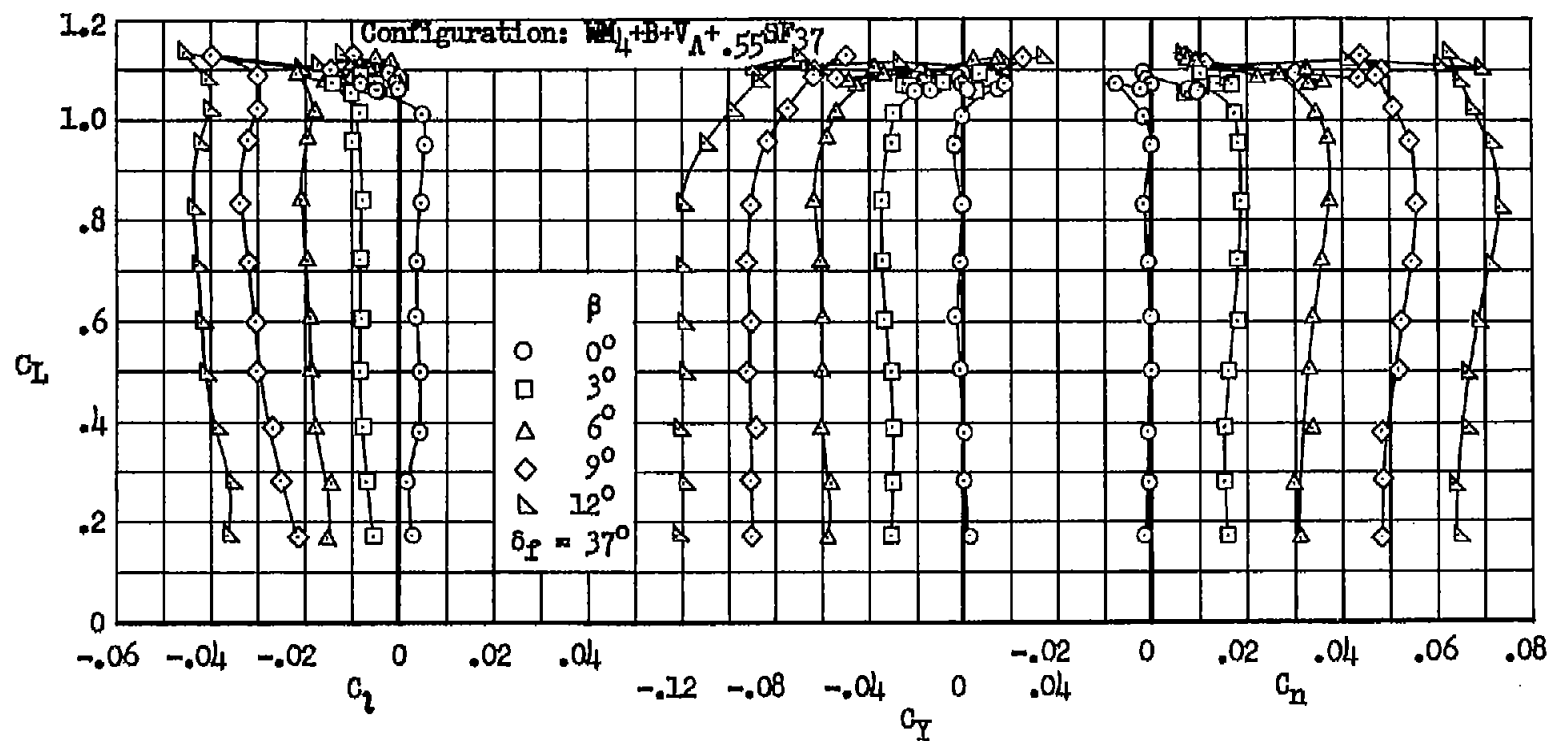
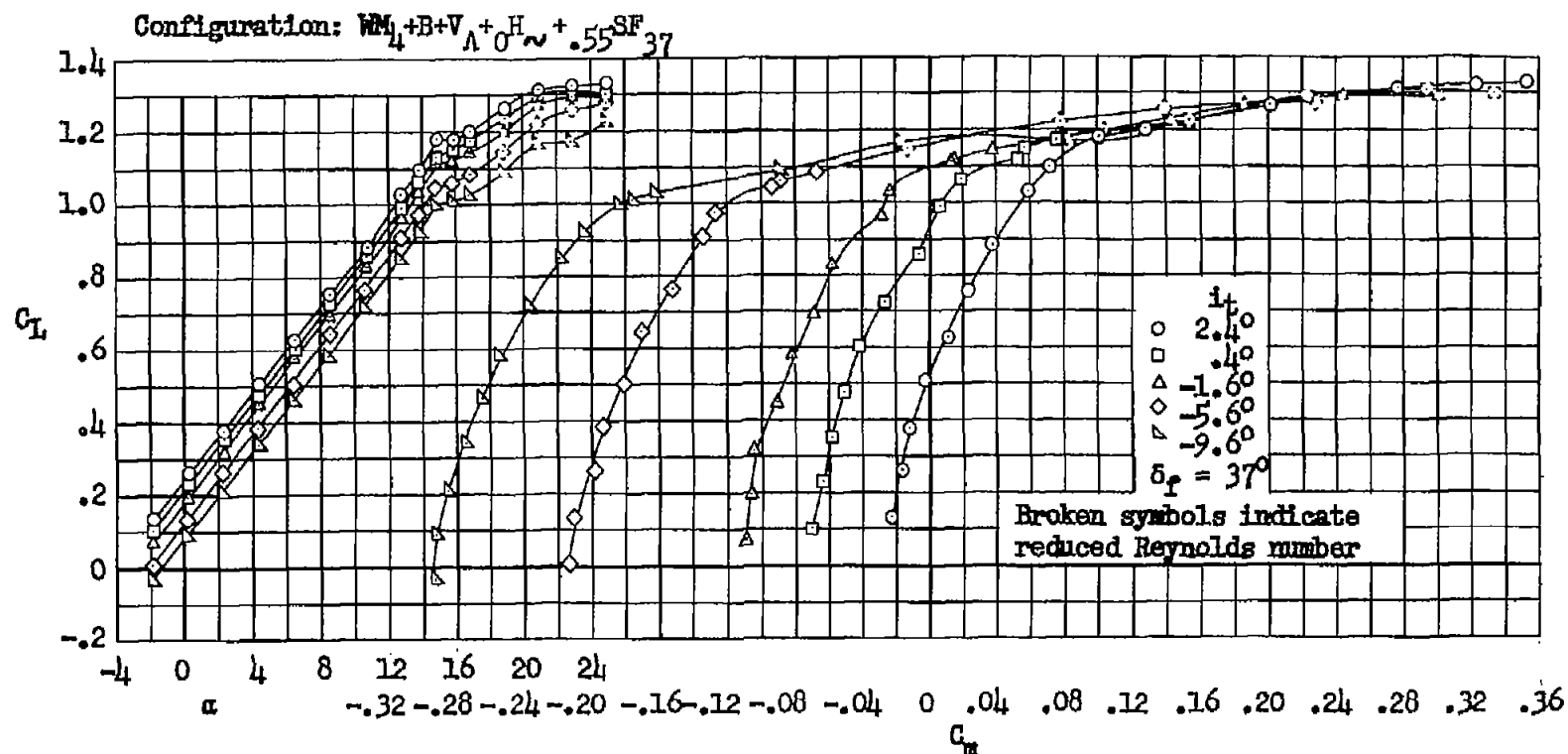
(b) C_L vs. C_D , C_Y , C_N

Figure 47.- Concluded.



(a) C_L vs. α , C_m

Figure 48.- Wing modification 4; longitudinal characteristics of the model with split flaps of span $0.55 b/2$, with the horizontal tail in the wing chord plane; moment center at 0.348 , Reynolds numbers 10 and 8×10^6 .

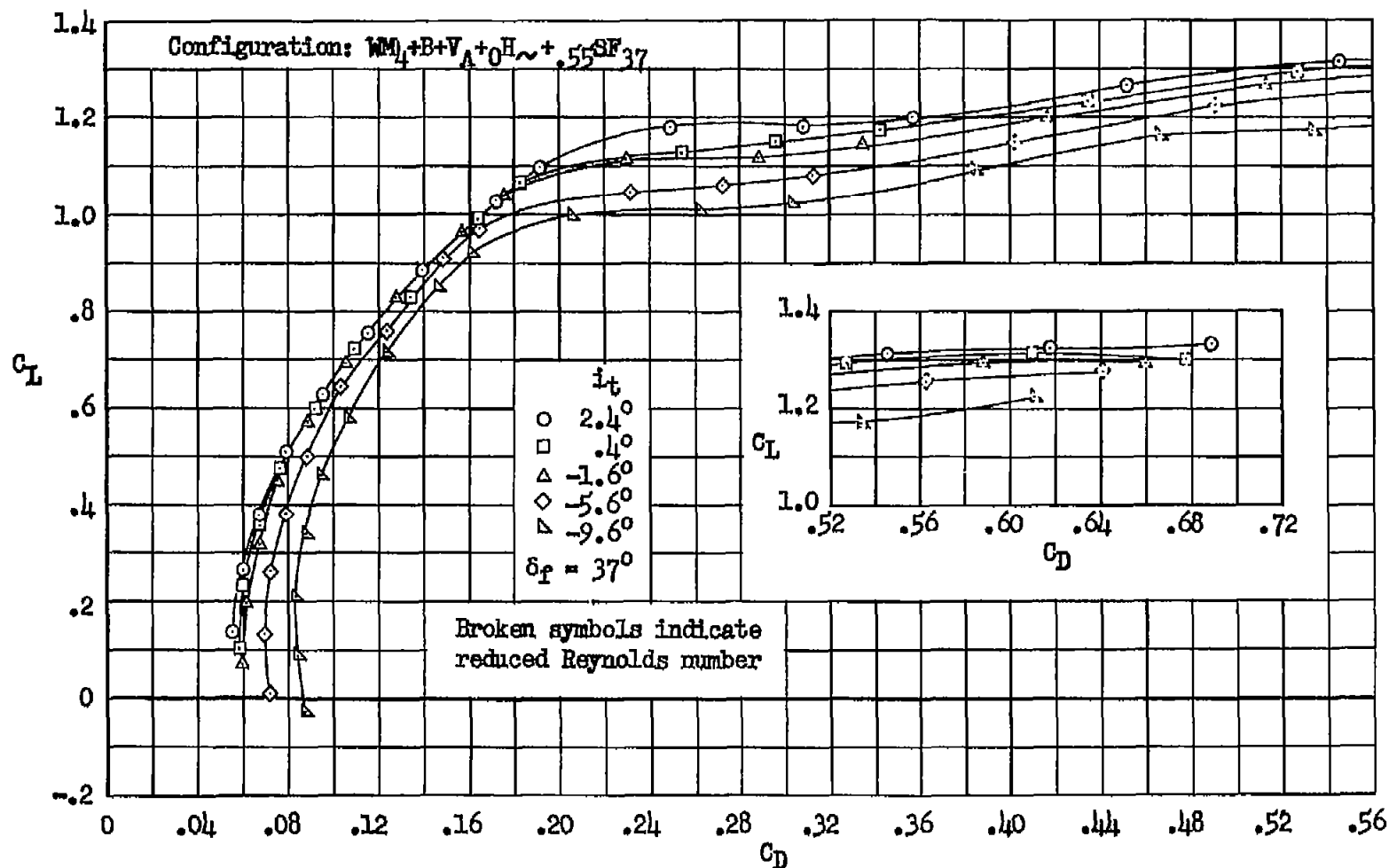


Figure 48.- Concluded.

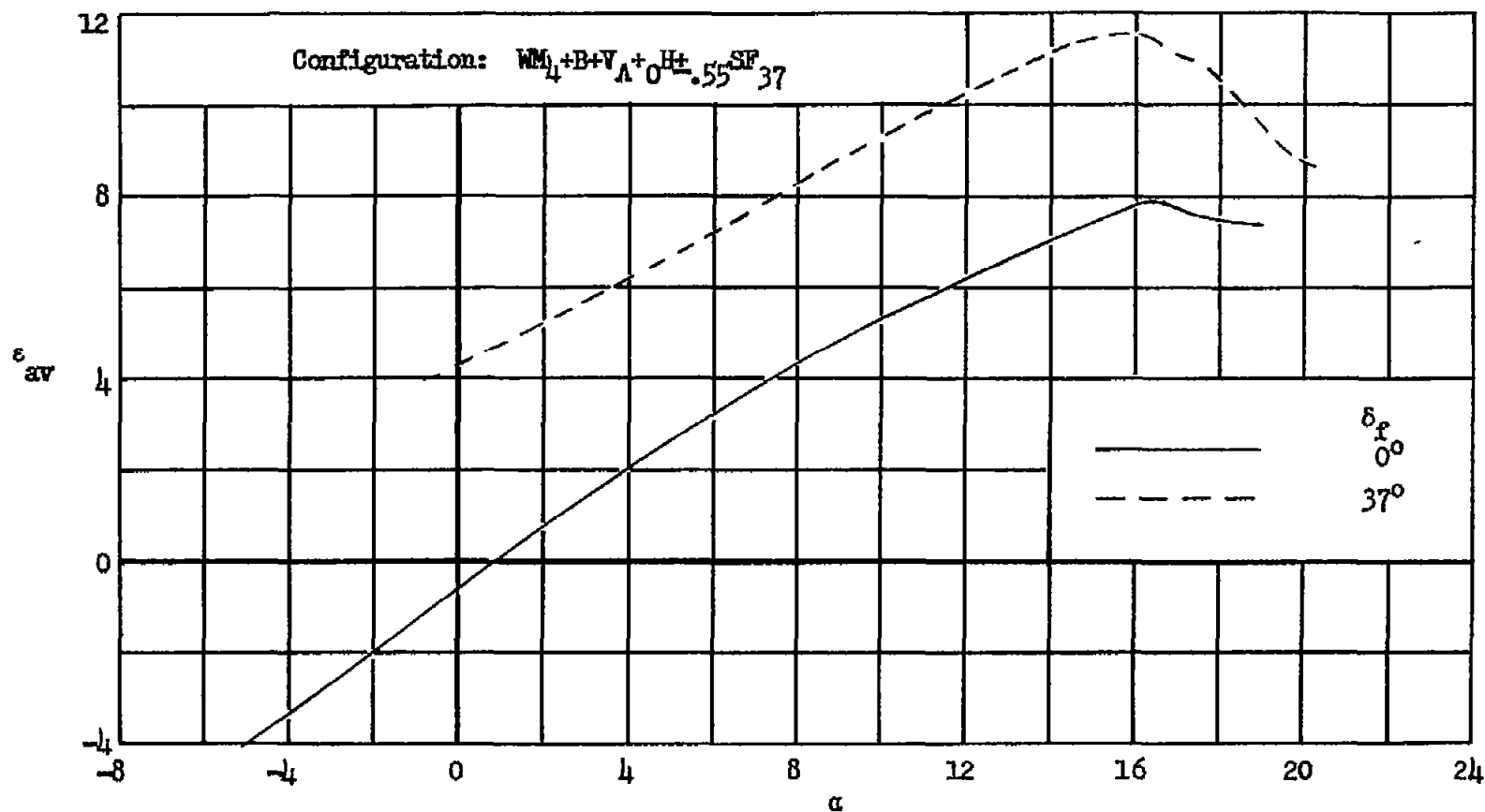


Figure 49.- Wing modification 4; average effective downwash at the position of the horizontal tail in the wing chord plane, both with and without split flaps of span $0.55 b/2$ on the wing; determined at Reynolds numbers of 10 and 8×10^6 .

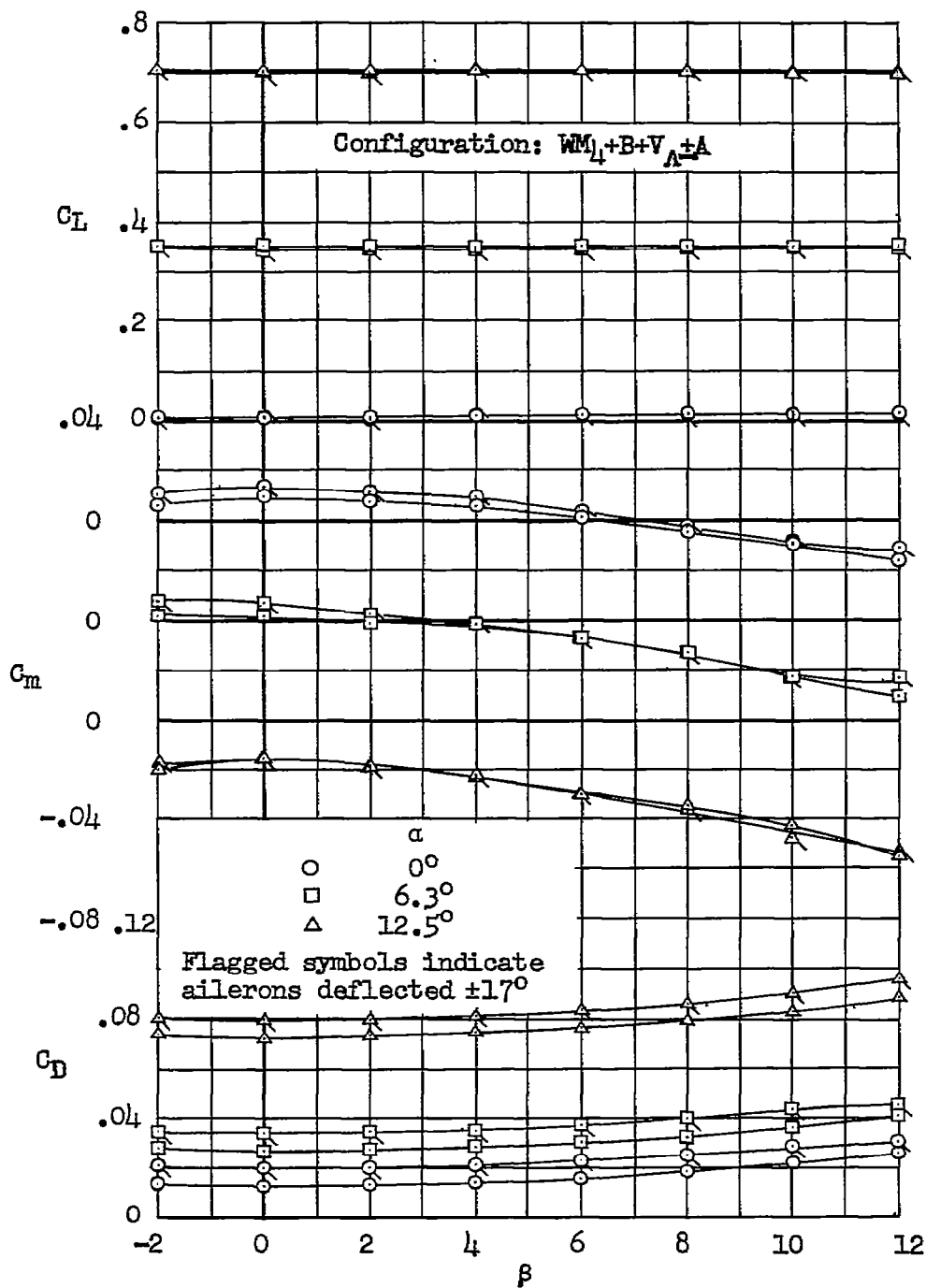
(a) C_L , C_m , C_D vs. β

Figure 50.- Wing modification 4; effect of simulated ailerons on the characteristics in sideslip of the model with the swept vertical tail, without the horizontal tail; Reynolds number 10×10^6 .

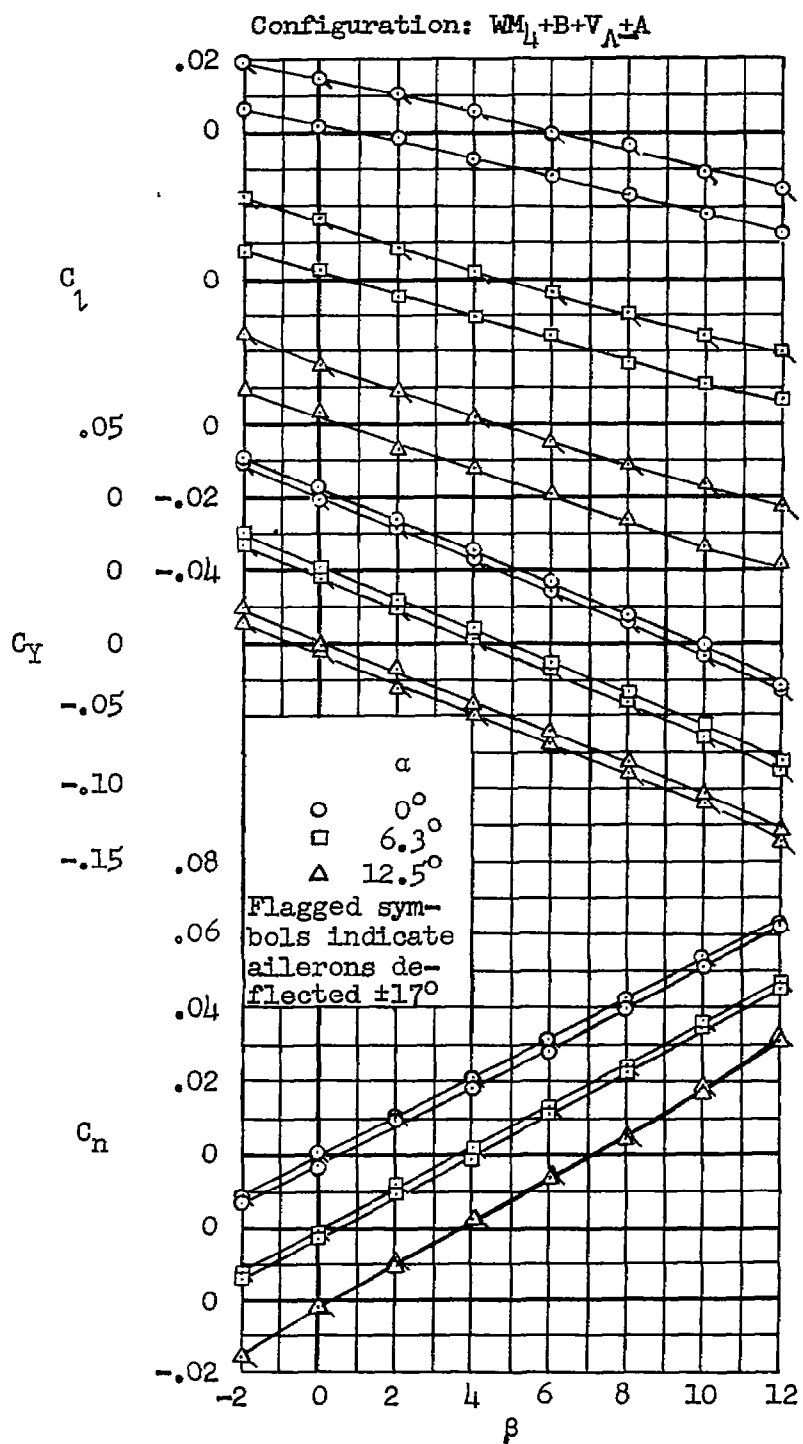


Figure 50.- Concluded.

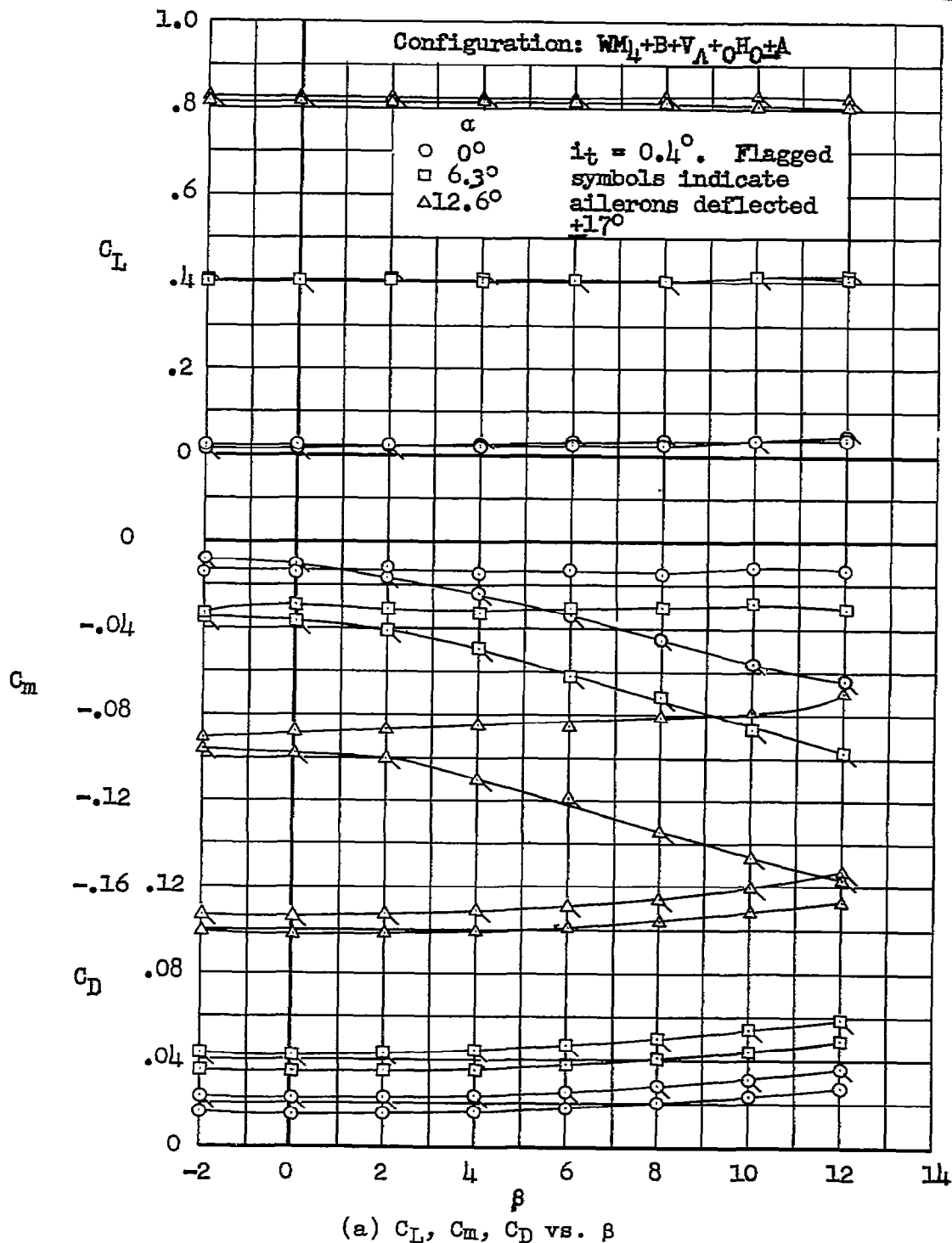


Figure 51.- Wing modification 4; effect of simulated ailerons on the characteristics in sideslip of the model with the swept vertical tail and the horizontal tail in the wing chord plane; moment center at $0.34\bar{c}$, Reynolds number 10×10^6 .

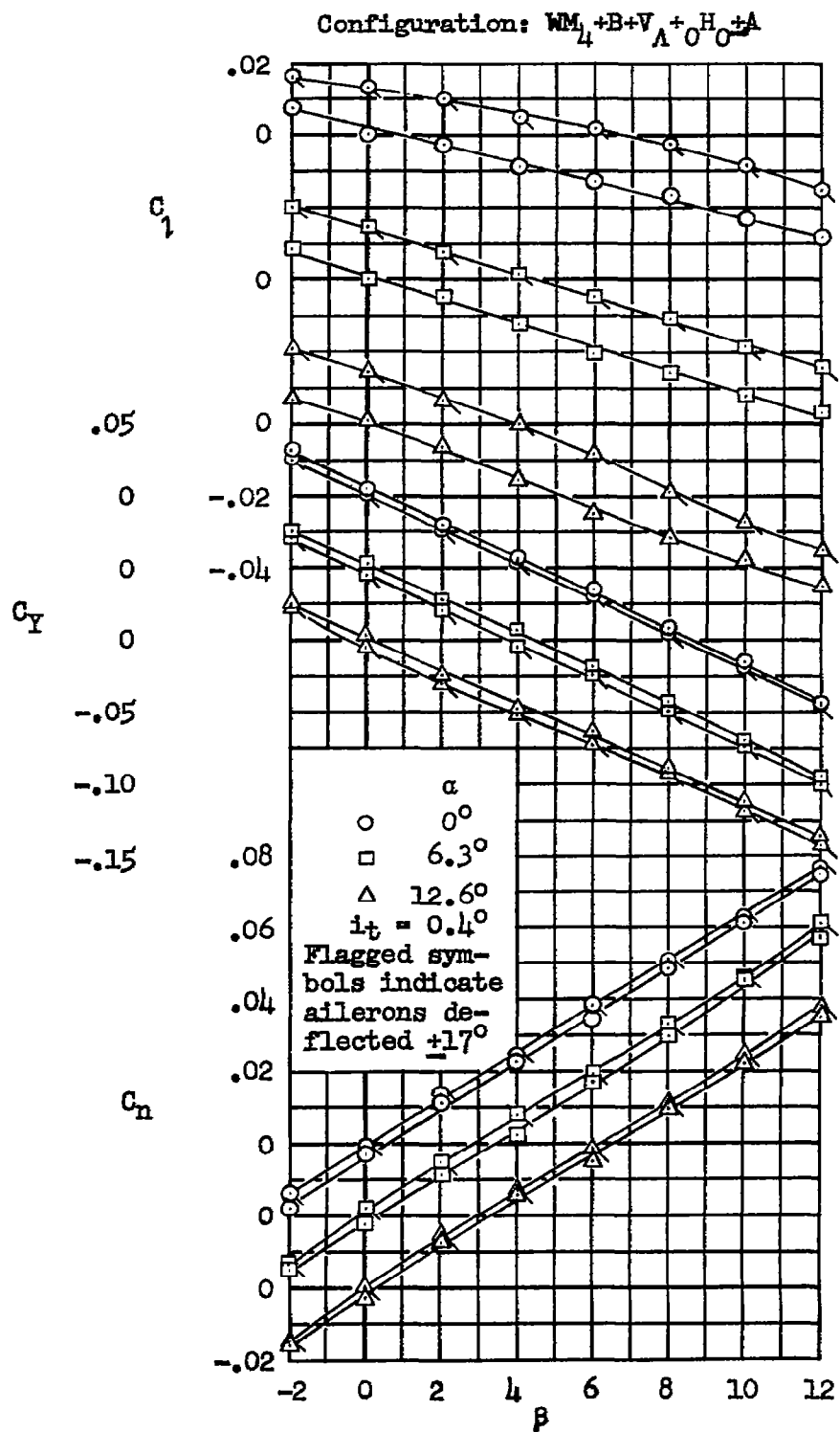
(b) C_l, C_Y, C_n vs. β

Figure 51.- Concluded.

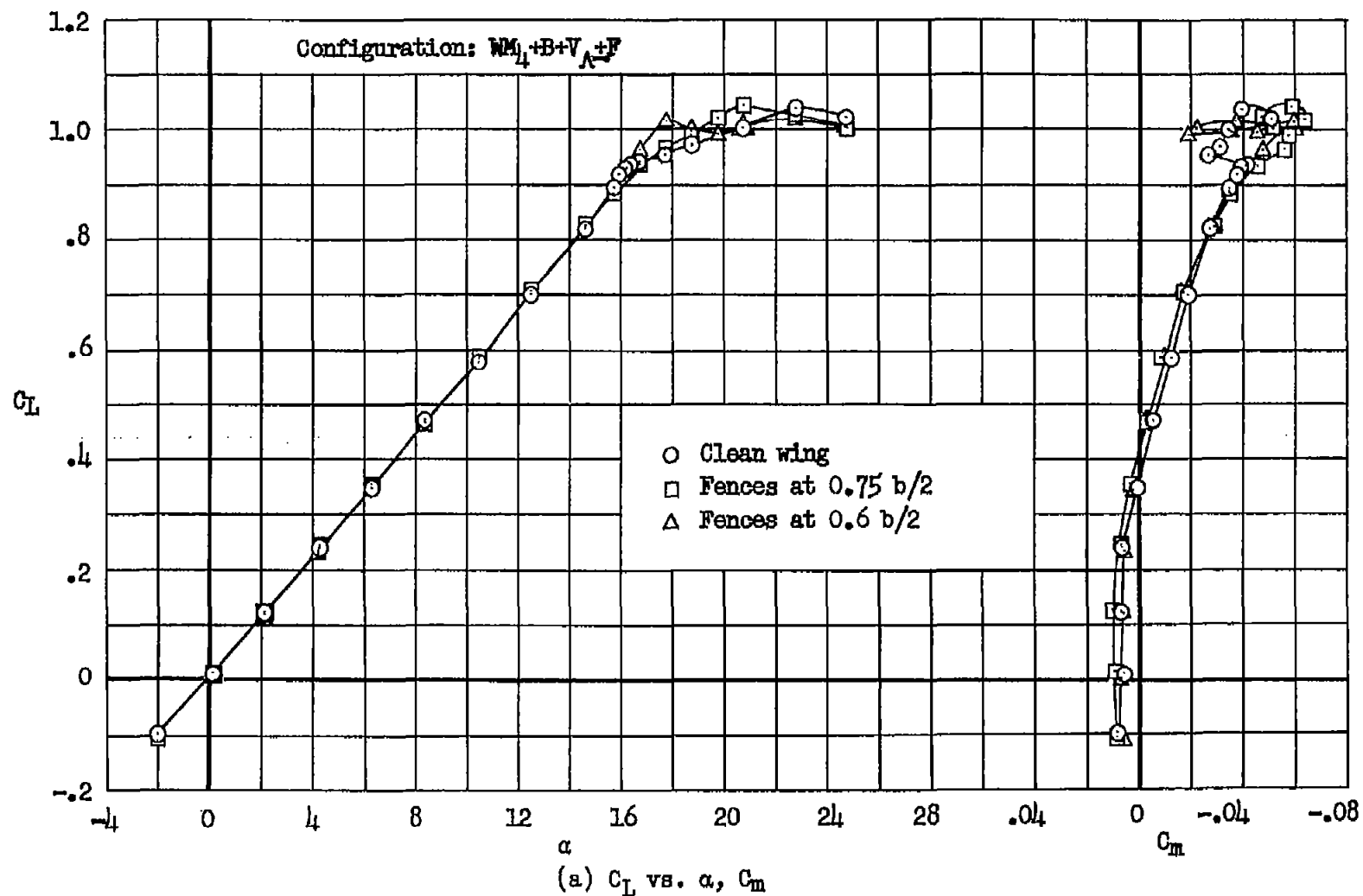


Figure 52.- Wing modification 4; effect of fences on the longitudinal characteristics of the model without the horizontal tail, Reynolds number 10×10^6 .

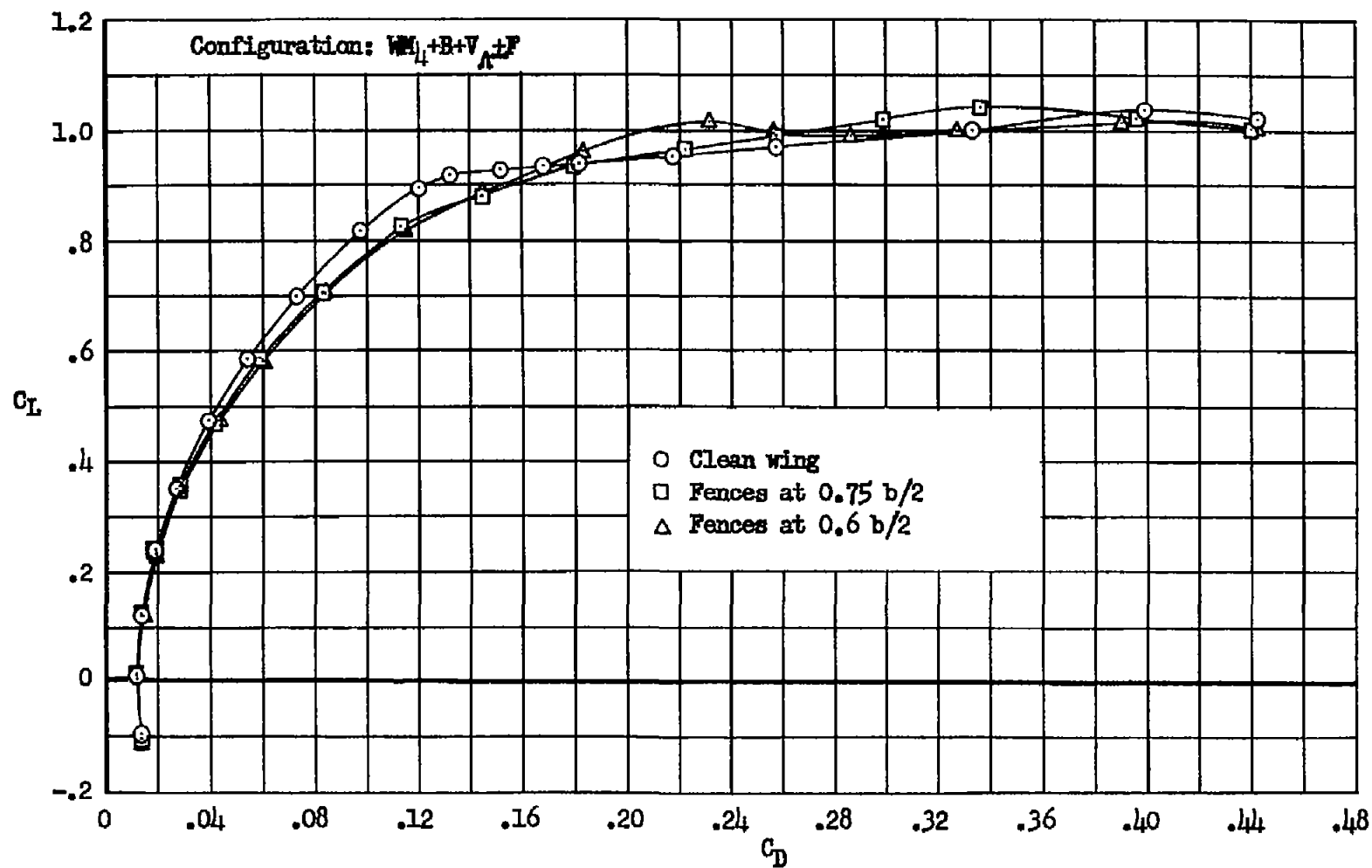
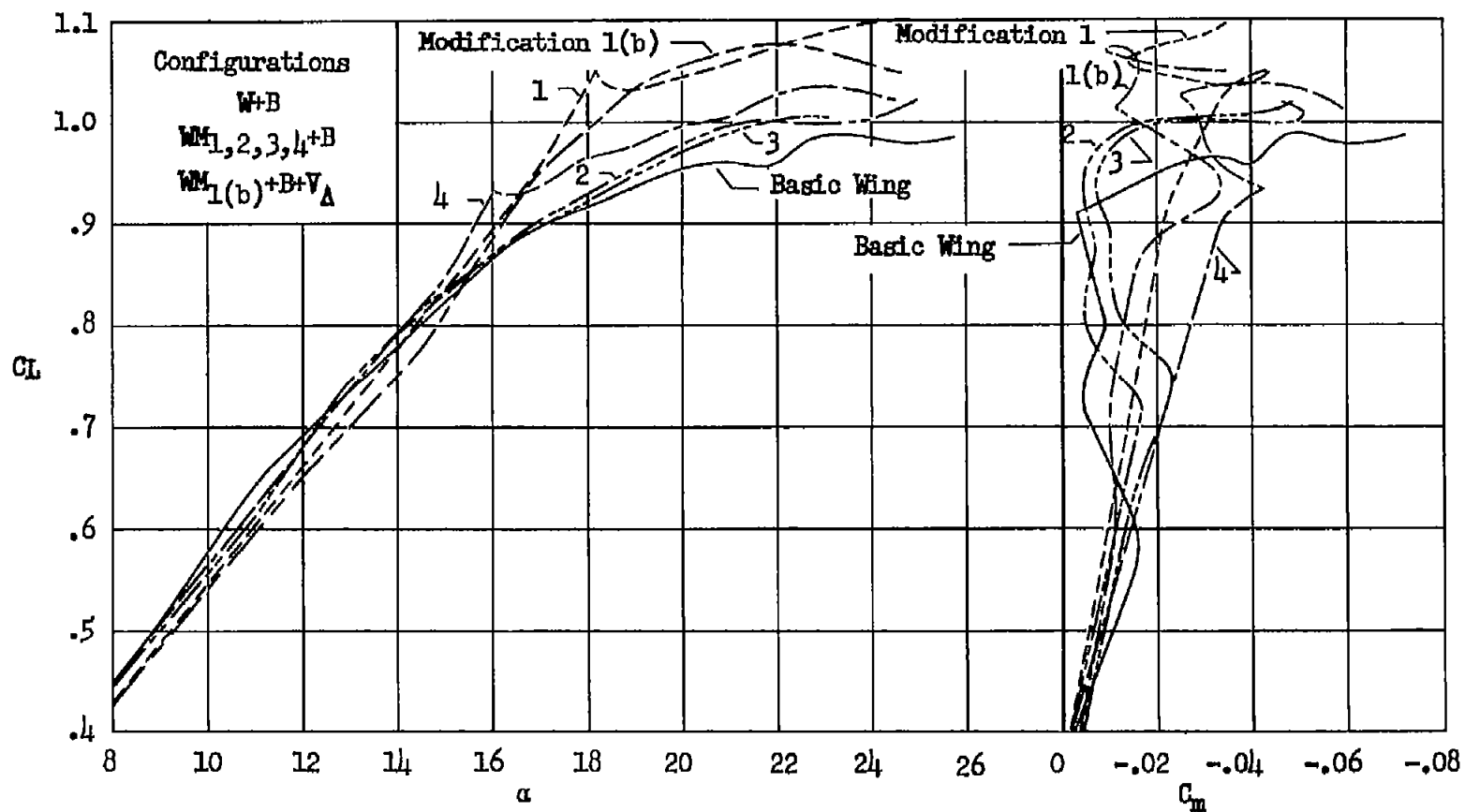
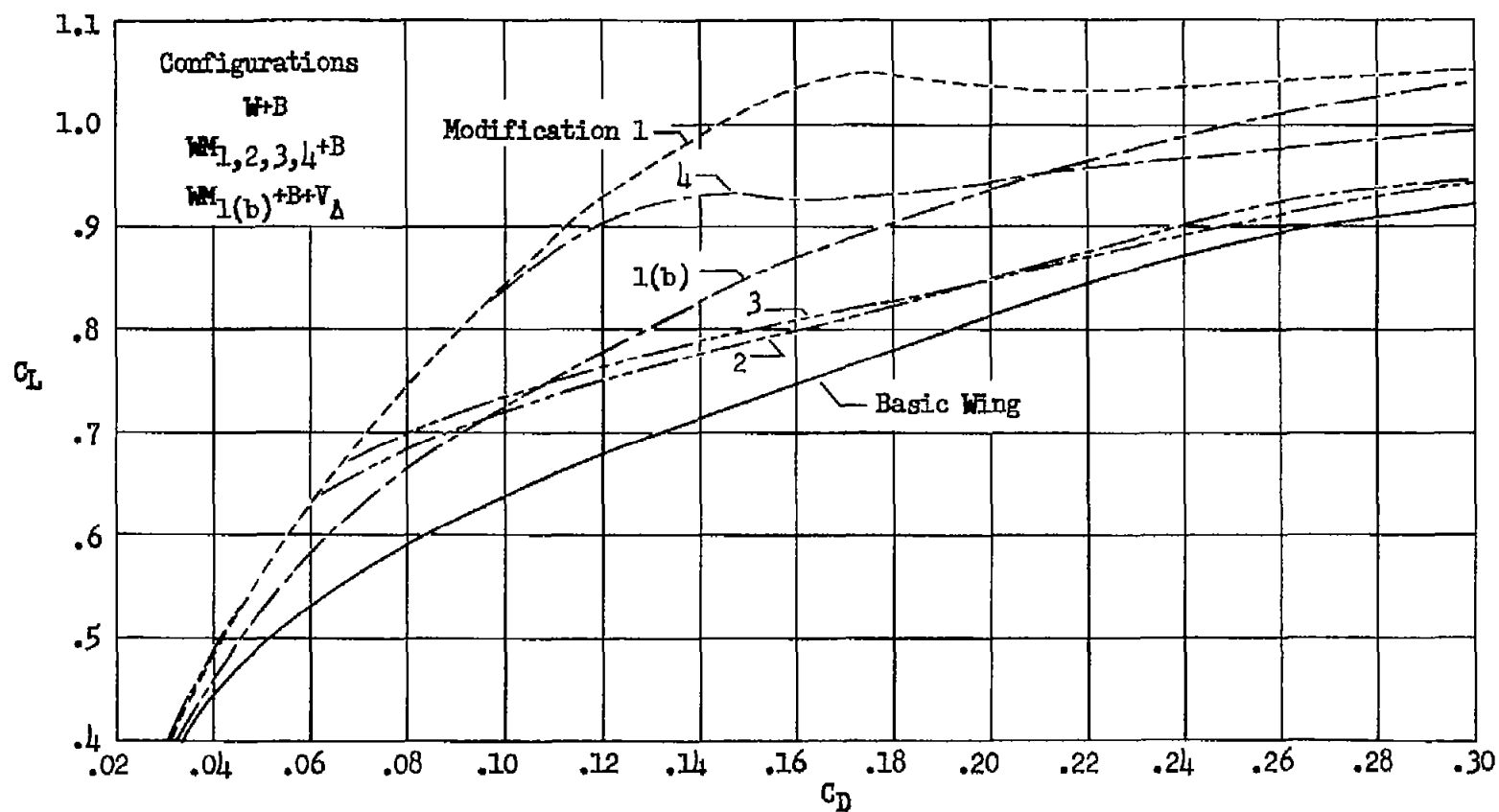
(b) C_L vs. C_D

Figure 52.- Concluded.



(a) C_L vs. α , C_m

Figure 53.- Basic wing and all modifications; comparison of the longitudinal characteristics of the wing-body configurations, Reynolds number 10×10^6 .



(b) C_L vs. C_D

Figure 53.- Concluded.

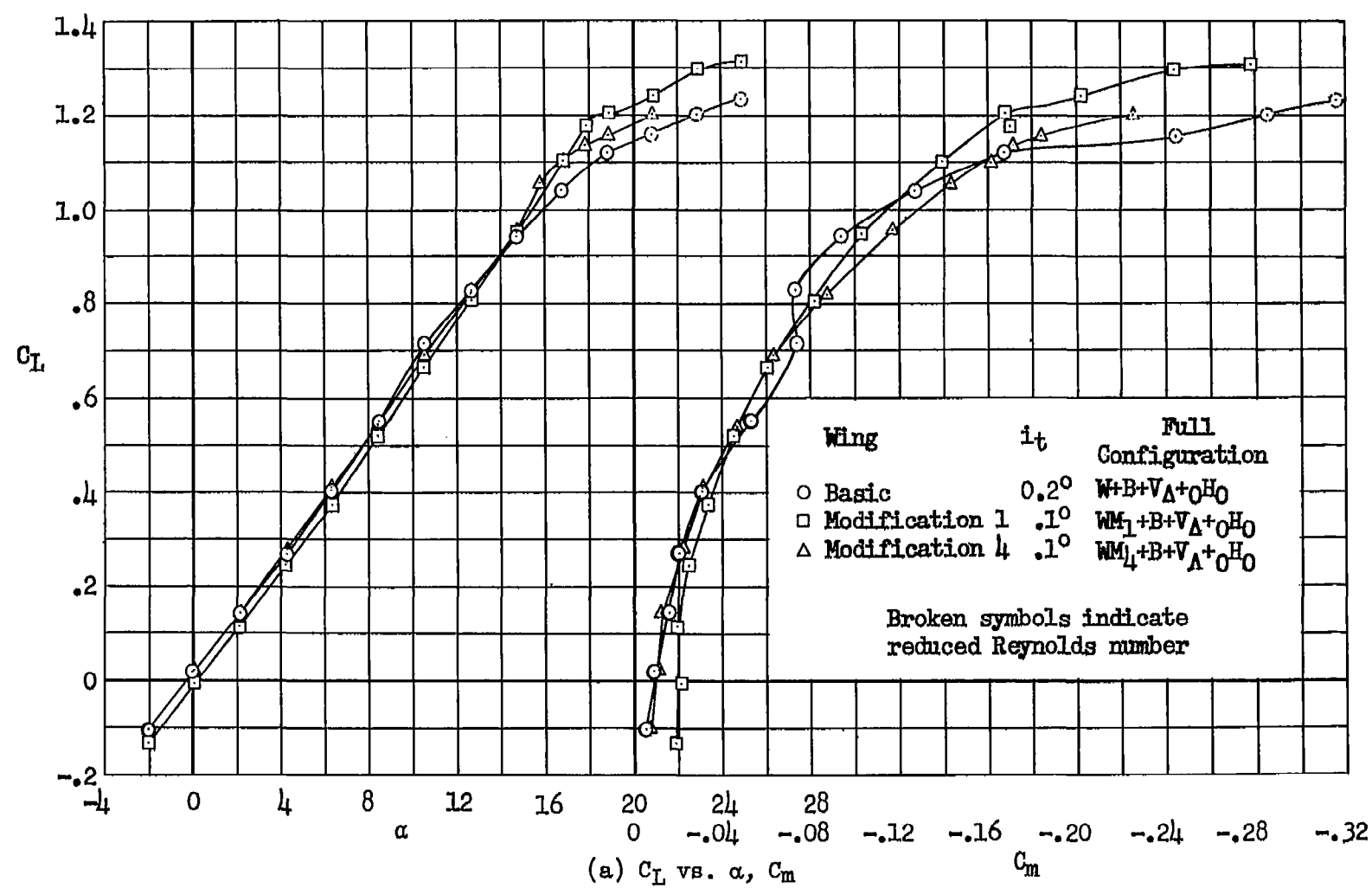


Figure 54.- Basic wing and modifications 1 and 4; comparison of the longitudinal characteristics of the models with the horizontal tail in the wing chord plane; moment center at $0.34\bar{c}$, Reynolds numbers 10 and 8×10^6 .

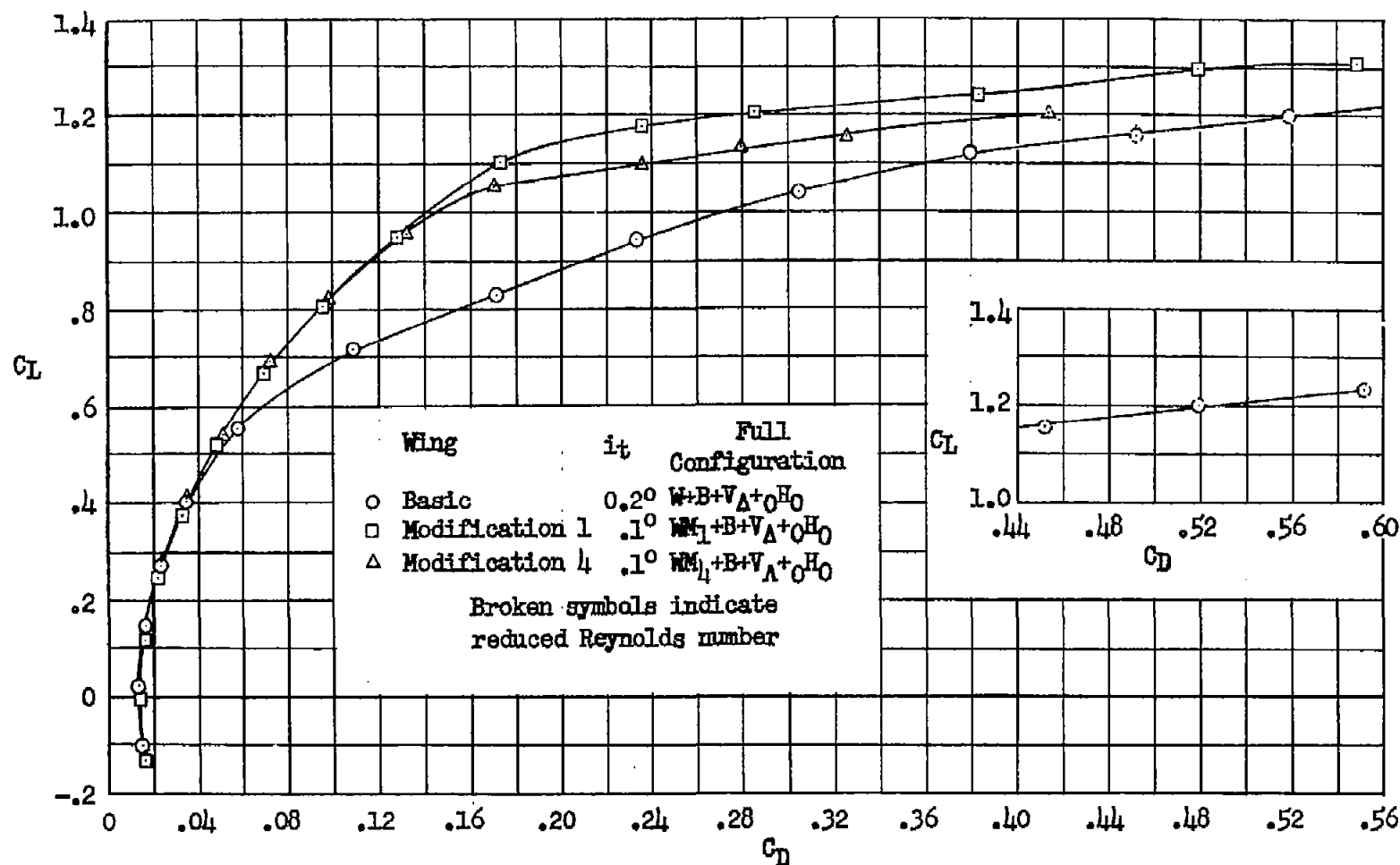
(b) C_L vs. C_D

Figure 54.- Concluded.

LANGLEY RESEARCH CENTER
3 1176 00511 4062